Novel and actionable high-resolution climate change information for adaptation of engineering systems in cold environments

by

Bernardo Stephan Teufel

Department of Civil Engineering,

McGill University, Montreal

December 2021

A thesis submitted to McGill University in partial fulfillment of the requirements of the degree of Doctor of Philosophy

Table of contents

List of Figures

List of Abbreviations

ALT	Active Layer Thickness
AMS	Annual Maximum Streamflow
ASR	Arctic System Reanalysis
CALM	Circumpolar Active Layer Monitoring
CanESM2	Second generation Canadian Earth System Model
CC	Clausius–Clapeyron
CLASS	Canadian Land Surface Scheme
CPM	Convection-Permitting Model
CRU	Climatic Research Unit
DSR	Daily Severity Rating
ECCC	Environment and Climate Change Canada
ECMWF	European Centre for Medium-Range Weather Forecasts
ERA	ECMWF Re-Analysis
FWI	Fire Weather Index
GCM	Global Climate Model
GEM	Global Environmental Multiscale
GEV	Generalized Extreme Value

GHG	Greenhouse Gas
GMT	Global Mean Temperature
HWSD	Harmonized World Soil Database
IPCC	Intergovernmental Panel on Climate Change
IQR	Interquartile Range
MODIS	Moderate Resolution Imaging Spectroradiometer
MSE	Mean Square Error
NARCCAP	North American Regional Climate Change Assessment Program
NWT	Northwest Territories
RCM	Regional Climate Model
RCP	Representative Concentration Pathway
ROS	Rain-On-Snow

Abstract

Engineering systems are designed to withstand their operating environment, which generally includes a variety of factors influenced by climate variability and extremes. Given that engineering systems usually have long lifespans, it becomes necessary to account for future environmental conditions, which due to climate change, are unlikely to be represented in historical archives. It follows that the first step to adapt engineering systems to the changing environmental conditions is the generation of actionable climate change information. Climate models are the primary tools available to develop projections of future climate, but these projections need to be of sufficiently high quality and resolution to be useful for the adaptation of engineering systems.

In this thesis, novel climate change information was developed using the state-of-the-art regional climate model GEM (Global Environmental Multiscale), which is extensively used for climate research. Contributions to original knowledge arose by applying innovative analysis methods to an ensemble of climate projections, including 4 km resolution projections over the Canadian Arctic, developed for the first time. Several knowledge gaps were addressed, which contributed significantly to the advancement of the understanding of climate-infrastructure interactions in cold regions.

Analysis of rainfall and snowmelt as flood-generating mechanisms across Canada demonstrated the importance of keeping global warming below the 2 °C threshold of the Paris Agreement. Under 2 °C of global warming, slight increases of rainfall contribution to flood peaks are projected, while a high-warming scenario leads to widespread increases in rainfall contribution and the emergence of hotspots of change in currently snowmelt-dominated regions. These changes influence flood magnitude and timing, which has implications for the management of flood risks and freshwater resources and for the development of flow regulation plans.

Large projected changes over northern regions motivated further analysis, which revealed the possibility of abrupt decreases in soil moisture in response to increased drainage due to permafrost degradation for the high-warming scenario. This regime shift is projected to result in abrupt changes to many variables and processes of high significance to northern interests, such as flood predictors and wildfire intensity. The abruptness of these changes presents additional challenges to climate change adaptation and potential retrofitting of engineering systems.

The adaptation of these systems requires high-resolution projections, which were developed here for the first time at 4 km resolution over the Canadian Arctic, for the investigation of hazards to northern transportation. By 2040, significant increases to short-duration rainfall and wind gust extremes, as well as further permafrost degradation, are expected to foment deterioration of northern infrastructure and transportation systems. A novel approach integrating climate model output and machine learning algorithms allowed deriving projections of fog – a complex variable. Overall fog frequency is projected to increase over most of the Canadian Arctic by 2040, presenting an additional hazard to northern transportation.

The main contribution of this thesis is the advancement of the understanding of several different pathways through which changing climatic conditions are expected to impact engineering systems in cold regions. On one hand, the projections highlight the crucial importance of climate change mitigation, as remaining below the 2 °C global warming threshold would prevent large changes over many regions and decrease the likelihood of abrupt changes. On the other hand, some climatic hazards are projected to soon exceed those in historical records regardless of emissions scenario, and the high-quality, high-resolution projections analyzed here contain useful and actionable information for the adaptation of engineering systems.

Résumé

Les systèmes d'ingénierie sont conçus pour résister à leur milieu opérationnel, qui comprend généralement une variété de facteurs influencés par la variabilité et les extrêmes climatiques. Étant donné que les systèmes d'ingénierie ont généralement une longue durée de vie, il devient nécessaire de tenir compte des conditions environnementales futures, qui, en raison du changement climatique, ont peu de probabilité d'être représentées dans les archives historiques. Il s'ensuit que la première étape pour adapter les systèmes d'ingénierie aux conditions environnementales changeantes est la génération d'informations fiables et exploitables sur le changement climatique. Les modèles climatiques sont les principaux outils disponibles pour développer des projections du climat futur, mais ces projections doivent être d'une qualité et d'une résolution suffisamment élevées pour être utiles à l'adaptation des systèmes d'ingénierie.

Dans cette thèse, des nouvelles informations sur le changement climatique ont été développées à l'aide du modèle climatique GEM (Global Environnemental Multi-échelle), un modèle de pointe qui est largement utilisé pour la recherche climatique. Des contributions originales sont nées de l'application de méthodes d'analyse innovantes à un ensemble de projections climatiques, dont des projections à résolution de 4 km couvrant l'Arctique canadien, développées pour la première fois. Plusieurs lacunes au niveau des connaissances ont été comblées, ce qui a contribué de manière significative à l'avancement de la compréhension des interactions climat-infrastructure dans les régions froides.

L'analyse de la pluie et de la fonte des neiges comme mécanismes générateurs d'inondations à travers le Canada a démontré l'importance de maintenir le réchauffement climatique sous le seuil de 2 °C de l'Accord de Paris. Sous 2 °C de réchauffement climatique, de légères augmentations de la contribution des précipitations liquides aux inondations sont prévues, tandis qu'un scénario de

réchauffement élevé entraîne une augmentation généralisée de la contribution des précipitations liquides et l'émergence de zones réactives dans les régions actuellement dominées par la fonte des neiges. Ces changements influencent l'amplitude et le calendrier des crues, ce qui a des implications pour la gestion des risques d'inondation et des ressources en eau douce, et pour l'élaboration de plans de régulation des débits.

Les importants changements projetés dans les régions nordiques ont motivé une analyse plus approfondie, qui a révélé la possibilité de diminutions abruptes de l'humidité du sol en réponse à la dégradation du pergélisol pour le scénario de réchauffement élevé. Ce changement de régime risquerait d'entraîner des changements soudains dans de nombreuses variables et processus de grande importance pour les intérêts nordiques, tels que des prédicteurs d'inondations et l'intensité des feux de forêt. La soudaineté de ces changements présente des défis supplémentaires pour l'adaptation des systèmes d'ingénierie au changement climatique.

L'adaptation de ces systèmes nécessite des projections à haute résolution, qui ont été développées ici pour la première fois à une résolution de 4 km couvrant l'Arctique canadien, pour l'étude des risques pour le secteur des transports. D'ici 2040, des augmentations importantes des chutes de pluie de courte durée et des rafales de vent extrêmes, ainsi que la poursuite de la dégradation du pergélisol, risquent de provoquer la détérioration des infrastructures et des systèmes de transport du Nord. Une nouvelle approche intégrant les sorties du modèle climatique et des algorithmes d'apprentissage automatique a permis de dériver des projections pour la fréquence du brouillard - une variable complexe. On prévoit que la fréquence du brouillard augmentera sur la majeure partie de l'Arctique canadien d'ici 2040, présentant un danger supplémentaire pour le transport dans le Nord.

La principale contribution de cette thèse est l'avancement de la compréhension de plusieurs voies par lesquelles les conditions climatiques changeantes risquent d'avoir un impact sur les systèmes d'ingénierie dans les régions froides. D'une part, les projections soulignent l'importance cruciale de l'atténuation du changement climatique, car rester en dessous du seuil de réchauffement global de 2 °C empêcherait des changements importants dans de nombreuses régions et réduirait la probabilité de changements soudains. D'un autre côté, certains risques climatiques devraient bientôt dépasser ceux des enregistrements historiques, quel que soit le scénario d'émissions, et les projections de haute qualité et à haute résolution analysées ici contiennent des informations utiles et exploitables pour l'adaptation des systèmes d'ingénierie.

Acknowledgements

First, I want to thank to my wife, Monica, who went through it all and never left my side – her strength inspires me every day and her encouragement helped me achieve this dream.

I am grateful to my parents, who taught me to think critically and question everything, putting me on this path that reaches a major milestone today. They have always supported my dreams, which has allowed me to come farther than I would ever have imagined.

I will always be indebted to Dr. Turcotte and the entire team at the Cedars Cancer Centre – without them, my path would have ended long before this moment.

I want to express my gratitude to my supervisor, Prof. Laxmi Sushama, for her guidance and support throughout my research career. Her knowledge and effective mentorship have led me to achieve this milestone. I appreciate the freedom and the encouragement to dig deeper – both have made me a better researcher. Over the course of my PhD studies, she also gave me unique opportunities to lead multi-institutional publications on other topical and critical societal issues, such as COVID-19 (doi: 10.3390/atmos12020243) and the 2017 Montreal flood (doi: 10.1007/s00382-018-4375-0).

I also want to thank all my past and present colleagues at the Climate Change and Sustainable Engineering and Design Lab, with special thanks to Vincent, Sasha, Gulilat and Seok-Geun, for their technical assistance and for all the interesting discussions we had over the years.

Finally, I want to acknowledge the financial support from the McGill Engineering Doctoral Award (MEDA), Natural Sciences and Engineering Research Council of Canada (NSERC), Trottier Institute for Sustainability in Engineering and Design (TISED), McGill Sustainability Systems Initiative (MSSI) and all resources provided by Compute Canada.

Chapter 1: Introduction

1.1. Problem statement

Engineering systems are designed to withstand the environment in which they operate. For instance, virtually all physical infrastructure is designed to be resilient to historical climate and its extremes. Given that climate is changing (IPCC, 2013), historical climate information will no longer be representative of the conditions to which infrastructure might be exposed throughout its lifespan, and thus it becomes necessary to account for future climatic conditions. This becomes even more important for infrastructure with long lifespans and/or located in regions where climate is changing rapidly.

Climate change in high-latitude regions of the northern hemisphere is among the greatest anywhere on Earth because warming over the region is amplified by positive feedbacks in the climate system (IPCC, 2013). For instance, Canada has warmed and will continue to warm at about double the global rate (Palko and Lemmen, 2017). Even greater warming rates have been observed for northern Canada, where the land surface has warmed at a rate of 0.5°C per decade over the past three decades, and temperatures in recent decades have been significantly higher than those seen over the past 2000 years (Kaufman et al., 2009). While climate change will bring some potential benefits, overall it will impose increasing economic costs on Canada (Warren and Lulham, 2021).

Climate-infrastructure interactions are numerous, given the large number of pathways through which various climate variables can impact different types of infrastructure, from gradual weathering of building facades to catastrophic failures during extreme storms. In this thesis, the focus is on climate-infrastructure interactions in cold regions, particularly those for which significant knowledge gaps exist, such as hazards related to extreme events, abrupt changes and complex phenomena, which could trigger catastrophic failures. Special attention is paid to the transportation sector, which is both vulnerable and vital for northern communities and industry. For instance, given that many northern communities rely entirely on air transportation during part of the year, they may be left temporarily uncommunicated due to low visibility conditions (Deton' Cho Stantec, 2013). In addition, climate-driven disruptions to mine access roads have forced supplies to be transported by air, causing tens of millions of dollars in losses (Perrin et al., 2015).

One fundamental component of northern landscapes that is particularly vulnerable to warming temperatures is permafrost, defined as ground (soil or rock) that remains at or below 0°C for two or more consecutive years, and which currently underlies about 40% of Canada's landmass. Permafrost thaw and associated soil subsidence, particularly in regions with high ice content, can damage infrastructure, both above ground and below ground. Transportation networks, pipelines and building foundations have already shown signs of deterioration and failure (Government of the NTW, 2008). In addition, permafrost acts as an impermeable barrier to soil water movement. When permafrost thaws, new hydraulic pathways might become available, with the potential to induce abrupt changes (Liljedahl et al., 2016; Perreault et al., 2016), which can have significant implications for northern communities and infrastructure (Lenton, 2012). This further increases the challenges associated with adaptation and potential retrofitting measures, as the potential for abrupt shifts is rarely considered when climate change information is incorporated into the decision-making process.

Near-surface permafrost degradation and its detrimental consequences are expected to continue in a warming climate (e.g., Slater and Lawrence, 2013), but are far from being the only environmental threat to engineering systems in cold regions. Increasing rainfall extremes over the northern high latitudes have already been observed (Westra et al., 2013), and further intensification is projected in future climate (Mladjic et al., 2011; Monette et al., 2012; Khaliq et al., 2015). Warmer temperatures favor faster snowmelt rates, which along with increasing rainfall has severe implications for flood risk. Additional threats due to climate change include increased wildfire risk, which is a major concern for the safety of communities and infrastructure (McGee et al., 2015), as well as potential changes to extreme wind and low visibility conditions, which have not been studied in depth and are highly uncertain. Given that much of the existing northern physical infrastructure was designed without consideration of climate change (e.g., Huntington et al., 2007), there is an urgent need to adapt the Canadian Arctic's engineering and infrastructure systems to the changing climatic conditions.

The first step to adapt engineering and infrastructure systems to the changing climatic conditions is the generation of actionable climate change information. Climate models, which are based on the fundamental laws of nature (e.g., energy, mass and momentum conservation) and encapsulate the current understanding of the climate system, are the primary tools available to make projections of future climate over the coming decades and beyond. Global climate models (GCMs) are able to reproduce the observed continental-scale surface temperature patterns and trends over many decades (IPCC, 2013). Regional and local-scale climate information can be obtained directly from global models; however, their horizontal resolution (typically hundreds of kilometers) is often too coarse to resolve features that are important at smaller scales, including most climate extremes.

Statistical and dynamical downscaling methods are both widely used to generate climate information at the smaller scales needed for many climate impact studies (IPCC, 2013). Statistical downscaling derives and applies empirical relationships to obtain local/regional climate information from model output, while regional climate models (RCMs) are applied over a limited-area domain with boundary conditions from GCM output (Rummukainen, 2010). Reducing the size of the domain enables the use of finer horizontal resolution (typically tens of kilometers), resulting in simulations that are richer in spatial and temporal detail (e.g., Feser et al., 2011; Jacob et al., 2014). Downscaling by RCMs adds value in regions with highly variable topography and for various small-scale phenomena, which are often responsible for climate extremes (Feser et al., 2011). Another benefit of RCMs is the explicit resolution of regional water bodies and land-surface heterogeneities, thus resolving feedback processes that increase the realism of climate simulations and improve climate change projections (Diro et al., 2014; Garnaud and Sushama, 2015; Huziy and Sushama, 2017b; Diro et al., 2018). Given the focus of this thesis on complex physical processes and mechanisms, dynamical downscaling is preferred over the statistical downscaling approach.

Even at RCM resolution, mismatches exist between actionable and modelled spatiotemporal information, as some engineering systems and their adaptation require higher resolution climate change information. Additional downscaling in the form of convection-permitting models (CPMs; Prein et al., 2015) can provide information for these engineering systems – at resolutions around 4 km and finer. The favored approach is to telescopically nest limited-area domains at decreasing horizontal grid spacing (with the outermost boundary conditions provided by a global model) until convection-permitting scales are reached. CPMs also offer the advantage of further improving the representation of fine-scale orography and surface heterogeneity when compared to RCMs. This can be especially beneficial in highly heterogeneous regions such as the Canadian Arctic (Diro and Sushama, 2019).

The main contribution of this thesis is to advance the understanding of several different pathways through which changing climatic conditions are expected to impact engineering systems in cold regions. This advancement is accomplished by applying innovative analysis methods to an ensemble of medium-resolution climate projections and by performing and analyzing high-resolution climate projections over the Canadian Arctic for the first time.

The climate model used in this thesis is a modified version of the Global Environmental Multiscale model (GEM; Côté et al., 1998), which is used for numerical weather prediction by Environment and Climate Change Canada (ECCC) and has also been extensively used for climate modelling studies. Research occurred in two main phases (Figure 1.1):

In phase 1, large-scale studies of climate-infrastructure interaction pathways were performed, based on medium resolution GEM simulations carefully designed to capture processes relevant to infrastructure. For instance, interactive modelling of streamflows in the RCM enabled physically consistent studies of floods and use of a deep soil configuration allowed large-scale permafrost degradation to be represented realistically. An ensemble approach was employed to capture more extreme events and to improve robustness of the conclusions drawn. The use of innovative analysis methods gave rise to the following original contributions:

(1) The novel assessment of projected changes to flood-generating mechanisms in terms of the relative contribution of snowmelt and rainfall across Canada, for both a high-warming scenario and in a 2 °C global warming context. Under high-warming, hotspots of change are projected to emerge in currently snowmelt-dominated regions across Canada. These findings are presented in Chapter 3, in the form of an article published in *Water*.

(2) The novel identification and quantification of abrupt changes to many variables and processes of high significance to northern interests (e.g., convective precipitation and wildfire intensity). These abrupt changes are projected to occur as a consequence of near-surface permafrost

degradation and subsequent drying of the land surface. These findings are detailed in Chapter 4, in the form of an article published in *Nature Climate Change*.

In phase 2, engineering-scale studies of specific climate-infrastructure interactions were performed. The focus on the northern transportation sector required the development of the very first climate projection at ~4 km horizontal spacing over northern Canada to accurately capture critical small-scale hazards such as extreme precipitation, extreme wind, and predictors of fog. These studies consumed significant high-performance computing resources, in the vicinity of 500 core-years and over 100 TB of storage, to achieve the required spatial and temporal detail.

Additional original contributions resulted from advanced analysis of projected changes to extreme short-duration rainfall, extreme wind, and the development of fog diagnostics for low visibility conditions – all for the first time at engineering relevant scales. These findings are presented in Chapter 5, in the form of an article submitted to *Climate Dynamics*.

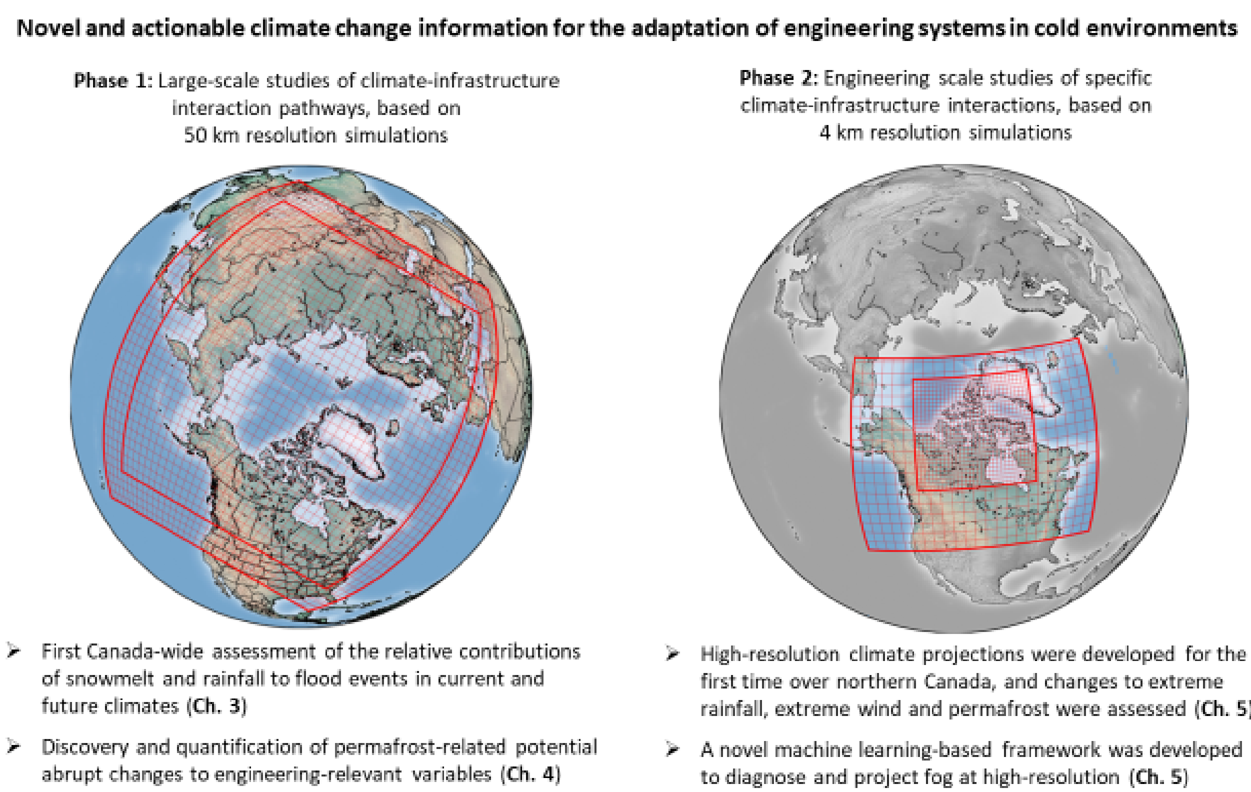

Figure 1.1. Overview of research phases, simulation/analysis domains and original contributions presented in each chapter.

1.2. Objectives

The main objective of this thesis is the generation of high-quality actionable climate change information for the adaptation of engineering systems in cold environments, with analysis focusing on hazards related to extreme events, abrupt changes and complex phenomena, for which significant knowledge gaps exist. Specific objectives leading to the accomplishment of the main objective are:

1) Assessment of the relative contributions of snowmelt and rainfall to flood events in current and future climates over Canada, as well as their influence on flood magnitudes and timings.
2) Identification of permafrost-related thresholds (tipping points), and quantification of the projected effects of crossing these thresholds, with particular emphasis on changes to variables relevant to engineering systems, such as flood predictors.
3) Development of a framework to diagnose complex climatic hazards, such as low visibility conditions, using outputs from high-resolution climate simulations, allowing these hazards to be estimated at unobserved locations and in future climate.
4) Assessment of the performance of GEM at simulating base variables and various climatic hazards at convection-permitting resolutions over northern Canada, and comparison with those derived from coarse-resolution simulations for the assessment of added value.
5) Generation of high-resolution projections of engineering-relevant climate hazards for northern Canada, including extreme short-duration rainfall, extreme wind, fog and permafrost thaw, which can have significant impacts on the northern transportation sector.

1.3. Thesis organization

In this manuscript-based thesis, Chapter 1 provides the motivation for the research, its objectives, and the main lines of the methodology. Chapter 2 presents a comprehensive literature review which identifies the knowledge gaps addressed by this thesis and explains methodological choices. Chapters 3 to 5 constitute the body of the thesis, where each of the chapters consists of an article published in or submitted to a peer-reviewed journal. The structure of each chapter follows the requirements of the respective journal. Chapter 6 summarizes the original contributions, along with insights and recommendations for future research to advance knowledge of climate-infrastructure interactions in northern environments. Supplementary material to Chapters 4 and 5 is provided in Appendices.

Chapter 2: Literature review

The first part of this chapter reviews previous studies on the variables and processes of interest for evaluating the vulnerability of engineering systems in cold regions and contextualizes the knowledge gaps addressed by this thesis. The review then proceeds to the strategies and datasets used for model validation, as any model needs to demonstrate satisfactory performance with respect to observed climate before projections of future climate can be attempted. The final part of this chapter presents concepts at the core of any climate projection, such as emission scenarios and uncertainties. Focused discussion on various concepts, diagnostics and climate model projections included here are also available in Chapters 3 to 5 that originated from the research carried out for this thesis.

2.1. Changes to hazards relevant to engineering systems in cold regions

Given the large number of pathways through which climate variability and extremes can impact different engineering systems, it becomes necessary to focus on a subset of climate impacts. In this thesis, the focus is on climatic hazards in cold regions, particularly those for which significant knowledge gaps exist, such as floods, permafrost degradation, wildfires, extreme precipitation, extreme wind and fog. Previous studies on changes to each of these hazards are reviewed, and existing knowledge gaps are highlighted.

Floods

Annual maximum streamflow is an important indicator of flood risk. Recently, Burn and Whitfield (2016) analyzed one-day maximum streamflow at 280 stations from 1961 to 2010 and concluded that 10% of hydrometric sites across Canada have shown significantly decreasing trends (i.e., lower maximum streamflow levels), while less than 4% have experienced increasing trends (i.e., higher maximum streamflow levels).

An intensification of the hydrological cycle in a future warmer climate is expected (IPCC, 2013), which is likely to impact the frequency and severity of extreme hydrological events, including floods. In Canada, fluvial flooding occurs mostly in spring due to snowmelt or due to combined rain/snowmelt events, while occasionally (mostly for southern watersheds) it can occur in summer and fall because of rainstorms (e.g., Javelle et al., 2002; Clavet-Gaumont et al., 2013). Increasing rainfall extremes over the northern mid-to-high latitudes have already been observed (Westra et al., 2013), and further intensification is projected in future climate (Mladjic et al., 2011; Monette et al., 2012; Bush et al., 2014; Khaliq et al., 2015). A warmer climate is expected to impact snowmelt events through multiple pathways: on one side, warmer temperatures favor increased snowmelt rates (Jeong and Sushama, 2018b); however, less shortwave energy is available earlier in the snowmelt season, favoring slower snowmelt (Musselman et al., 2017).

Projected changes to both rainfall and snowmelt highlight the potential for significant shifts in flood-generating mechanisms across Canada. Previous studies on the projected impact of global warming on flood generating mechanisms have suggested extensive, landscape-scale transformations. For example, large areas of the northwestern United States are projected to experience shifts from mixed-rain-and-snow to rain-dominant behaviour, along with increased flood risk by the end of the 21st century (Hamlet et al., 2013). Projections over Norway also show increasing relevance of rainfall as a flood-generating mechanism, where it is projected to replace snowmelt as the dominant mechanism for several basins (Vormoor et al., 2015).

Interactions between flood-generating factors at the basin scale lead to large uncertainties regarding the frequency and intensity of future floods (Whitfield, 2012). Projected changes to streamflow (and flooding) are often assessed using hydrological models driven by climate model outputs for various scenarios. RCMs have also been increasingly used to study projected changes to various components of the hydrological cycle, including streamflow (Kay et al., 2006; Sushama et al., 2006; Poitras et al., 2011; Clavet-Gaumont et al., 2013; Huziy et al., 2013; Jeong et al., 2014; Huziy and Sushama, 2017b, 2017a). For many basins, it is difficult to project whether flood magnitude will increase or decrease, due to significant variability among climate models (Rasmussen, 2016). The multitude of climate and hydrological models used adds further uncertainty to projections of future streamflow and flooding (e.g., IPCC, 2012).

Large knowledge gaps remain regarding projected changes to the frequency and intensity of floods in Canada, which cannot be adequately addressed by a single model, given the large variability among models. However, exploring projected changes to flood-generating mechanisms in terms of the relative contribution of snowmelt and rainfall would improve understanding of future changes to floods, and this assessment has so far not been performed across Canada. GEM includes both the atmospheric and land surface branches of the water cycle and is thus an ideal tool to better understand the linkages and feedbacks between climate and hydrological systems, and to evaluate the impact of climate change on streamflow and its generating mechanisms, which is analyzed in Chapter 3.

Permafrost degradation

Understanding current permafrost conditions and how they may evolve in response to a changing climate is essential for the assessment of climate change impacts and the development of adaptation strategies in northern Canada, given that many existing northern buildings were designed without consideration of climate change. Permafrost thaw and soil subsidence, particularly in regions with high ice content, can damage infrastructure. Geo-hazards in the form of slope failure, thaw settlement and frost heave pose significant threats to the structural integrity of infrastructure in cold regions (Li et al., 2019). Transportation networks, pipelines and building foundations have already shown signs of deterioration and failure (Government of the NTW, 2008).

Current permafrost conditions are determined largely from in situ monitoring, which results in large gaps in the spatial distribution of measurement sites because of the relative inaccessibility of large portions of northern Canada. Regional observations over the last few decades show that permafrost temperature has warmed at rates of about 0.1ºC per decade in the central Mackenzie Valley and 0.3ºC to 0.5ºC per decade in the high Arctic. Active layer thickness has increased by approximately 10% since 2000 in the Mackenzie Valley (Duchesne et al., 2015; Smith et al., 2017).

Given the strong projected warming across the northern high latitudes, substantial near-surface permafrost degradation is expected during the 21st century (Slater and Lawrence, 2013). Permafrost degradation at greater depths occurs much more slowly, but is less relevant to surface conditions (Delisle, 2007). Following a high-warming scenario, a reduction of around 80% by the end of the 21st century in near-surface permafrost area (areas with permafrost in the top 3.5 m of soil) is projected by GCMs (Koven et al., 2013; Slater and Lawrence, 2013). Future projections of permafrost remain limited given the lack of representation of processes within current climate models. Even if processes are included, validating them is often problematic due to the scarcity of actual measurements from these remote landscapes (Schuur et al., 2013).

Permafrost thaw alters soil structural and hydrologic properties, with impacts on the spatial extent of lakes and wetlands (Smith et al., 2005). As permafrost degrades, new hydraulic pathways might become available, increasing drainage (Liljedahl et al., 2016) and rapidly reducing surface soil moisture (Perreault et al., 2016). Abrupt decreases in soil moisture due to permafrost degradation were also recently first reported in climate model simulations (Avis et al., 2011; Drijfhout et al., 2015). A significant knowledge gap exists in terms of the potential effects of these abrupt changes in surface conditions on other engineering-relevant variables, which is addressed in Chapter 4.

As the degradation of permafrost is a regional phenomenon, high-resolution simulations are expected to provide more reliable projections, but need to account for feedbacks with other components of the land surface. Examples include terrain (topography, slope, aspect, geomorphology), hydrology (surface drainage, site wetness, proximity of nearby water bodies, presence of underground water, flooding), vegetation (insulation, shading and insolation, snow interception), geology (type of soil and rock, tectonic setting and geothermal heat flow), and disturbances (human, animal, and fire related). These factors operate at different timescales (days to millennia) and spatial scales (local to continental) (Osterkamp, 2007). Many of these factors are considered in GEM, and thus the high-resolution simulations in Chapter 5 are expected to improve the representation of permafrost with respect to coarser-resolution simulations and produce more reliable projections of permafrost degradation and its impacts on engineering systems.

Wildfires

Fire hazards have been identified as a major concern by many northern communities and organizations. The transportation sector is particularly at risk, as wildfires often result in the closure of road segments. In addition, wildfires and smoke considerably reduce visibility for aircrafts, which must adapt their flying methods to ensure safety (Palko and Lemmen, 2017). Permafrost is becoming increasingly vulnerable to substantial thaw and collapse after moderate to high-severity fire, and the ability of permafrost to recover is diminishing as the climate continues to warm (Brown et al., 2015).

Fire could be an important additional mechanism for releasing permafrost carbon to the atmosphere. Fire frequency and severity are increasing in some parts of the Canadian boreal permafrost zone. Thawing and fires could act together to expose and transfer permafrost carbon to the atmosphere very rapidly, especially in ecosystems with organic surface soils (Turetsky et al., 2010).

In sparsely populated regions, such as the Arctic, cloud-to-ground lightning is the process responsible for the ignition of most wildfires (Stocks et al., 2002). Veraverbeke et al. (2017) found that lightning ignitions for boreal North America have increased since 1975 and explained more than 55% of the interannual variability in burned area. Lightning frequency in boreal regions is projected to increase in future climate due to increases in convective storm activity (Krause et al., 2014), given previously found relationships between lightning and other thunderstorm-related variables, such as convective precipitation and mass flux (e.g., Magi, 2015).

In addition to lightning, combustibility of available fuel is an essential condition for the ignition and growth of wildfires. The Canadian Forest Fire Weather Index (FWI; Van Wagner, 1987) uses daily weather observations to model the combustibility of different types of forest fuels and has been shown to be successful in estimating wildfire intensity. Higher temperatures in the future will contribute to increased values of the FWI and, therefore, increased fire risk. Several studies project increases in the FWI indices and the length of the fire season in Canada in the future (e.g., de Groot et al., 2013; Flannigan et al., 2013).

Reductions in surface soil moisture (Perreault et al., 2016) due to increasing drainage in permafrost regions (Liljedahl et al., 2016) would be expected to increase fire risk. Despite the threat that wildfires pose to northern communities and ecosystems, this line of research has not been thoroughly explored nor quantified in previous studies, representing a significant knowledge gap which is addressed in Chapter 4.

Extreme precipitation

It is likely that the frequency of heavy precipitation will increase in the 21st century over many areas of the globe. Based on a range of emissions scenarios, a 1-in-20 year annual maximum daily precipitation amount is likely to become a 1-in-5 to 1-in-15 year event by the end of the 21st century in many regions (IPCC, 2012). Over Canada, Mladjic et al. (2011) projected a widespread increase in the return levels in future climate, with the largest percentage increase for the northern regions. For the 1-in-20-year return levels of 1–7-day precipitation extremes during the April to September period, increases in the 5%–12% range were found for most regions, while larger increases in the 13%–19% range were noticed for the northern regions.

Using a similar approach, Monette et al. (2012) analyzed projected changes to seasonal (May–October) single- and multiday (i.e., 1-, 2-, 3-, 5-, 7-, and 10-day) precipitation extremes for 21 Northeast Canadian watersheds using a multi-RCM ensemble available through the North American Regional Climate Change Assessment Program (NARCCAP). Projected changes to precipitation extremes were studied at the watershed/regional scale by comparing the selected return levels derived from simulations for the future 2041–70 period with those for the current 1971–2000 period, for the eight ensemble members. An increase in return levels in future climate is projected for nearly all watersheds. Return levels of 1- and 3-day precipitation extremes are associated with larger increases compared to 7-day cases. Average change for all watersheds, return periods and precipitation durations is of the order of 13%, with minimum changes in the 5 to 9% range for the southeastern watersheds, while maximum changes of the order of 16 to 18% is noted for the northern watersheds.

Khaliq et al. (2015) also used NARCCAP multi-RCM simulations to evaluate projected changes to characteristics of seasonal precipitation and rain and snow dominated daily precipitation extremes for 47 watersheds, located mainly in Alberta, Saskatchewan and Manitoba. Analysis of ensemble-averaged projected changes to 10-, 30- and 50-year return levels of rain dominated precipitation extremes for the future 2041–2070 period with respect to the current 1971–2000 period shows an increase in return levels in future climate for nearly all watersheds/regions. The majority of the ensemble members suggest significant positive changes (i.e., increases) in 10-year return levels for most of the watersheds/regions. While 30- and 50-year return levels are associated with relatively larger increases compared to 10-year return level for some parts of the study domain, the number of ensemble members that suggest significant changes reduces with increasing return period.

Since extreme short-duration rainfall is controlled by small-scale processes, it is expected to be better represented as model resolution increases. Previous studies have shown that high-resolution models perform better at reproducing the observed intensity of extreme precipitation (Wehner et al., 2010; Endo et al., 2012; Sakamoto et al., 2012). No high-resolution projections of changes to extreme rainfall currently exist over northern Canada, a knowledge gap which is addressed in Chapter 5, given that excessive rainfall can lead to flooding and damage to infrastructure.

Extreme wind

Wind load is defined as the external pressure or suction due to wind on the surface of a building or structure and varies proportional to the square of the wind speed. The National Building Code of Canada (NRCC, 2015) specifies the design wind pressure for various return periods for selected locations across Canada based on the design wind speed estimated from the Gumbel distribution fitted to the annual maximum series of hourly mean wind speed.

Near-surface intense wind speeds are caused by high momentum air being brought towards the surface. The driving phenomena associated with high-magnitude wind events (including extreme near-surface wind gusts) span many scales and include: intense extra-tropical cyclones (and frontal activity therein), boundary-layer turbulence (generated by shear due to rough/inhomogeneous terrain/land cover), deep convection and topographic-flow interactions (Letson et al., 2018).

Pryor et al. (2012) compared wind climates in eight RCM simulations from NARCCAP for the middle-twenty-first century (2041–2062) to those for the historical period (1979–2000). Over North America, no robust change was observed in the extreme wind speeds, as only 1% of grid cells indicated a consistent signal of either higher or lower values of either the 20- or 50-year return period wind speed in the future period.

Over Canada, Jeong and Sushama (2018a) noted potential increases in extreme wind speed and pressure for many grid cells over the eastern, central and Arctic regions of Canada, although these projected changes vary considerably with the driving GCM and the emission scenario. However, given that wind pressure is directly proportional to the square of the wind speed, small increases in extreme wind speed could have significant implications for design and management of buildings and structures (Jeong and Sushama, 2018a).

There is low confidence in projections of changes in extreme winds, due to relatively few studies on projected extreme winds, combined with shortcomings in the simulation of extreme winds and the different models, regions, and methods used to develop projections of this variable (IPCC, 2012). Since extreme winds are small-scale processes that are strongly influenced by local factors, they are expected to be much better represented in high-resolution simulations, resulting in more credible projections. No high-resolution projections of changes to extreme winds and associated diagnostics exist over northern Canada, a knowledge gap that is addressed in Chapter 5, allowing for the assessment of extreme wind as a potential hazard to structures and operations.

Fog

Any obstructions to visibility in the lowest 300 m of the air space restrict many smaller aircraft from flying because instrument flight rules apply. As of 2013, eight airports in the Northwest Territories did not have the navigational systems in place to assist pilots in landing during their approach. Thus, under low visibility conditions, these airports are forced to suspend operations. For example, the airport in Wekweeti, Northwest Territories, was shut down for a week in September 2011 due to dense fog (Deton' Cho Stantec, 2013).

Fog is reported as an official event if it reduces visibility to less than 1 km (ECCC, 2019). Presence of fog can be problematic for transportation (aerial, marine and terrestrial) due to its direct effects on visibility. Fog in the Arctic can form as a result of radiative cooling, advection, and strong vertical heat and moisture fluxes. Fog becomes frequent when strong temperature contrasts exist between the surface and atmosphere under weaker wind regimes. Climatologically, Arctic fog is characterized by a highly variable seasonal occurrence and strong local influences (terrain and proximity to open water), with higher frequencies in coastal regions. The frequency of fog occurrence has changed significantly in some regions of the Canadian Arctic (Hanesiak and Wang, 2005). The observed changes can be associated with many different changing processes, such as open water sources for coastal areas, temperature and humidity regimes, light winds, stability regimes, large-scale circulation patterns, etc. Despite the importance of fog for all modes of transportation, little research has been done to explain observed trends, or to attempt future projections, a knowledge gap that is addressed in Chapter 5 through the development of a novel framework to diagnose fog, using outputs from high-resolution climate model simulations.

2.2. Strategies and approaches for validation of climate models

Systematic evaluation of models through comparisons with observations is a prerequisite to applying them confidently. Climate models need to represent the observed behaviour of past climate to be considered a viable tool for future projections (IPCC, 2013). GEM has been widely used for climate research, and previous climate modelling studies have shown that the GEM model can reasonably well reproduce processes such as land-atmosphere coupling (Diro et al., 2014), lake-atmosphere interactions (Huziy and Sushama, 2017b) and snow-atmosphere coupling (Diro et al., 2018), as well as permafrost extent (Paquin and Sushama, 2014), rain-on-snow events (Jeong and Sushama, 2018b) and wind/snow loads (Jeong and Sushama, 2018a). At convection-permitting resolutions, Diro and Sushama (2019) noted that the observed temperature–extreme precipitation scaling over northern Canada is realistically reproduced by GEM, in part due to improved representation of extreme precipitation events during summer.

Whenever a climate model is applied over a new domain, at higher resolution, or for a new variable/process, it is fundamental to perform the appropriate validation on multiple aspects. Given the focus of this thesis on engineering systems, the validation datasets of interest are those based on measurements of various surface and near-surface variables. During validation, it is important to consider the spatial scales of both observed and modelled data. For instance, a point measurement (e.g., at a weather observing site) might not be representative of the average value across a medium-resolution model grid cell spanning thousands of square kilometers. Whenever possible, the observational estimate and the modelled data should be compared at roughly similar scales. This also implies that the most appropriate dataset for validation might differ between medium and high-resolution climate simulations.

The Meteorological Service of Canada (MSC) archives climatological data from all sites where official weather observations are taken. Most of these observing stations are concentrated in the southern parts of the country, while northern regions have a significantly less dense network of stations. Weather observations are taken at regular intervals (e.g., hourly, daily) and include various surface and near-surface variables of interest, such as temperature, precipitation, humidity, wind speed and direction, visibility, and the occurrence of weather phenomena such as thunderstorms, fog, blowing snow, etc.

One of the advantages of high-resolution modelled data is that it can often be directly compared to point observations that fall within the respective model grid cell, given that sub-grid scale variations are expected to be relatively small for most variables. At coarser resolutions, sub-grid scale variations are larger, and gridded datasets based on sophisticated interpolation of station observations provide a more appropriate reference for validation. These gridded datasets usually include only a subset of the observed variables (most commonly, temperature and precipitation) and their temporal frequency is generally daily or coarser. Gridded datasets covering Canada include the global Climatic Research Unit (CRU; Harris et al., 2020) monthly timeseries on a 0.5° grid (~50 km), a thin plate smoothing spline surface fitting method (ANUSPLIN; Hutchinson et al., 2009) at 10 km resolution, and the Daymet dataset, developed using truncated Gaussian interpolation (Thornton et al., 2016) at 1 km resolution.

Dynamical reanalyses are an additional tool for assessing weather and climate phenomena. They aim to produce continuous reconstructions of past atmospheric states that are consistent with all observations as well as with atmospheric physics (IPCC, 2013). Unlike real-world observations, reanalyses are uniform in space and time and provide non-observable variables, making them very valuable for model validation. Several groups are actively pursuing reanalysis development at the global scale, and many of these have produced several generations of reanalyses products (e.g., Saha et al., 2010; Dee et al., 2011; Rienecker, 2011; Hersbach et al., 2020). In addition to the global reanalyses, several regional reanalyses include Canada in their domain (e.g., Mesinger et al., 2006; Bromwich et al., 2018).

In this thesis, the ability of GEM to reproduce near-surface climate characteristics is assessed by comparing simulated fields with various observation and reanalysis datasets. The high-resolution simulations are also validated at station level against available observations. Some of the engineering-relevant variables simulated by GEM, such as permafrost and streamflow, require additional specialized datasets for their validation, which are described below.

Permafrost validation

The land surface scheme in GEM models the temperature of a number of soil layers, which can be used to infer modelled permafrost extent and active layer thickness (ALT), defined as the maximum annual thaw depth. The circum-Arctic map of permafrost and ground-ice conditions (Brown et al., 1997) is used to validate the modelled permafrost extent. In this map, permafrost is categorized as continuous (> 90% coverage), discontinuous (50–90% coverage), sporadic (10–50% coverage) and isolated (< 10% coverage). The circumpolar active layer monitoring (CALM) dataset (Brown et al., 2000) contains yearly observations of ALT at specific sites, from 1990 to present. ALT is estimated in the field using a variety of methods, including mechanical probing with steel rods, thaw tubes and interpolation from ground temperature measurements at different depths. In addition, observed permafrost temperatures for select locations in Nunavut are available in the database by Smith et al. (2013).

Streamflow validation

Streamflows are simulated interactively in GEM using a hydrological routing scheme (Soulis et al., 2000; Poitras et al., 2011). These can be validated using observed streamflows at hydrometric stations, which are recorded in the Canadian National Water Data Archive HYDAT database. Given that the focus in this thesis is on events potentially leading to flooding, both the magnitude and date of annual maximum streamflow events are validated. As GEM does not consider flow regulation, it is important to only consider HYDAT stations recording natural streamflow and having sufficient data in the validation period.

2.3. Scenarios and other uncertainties in climate projections

Scenarios are used in climate research to provide plausible descriptions of how the future may evolve with respect to a range of variables including socioeconomic change, technological change, energy and land use, and emissions of greenhouse gases (GHGs) and air pollutants. They take into account the inertia in both the socio-economic and physical systems and are designed to allow researchers to explore the long-term consequences of decisions made today. As such, scenarios help to explore the costs and benefits of climate policy (IPCC, 2013).

Scenarios are used as input for climate model runs and as a basis for assessment of possible climate impacts and mitigation options and associated costs. In this thesis, the scenarios known as Representative Concentration Pathways (RCPs; van Vuuren et al., 2011) are considered. These include: one mitigation scenario (RCP2.6) leading to very low GHG concentration levels through substantial reductions in emissions; two medium stabilization scenarios, where emissions are reduced and radiative forcing is stabilized before 2100 (RCP4.5) or after 2100 (RCP6.0); and one baseline emissions scenario (RCP8.5), characterized by increasing emissions over time leading to high GHG concentration levels.

Given the significant computational expense associated with performing climate simulations, only the RCP8.5 scenario is used for the projections developed in this thesis. This scenario is chosen as it allows the signal-to-noise ratio to be maximized and represents a 'business as usual' scenario given recent trends in GHG emissions. Moreover, the choice of RCP8.5 does not preclude the assessment of risks and impacts of climate change at lower levels of warming. For example, projections can be assessed by assuming that the 2 °C warming level is not exceeded, given ongoing efforts to "hold the increase in the global mean temperature (GMT) to well below 2 °C above pre-industrial levels" (Paris Agreement; Schleussner et al., 2016). A simple procedure allows determining the time slice with a GMT increase of 1.4 °C above reference (1986–2005) levels, given that this reference period is known to have been 0.6 °C warmer than pre-industrial levels (IPCC, 2013). Impacts at this 2 °C warming level can then be compared to impacts at higher levels of warming to highlight the potential benefits of climate change mitigation.

Projections of future climate are uncertain, first because they are dependent on scenarios of future anthropogenic and natural forcings that are uncertain, second because of incomplete understanding and imprecise models of the climate system and finally because of the existence of internal climate variability (i.e., sampling uncertainty). The relative importance of the different sources of uncertainty depends on the variable of interest, the space and time scales involved, and the lead-time of the projection (IPCC, 2013). In general, internal variability becomes more important on shorter time scales and for smaller scale variables, but remains approximately constant across the forecast horizon (Hu et al., 2012), with model and scenario uncertainty increasing over time. Due to inertia in both the socio-economic and physical systems, scenario uncertainty is relatively small for projections with short lead-times. For instance, prior to 2040 the differences in projected CO_2 concentrations between the four RCP scenarios are less than 10%.

The uncertainty associated with internal variability can be reduced by running ensembles of simulations with slightly different initial conditions, designed explicitly to represent internal variability. At the same time, these ensembles also improve the sampling of extreme events, which is important given that the impacts of climate change are often experienced more profoundly in terms of the frequency, intensity or duration of these extreme events. In the first phase of this thesis, an ensemble of five medium-resolution GEM simulations was developed to represent internal variability, which is the main basis for the findings presented in Chapters 3 and 4.

The ability of models to mimic nature is achieved by simplification choices that can vary from model to model in terms of the fundamental numeric and algorithmic structures, forms and values of parameterizations, and number and kinds of coupled processes included. Simplifications and interactions between parameterized and resolved processes induce 'errors' in models, which can have a leading-order impact on the uncertainty in climate projections (IPCC, 2013).

For instance, the horizontal resolution of most existing climate projections from GCMs and RCMs is insufficiently fine (e.g., Jacob et al., 2014) to describe important processes that rarely extend beyond a few kilometres (e.g., convective cloud systems), which are consequently approximated using parameterizations. These approximations are a significant source of uncertainty in climate simulations (Dai, 2006; Hohenegger and Brockhaus, 2008; Zhang and Song, 2010; Ban et al., 2014; Palmer, 2014; Prein et al., 2015), and lead to limited confidence in model projections of precipitation extremes and other local phenomena, which are crucial in local planning and decision-making processes.

Shorter time scale extreme events are often associated with smaller scale spatial structures and are expected to be better represented as model resolution increases. Decreasing the size of grid cells of the climate model to kilometre scale allows major convective cloud systems to be resolved explicitly and is consequently termed as convection-permitting model (CPM). Growing evidence has shown that high-resolution models perform better at reproducing the observed intensity of extreme precipitation (Wehner et al., 2010; Endo et al., 2012; Sakamoto et al., 2012). Besides explicitly resolving deep convection, CPMs also offer the advantage of improving the representation of fine-scale orography and surface heterogeneity when compared to coarser models (e.g., Lauwaet et al., 2012; Prein et al., 2013a; Prein et al., 2013b; Trusilova et al., 2013). These substantial benefits inspired the novel development of CPM projections and advanced diagnostics over the Canadian Arctic in the second phase of this thesis (i.e., Chapter 5).

Preface to Chapter 3

In this first phase of research, the focus is on flooding, which has historically caused billions of dollars in damage and is one of the main threats to infrastructure in Canada. Improved understanding of projected changes to flood magnitude and timing is sought, which is obtained through the first Canada-wide assessment of the relative contributions of snowmelt and rainfall to flood events in current and future climates. The analysis is based on a newly developed ensemble of medium-resolution transient climate change simulations performed using a state-of-the-art regional climate model, with interactive modelling of streamflows.

Chapter 3: 2 °C vs. High Warming: Transitions to Flood-Generating Mechanisms across Canada

Bernardo Teufel and Laxmi Sushama

Abstract

Fluvial flooding in Canada is often snowmelt-driven, thus occurs mostly in spring, and has caused billions of dollars in damage in the past decade alone. In a warmer climate, increasing rainfall and changing snowmelt rates could lead to significant shifts in flood-generating mechanisms. Here, projected changes to flood-generating mechanisms in terms of the relative contribution of snowmelt and rainfall are assessed across Canada, based on an ensemble of transient climate change simulations performed using a state-of-the-art regional climate model. Changes to flood-generating mechanisms are assessed for both a late 21st century, high warming (i.e., Representative Concentration Pathway 8.5) scenario, and in a 2 °C global warming context. Under 2 °C of global warming, the relative contribution of snowmelt and rainfall to streamflow peaks is projected to remain close to that of the current climate, despite slightly increased rainfall contribution. In contrast, a high warming scenario leads to widespread increases in rainfall contribution and the emergence of hotspots of change in currently snowmelt-dominated regions across Canada. In addition, several regions in southern Canada would be projected to become rainfall dominated. These contrasting projections highlight the importance of climate change mitigation, as remaining below the 2 °C global warming threshold can avoid large changes over most regions, implying a low likelihood that expensive flood adaptation measures would be necessary.

3.1. Introduction

The significance of flooding for society is evident, given that flooding frequently leads to fatalities (Ashley and Ashley, 2008; Mohanty and Simonovic, 2021) and multi-billion dollar damage (Jongman et al., 2012; Winsemius et al., 2016). Fluvial flooding, which occurs when water overflows or breaches a river's banks and then inundates the surrounding area, is responsible for a majority of the most damaging floods in Canadian history (Teufel et al., 2017; Teufel et al., 2019).

An intensification of the hydrological cycle in a future warmer climate is expected (IPCC, 2013), which is likely to impact the frequency and severity of extreme hydrological events, including flooding. In Canada, fluvial flooding occurs mostly in spring due to snowmelt or due to combined rain/snowmelt events, while occasionally (mostly for southern watersheds) it can occur in summer and fall because of rainstorms (Javelle et al., 2002; Clavet-Gaumont et al., 2013). Increasing rainfall extremes over the northern mid-to-high latitudes have already been observed (Westra et al., 2013), and further intensification is projected in future climates (Mladjic et al., 2011; Monette et al., 2012; Khaliq et al., 2015). A warmer climate is expected to impact snowmelt events through multiple pathways: on one side, warmer temperatures favor increased snowmelt rates (Jeong and Sushama, 2018b); however, less shortwave energy is available earlier in the snowmelt season, favoring slower snowmelt (Musselman et al., 2017). Projected changes to both rainfall and snowmelt highlight the potential for significant shifts in flood-generating mechanisms across Canada.

Previous studies on the projected impact of global warming on flood-generating mechanisms have suggested extensive, landscape-scale transformations. For example, large areas of the northwestern United States are projected to experience shifts from mixed-rain-and-snow to rain-dominant behaviour, along with increased flood risk by the end of the 21st century (Hamlet et al., 2013).

Projections over Norway also show the increasing relevance of rainfall as a flood-generating process, where it is projected to replace snowmelt as the dominant process for several basins (Vormoor et al., 2015). Rain-on-snow (ROS) events can trigger major floods due to the contribution of both rainfall and snowmelt, and projections over the Swiss Alps suggest that the number of ROS events could increase by close to 50% with temperatures 2–4 °C warmer than present, before declining when temperatures go beyond 4 °C of warming (Beniston and Stoffel, 2016). ROS events are an important flood-generating mechanism for most of Canada, and increases in ROS characteristics (frequency, rainfall amount, and runoff) are projected during the November to March period for most regions of Canada by 2041–2070, due to increases in rainfall (Jeong and Sushama, 2018b).

Projected changes to streamflow (and flooding) are often assessed using hydrological models driven by climate model outputs for various scenarios. Global and regional climate models (GCMs and RCMs), with their water budget including both the atmospheric and land surface branches, are ideal tools to better understand the linkages and feedbacks between climate and hydrological systems, and to evaluate the impact of climate change on streamflow and its generating mechanisms. RCMs offer higher spatial resolution than GCMs, allowing for finer-scale dynamics to be simulated, and are a more adequate tool for generating the information required for regional impact studies. RCMs have been increasingly used to study projected changes to various components of the hydrological cycle, including streamflow (Kay et al., 2006; Sushama et al., 2006; Poitras et al., 2011; Clavet-Gaumont et al., 2013; Huziy et al., 2013; Jeong et al., 2014; Huziy and Sushama, 2017b, 2017a).

While previous studies have assessed projected changes to streamflow, this is the first study to explore projected changes to flood-generating mechanisms in terms of the relative contribution of snowmelt and rainfall across Canada, based on an ensemble of transient climate change simulations performed using a state-of-the-art regional climate model. Changes to flood-generating mechanisms are assessed for both a late 21st century, high-warming scenario (i.e., the Representative Concentration Pathway 8.5—RCP8.5), and a 2 °C global warming context, highlighting the benefits of climate change mitigation and simultaneously informing adaptation measures.

The paper is organized as follows. Section 2 describes the model and simulations used for this study. Section 3 discusses the results, from the validation of streamflow in the current climate, to the evolution of flood-generating mechanisms in future climates, followed by conclusions in Section 4.

3.2. Methods

This study is based on the limited area version of the Global Environmental Multiscale (GEM) model, used for numerical weather prediction at Environment and Climate Change Canada (Côté et al., 1998). It employs semi-Lagrangian transport and a (quasi) fully implicit time-stepping scheme. In its fully elastic nonhydrostatic formulation (Yeh et al., 2002), it uses a vertical coordinate based on hydrostatic pressure (Laprise, 1992). In this study, the GEM physics package includes: deep convection following Kain and Fritsch (1990), shallow convection based on a transient version of the Kuo (1965) scheme (Belair et al., 2005), large-scale condensation (Sundqvist et al., 1989), correlated K solar and terrestrial radiation (Li and Barker, 2005), sub-grid-scale orographic gravity wave drag (Mcfarlane, 1987), low-level orographic blocking (Zadra et al., 2003), and turbulent kinetic energy closure in the planetary boundary layer and vertical diffusion (Benoit et al., 1989; Delage and Girard, 1992; Delage, 1997).

The land surface scheme used is CLASS v3.6 (Verseghy, 2011), which is permafrost-enabled as the soil model is 60 m deep and has both mineral and organic soils represented, important components of high-latitude soils (Teufel et al., 2018; Teufel and Sushama, 2019). The surface and sub-surface runoff calculated by the surface scheme are used to simulate streamflows interactively in GEM using the modified WATROUTE hydrological routing scheme (Soulis et al., 2000; Poitras et al., 2011). The routing scheme solves the water balance equation at each grid cell and relates water storage to outflow from the grid cell, using Manning's equation. The flow directions, river lengths, and slopes required by the routing scheme are derived from the HydroSHEDS database (Lehner et al., 2008), available at 30-arcsecond spatial resolution, following the upscaling method employed by Huziy et al. (2013). Sub-grid lakes are represented using FLake (Mironov, 2008).

An ensemble of five GEM simulations are performed for the 1950–2099 period over a pan-Arctic domain at 0.5° (~50 km) grid spacing, covering all areas north of 49° N and including the entirety of Canada's landmass (Figure 3.1), using a 20-min time step. Each of these simulations is driven at the boundaries by the corresponding member of the second-generation Canadian Earth System Model (CanESM2) ensemble, following the high-emissions RCP8.5 scenario. Given efforts to significantly reduce the risks and impacts of climate change by "holding the increase in the global mean temperature (GMT) to well below 2 °C above pre-industrial levels" (Paris Agreement), the simulations are also assessed by assuming that this 2 °C warming level is not exceeded (Schleussner et al., 2016). According to the Fifth Assessment Report of the Intergovernmental Panel on Climate Change (IPCC, 2013), the 1986–2005 reference period is 0.6 °C warmer than pre-industrial levels. For CanESM2 RCP8.5, the 30-year time slice with a GMT increase of 2 °C above pre-industrial levels (1.4 °C above reference levels) corresponds to the 2017–2046 period.

3.3. Results and Discussion

The results are presented in two sections. In the first, floods and their generating mechanisms in GEM are explored in the current climate and validated against observations. In the second, projected changes to flood-generating mechanisms are assessed, for both a 2 °C warmer globe, and for a high-emissions scenario.

3.3.1. Flood-Generating Mechanisms in the Current Climate

3.3.1.1. Streamflow Validation

As discussed in Section 2, the version of GEM used for this study simulates streamflow at every model time step. To focus on the performance of GEM for events potentially leading to flooding, the peak daily streamflow is selected for each year, and its magnitude and date of occurrence compared to those at hydrometric stations in the Canadian National Water Data Archive HYDAT database. A total of 747 HYDAT stations recording natural streamflow and having at least 30 years of data in the 1971–2020 period are considered for validation. Both the magnitude and date of annual maximum streamflow (AMS) events are recorded. The average date of maximum streamflow occurrence is derived using circular statistics (i.e., by mapping the days of the year on the unit circle). This date is assumed to be representative of most events at the station when at least 50% of events occur within 30 days of the average date. The magnitude of the 1 in 10-year event is approximated by the 90th percentile, and its magnitude normalized by the median event, giving a measure of the variability of streamflow at each station.

Figure 3.2 shows that GEM captures all the major rivers in Canada, and the timing of peak streamflow appears reasonable, generally occurring earlier for the warmer southern regions and later farther north. In some regions of central Canada (shown in grey), the average timing of peak streamflow is very variable, suggesting that more than one mechanism could lead to flooding in this region. As in observations, GEM suggests that streamflow in the Prairie region is more variable from year to year than for rest of Canada. Direct comparison at HYDAT stations where drainage area is within 20% of the value used in GEM reveals that GEM underestimates the median AMS by around 30%, and the AMS occurs on average 6 days later in GEM, for the median station. Compared to similar studies, it can be said that GEM is able to reasonably capture the magnitude, the timing, and the variability of peak streamflow with respect to observations over most regions.

3.3.1.2. Flood-Generating Mechanisms

Given that the two processes contributing virtually all liquid water at the surface are snowmelt and rainfall, any streamflow peak can be traced back to these two components, after considering delays in surface and groundwater transport. These delays also imply that an extended period of snowmelt and/or rainfall is required to generate a notable streamflow peak, at least at the scales considered in this study, which exclude flash flooding.

The analysis of flood-generating mechanisms in the current climate (1981–2010) focuses on the 150 largest streamflow events (30 years times 5 ensemble members) at each grid point. To ensure that these events are independent, a minimum 90-day separation between events is enforced. It is hypothesized that each of these events is caused by snowmelt, rainfall, or both, falling over the upstream contributing basin prior to the event. To take into account some of the hydrological characteristics of each basin, varying moving windows for accumulation of rainfall and snowmelt (from 1 to 90 days), and varying delays between the accumulation window and the date of maximum streamflow (also from 1 to 90 days) are considered at each grid point. The accumulation window and delay that best explain the variability in streamflow are chosen on the basis of the maximum correlation coefficient between accumulated snowmelt/rainfall and streamflow for the

150 events. To establish the relative contribution of snowmelt and rainfall, it suffices to compare the contribution of each over the accumulation window at each location.

Figure 3.3 shows that the amount of snowmelt/rainfall falling over the contributing basin is strongly correlated with the magnitude of the corresponding ensuing streamflow event. The value of the correlation coefficient is close to one over some parts of the high Arctic, where permafrost forces hydrological processes to occur very close to the land surface. Lower correlations over central Canada again suggest multiple flood-generating mechanisms over this region, with potentially varying accumulation windows and delays. Figure 3.3 also shows the relative contribution of snowmelt and rainfall to streamflow events. As expected, both snowmelt and rainfall contribute significantly to flood generation over most of Canada, with warmer regions having slightly more rainfall contribution. Over northern Canada, as well as the western mountain ranges, the snowmelt contribution exceeds (often significantly) the rainfall contribution.

3.3.1.3. Intense Floods

Given that higher streamflows are more likely to lead to flooding, it should be assessed whether the relative contribution of rainfall and snowmelt varies with the magnitude of the streamflow event. To assess whether 1 in 10-year events behave differently, the average relative contribution is calculated using only the 15 largest events (instead of 150). Figure 3.4 shows that, over many regions, the largest events are characterized by decreased rainfall contribution (i.e., increased snowmelt contribution). Interestingly, this also occurs along the course of several large rivers (e.g., Mackenzie).

3.3.2. Projected Changes to Flood-Generating Mechanisms

3.3.2.1. Projected Changes to Streamflow

As discussed in Section 1, a warmer climate is expected to impact streamflow events through multiple pathways, including changes to rainfall, snow accumulation, and melt rates, as well as evapotranspiration and infiltration rates. Figure 3.5 shows that GEM projects both increases and decreases in median annual maximum streamflow over Canada, with the strongest relative increases projected for the high Arctic (where both snowmelt and rainfall are projected to increase significantly), while large regions of central and western Canada are projected to experience decreases in peak streamflow. The date of occurrence of peak streamflow is projected to become earlier in spring over virtually all regions where such a projection can be made (Figure 3.5), as a consequence of earlier snowmelt. The year-to-year variability in streamflow is not projected to change significantly over most regions (not shown). Under a 2 °C warming, changes are projected to be relatively small, with most regions projected to stay within 10% in magnitude and 15 days in timing of peak streamflow. In contrast, following a high-emissions scenario leads to significant changes in streamflow magnitude over large regions, and shifts of up to 2 months in the average date of occurrence of peak streamflow, thereby increasing the likelihood that adaptation measures would be required.

3.3.2.2. Transitions to Flood-Generating Mechanisms

Figure 3.6 shows that the amount of snowmelt/rainfall falling over the contributing basin is projected to remain strongly correlated with the magnitude of the corresponding ensuing streamflow event in a warmer climate, with spatial patterns resembling those seen in Figure 3.3 and discussed in Section 3.1.2. Under 2 °C of global warming, the relative contribution of snowmelt and rainfall to streamflow peaks is projected to remain close to the 1981–2010 reference period, with some projected increases in rainfall contribution over Ontario and southern Quebec (Figure 3.6), but both components remain close in magnitude. In contrast, following a high-emissions scenario leads to generally higher rainfall contributions over Canada and the emergence of hotspots of change over central Nunavut, Nunavik, the west coast, and northern Ontario, where rainfall contribution is projected to significantly alter the currently snowmelt-dominated regime, as well as the southern Prairies, where rainfall is projected to become the dominant factor. In addition, warmer regions such as Vancouver Island, southern Ontario, and parts of the Maritimes are also projected to become rainfall-dominated.

3.4. Conclusions

The implications of the projections presented in Section 3 vary depending on the region and the vulnerability of natural and built systems in the region. Increased peak streamflow, as projected for several regions, has the direct implication of increased flood risk. Decreased peak streamflow, while positive from the flooding perspective, hints at potential decreases in total streamflow, which has important implications for freshwater resources. The same can be said for shifts in streamflow distribution throughout the year, linked to shifts in the average date of peak streamflow, which additionally have implications for flow regulation plans in the affected regions.

Like most previous RCM-based studies on flooding, this study uses high streamflow (or discharge) as a proxy for flooding, which constitutes a good approximation under the assumption of a fixed stage–discharge relationship. However, extreme flooding in Canadian rivers is frequently the result of ice jams (de Rham et al., 2020), particularly for north-flowing rivers, with water levels for a given discharge greatly exceeding those occurring under open-water conditions, due to the well-known hydraulic effects of ice on flow conveyance. Given warming temperatures, the probability of mid-winter ice jams is likely to increase across many regions, constituting a major threat to riverside communities and infrastructure (Beltaos, 2002; Beltaos et al., 2003). Simulations of projected changes to river ice and ice jam mechanisms are thus needed and are currently being implemented in models.

While the ~50 km grid spacing used in this study is sufficient for the identification of potential hotspots of change at regional scales, higher resolution is required for assessing impacts at local scales. This would also allow studying flash flooding in smaller basins, which might increase in a warmer climate, given the significant projected increases in short-duration rainfall (Oh and Sushama, 2020). Site-specific impact studies can be performed with the aid of hydrodynamic models, which can explicitly simulate inundation area and flood depths, and are often used to provide flood-risk mapping (Teng et al., 2017). The flow boundary conditions required for mapping purposes could be taken from high-resolution RCM simulations of streamflow.

Author Contributions

Conceptualization, L.S. and B.T.; methodology, L.S. and B.T.; formal analysis, B.T.; investigation, B.T.; resources, L.S.; writing—original draft preparation, B.T.; writing—review and editing, L.S.; visualization, B.T.; supervision, L.S.; funding acquisition, L.S. All authors have read and agreed to the published version of the manuscript.

Funding

This research was funded by the Trottier Institute for Sustainability in Engineering and Design (TISED) and the Natural Sciences and Engineering Research Council of Canada (NSERC).

Acknowledgments

The GEM simulations considered in this study were performed on supercomputers managed by Calcul Québec and Compute Canada.

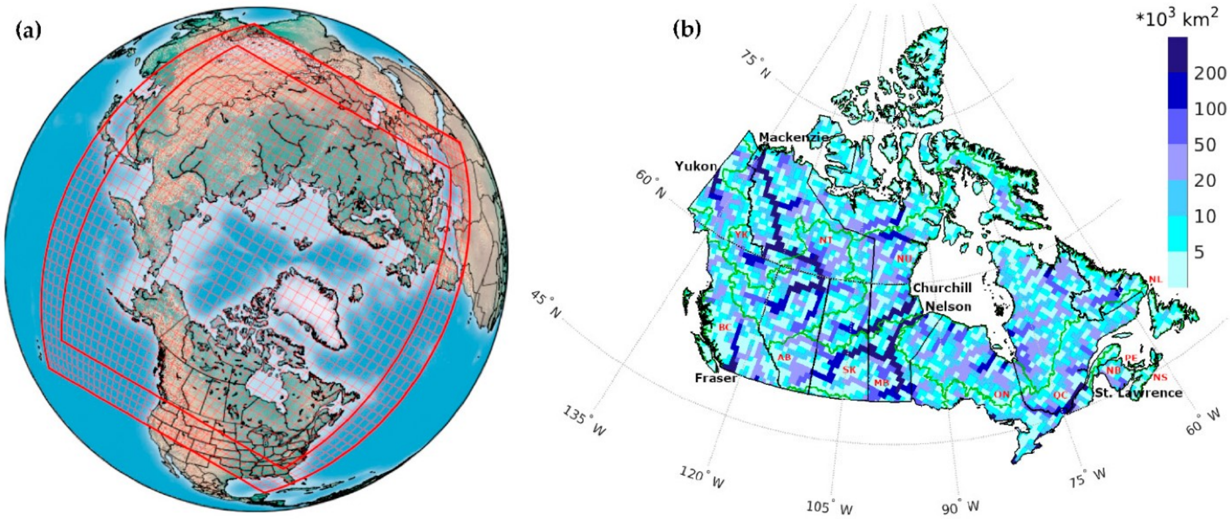

Figure 3.1. (a) Experimental domain of Global Environmental Multiscale (GEM) simulations, with every fifth grid point shown. The outer thick lines represent the full domain, while the inner thick lines represent the free domain. (b) Upstream drainage area over the analysis domain. Major rivers are named near their outlet. Black lines show the boundaries of Canadian provinces and territories, named with their two letter codes. Green lines show the boundaries of major drainage areas as defined by Water Survey of Canada.

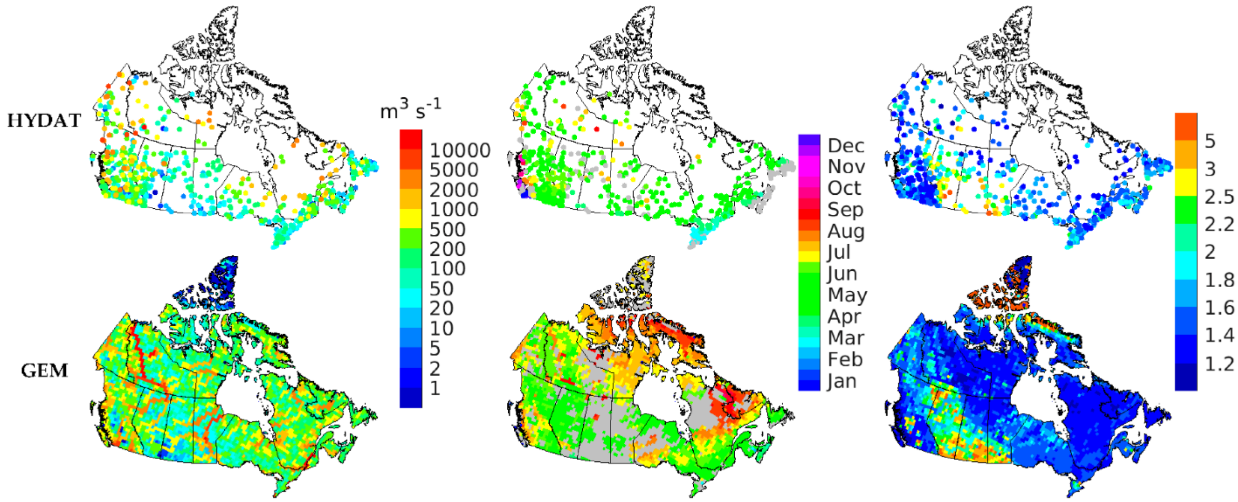

Figure 3.2. Median annual maximum streamflow (first column), its average date of occurrence (second column), and ratio between 1 in 10-year and median annual maximum streamflow (third column), for the 1971–2020 period, from HYDAT (top row) and GEM (bottom row). Grey is used for the date at locations where less than 50% of annual maximum events occur within 30 days of the average date. Where multiple HYDAT observations overlap, the one with the highest streamflow is shown on top.

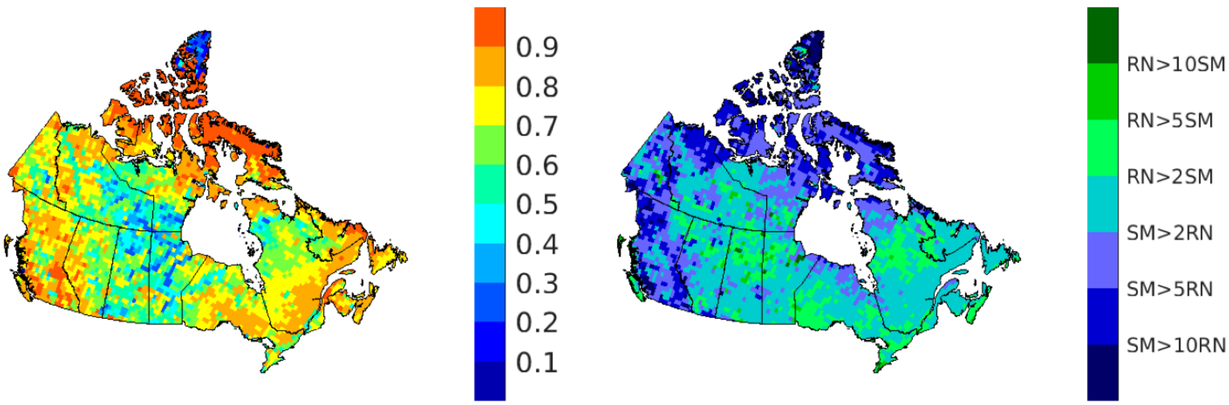

Figure 3.3. Correlation coefficient between streamflow and accumulated snowmelt/rainfall upstream of respective grid cell in GEM for the 150 largest streamflow events during the 1981–2010 period (left). Relative average snowmelt (SM) and rainfall (RN) contribution during those events (right).

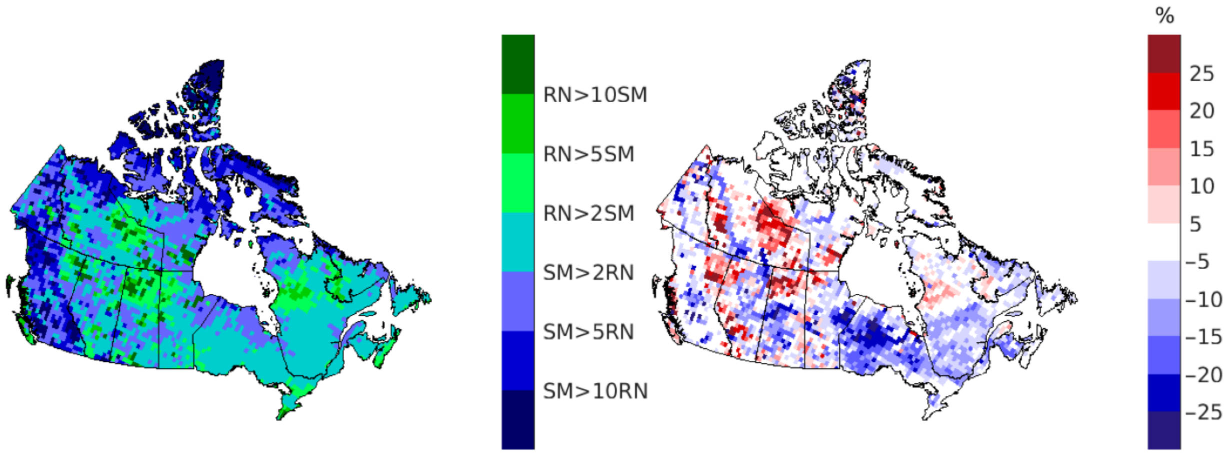

Figure 3.4. Relative average snowmelt and rainfall contribution in GEM for the 15 largest streamflow events during the 1981–2010 period (left). Difference in rainfall contribution with respect to the average rainfall contribution during the 150 largest streamflow events (right).

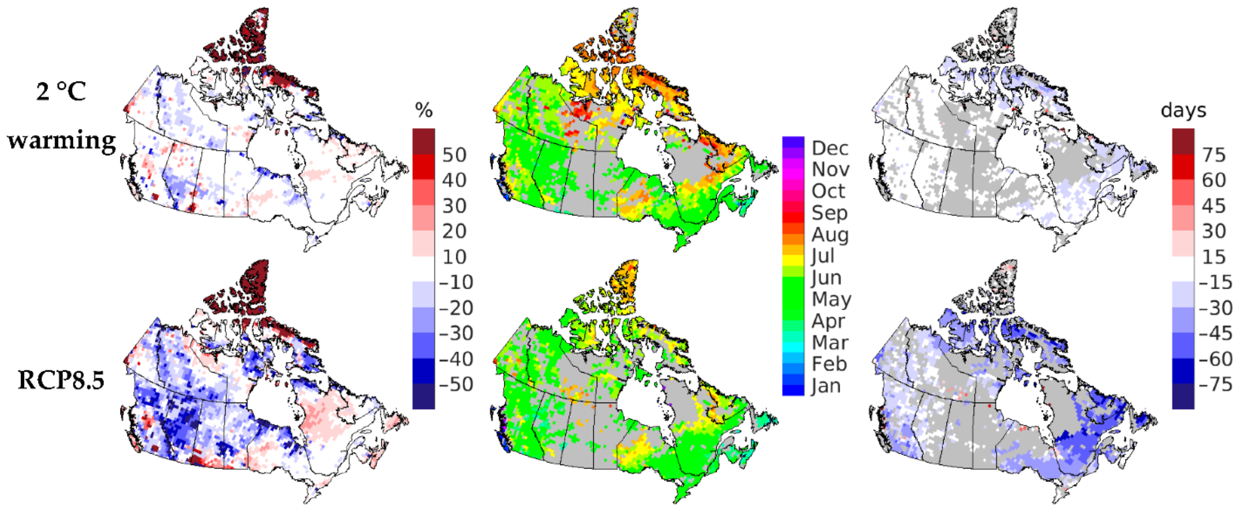

Figure 3.5. Projected changes to median annual maximum streamflow with respect to 1981–2010 (first column), projected average date of occurrence of annual maximum streamflow (second column), and its projected changes with respect to 1981–2010 (third column). Projections for both 2 °C warming (top row) and RCP8.5 2070–2099 (bottom row) are shown. Grey is used for the date at locations where less than 50% of annual maximum events occur within 30 days of the average date.

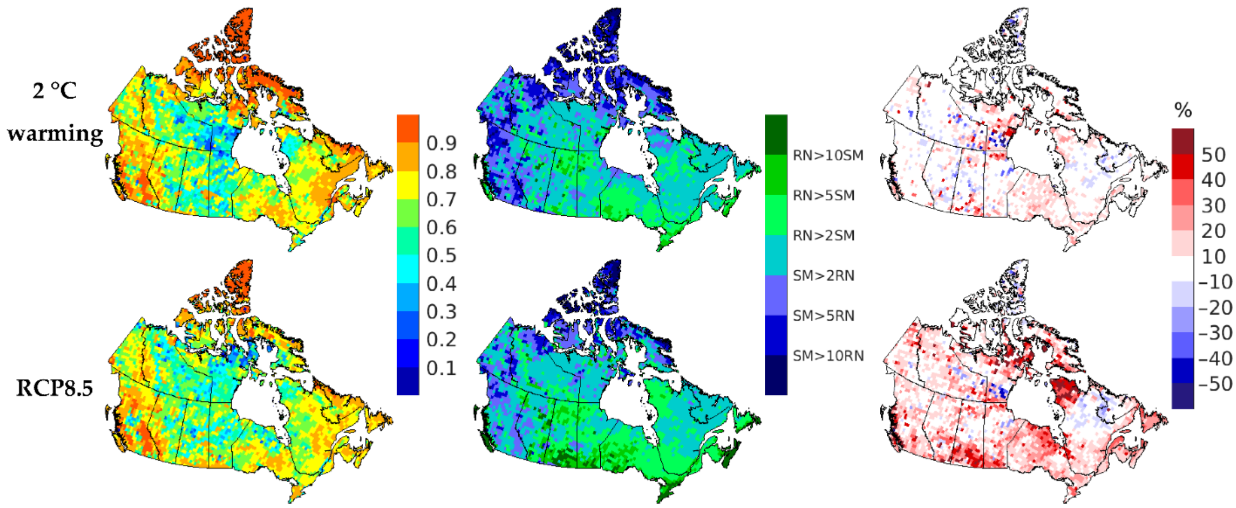

Figure 3.6. Correlation coefficient between streamflow and accumulated snowmelt/rainfall upstream of respective grid cell in GEM for the 150 largest streamflow events (first column), relative average snowmelt and rainfall contribution during those events (second column), and projected changes to the rainfall contribution during those events with respect to 1981–2010 (third column). Projections for both 2 °C warming (top row) and RCP8.5 2070–2099 (bottom row) are shown.

Preface to Chapter 4

In Chapter 3, the largest projected changes to flood magnitude were seen over northern regions of Canada, due to projected increases to both rainfall and snowmelt. This motivated further analysis over these regions, focusing on the role of permafrost degradation on regional hydrology, specifically on the transition between surface and subsurface flows, which were hypothesized to have a significant influence on flood regimes. Chapter 4 explores this line of research, which ultimately demonstrated changes to flood regimes, but also resulted in the discovery of the possibility of abrupt changes to many other variables relevant to northern engineering systems.

Chapter 4: Abrupt changes across the Arctic permafrost region endanger northern development

Bernardo Teufel and Laxmi Sushama

Abstract

Extensive degradation of near-surface permafrost is projected during the twenty-first century (Koven et al., 2013), which will have detrimental effects on northern communities, ecosystems and engineering systems. This degradation is predicted to have consequences for many processes, which previous modelling studies have suggested would occur gradually. Here we project that soil moisture will decrease abruptly (within a few months) in response to permafrost degradation over large areas of the present-day permafrost region, based on analysis of transient climate change simulations performed using a state-of-the-art regional climate model. This regime shift is reflected in abrupt increases in summer near-surface temperature and convective precipitation, and decreases in relative humidity and surface runoff. Of particular relevance to northern systems are changes to the bearing capacity of the soil due to increased drainage, increases in the potential for intense rainfall events and increases in lightning frequency. Combined with increases in forest fuel combustibility, these are projected to abruptly and substantially increase the severity of wildfires, which constitute one of the greatest risks to northern ecosystems, communities and infrastructures. The fact that these changes are projected to occur abruptly further increases the challenges associated with climate change adaptation and potential retrofitting measures.

4.1. Main

The pan-Arctic permafrost region is expected to warm at least at twice the global average during the twenty-first century (Miller et al., 2010), resulting in substantial near-surface permafrost degradation and thaw-depth deepening, with specific projections depending on the underlying climate forcing scenario and model physics (Koven et al., 2013). Given that permafrost acts as an impermeable barrier to soil water movement (Woo et al., 2008), the deepening of the annual thaw depth has important implications for the hydraulic behaviour of soils. In regions with the permafrost table close to the surface, hydrological processes are confined close to the surface and the water storage capacity of soils is small, meaning that available liquid water (from precipitation and/or snowmelt) has a strong influence on the soil moisture content closest to the surface. In regions with a deep permafrost table, the water storage capacity of soils is larger, often resulting in drier surface soil layers as water is stored at greater depths (White et al., 2007; Jorgenson et al., 2013). The timing of the transition between these regimes as near-surface permafrost degrades due to rising temperatures has received little attention in past modelling studies. Field observations have shown that additional hydraulic pathways might become available as permafrost degrades, increasing drainage (Liljedahl et al., 2016) and rapidly reducing surface soil moisture (Perreault et al., 2016). Abrupt decreases in soil moisture due to permafrost degradation were only recently first reported in climate model simulations (Avis et al., 2011; Drijfhout et al., 2015). The implications of abrupt changes are significant for northern communities and for the built environment (Lenton, 2012). Although the importance of incorporating climate change information in their decision-making process has gained recognition in recent years, often only mean projected changes and smooth trends are considered, ignoring the potential for abrupt climatic shifts.

Analysis of an ensemble of five pan-Arctic realizations performed using the limited area version of the Global Environmental Multiscale (GEM) model for the Representative Concentration Pathway 8.5 (RCP8.5) reveals that for a region covering around 4.4 million km^2 of the present-day permafrost area, an abrupt decrease in soil moisture occurs during the year in which permafrost degrades enough to stop acting as a hydraulic barrier. This abrupt decrease, described here for the first time, marks the transition between two soil moisture regimes (Fig. 4.1a). The years before this abrupt change are characterized by soil moisture near saturation, while the years following the change are characterized by much drier soils, with the median grid cell losing around 34% of its vertically integrated soil moisture-interquartile range (IQR) of 28 to 41%. Soil moisture values for the dry regime are generally outside the range of interannual variability of the wet regime and these low values persist until the end of the climate simulation (that is, the end of the twenty-first century). Figure 4.1b shows the regions affected by these abrupt changes and their timings, and Fig. 4.1c shows the relative magnitude of the decrease in soil moisture at each grid cell. Northern ecosystems will probably be disrupted by this abrupt decrease in soil water availability (Wrona et al., 2016), impacting high-latitude carbon emissions (Lawrence et al., 2015). In addition, these abrupt changes will modify the bearing capacity of the soil, conditional on site-level soil properties and foundation characteristics, leading to potentially catastrophic situations for infrastructure (Streletskiy et al., 2012). Given the abruptness of this change and that it is expected to occur with little or no warning, adaptation measures would need to be made very quickly to minimize impact.

Given that annual frost depth and thaw depth vary from year to year as a function of near-surface climate, it is possible for soil ice to again act as a hydraulic barrier in the years after permafrost first degraded, resulting in a transition period where soil moisture varies between high and low values, as shown in Fig. 4.1a (lower panel). The median duration of this transition period at each grid cell is shown in Fig. 4.1d. Slightly more than one-third of the modelled transitions occur within 1 year, while the other two-thirds occur over an average of 15 years (IQR: 8–25 years). In regions where the permeable soil is deep, soil moisture is unlikely to return to its original range from the wet regime because replenishment often takes years and the possibility of permafrost being present decreases as temperature increases.

River flows in these northern regions are generally dominated by snowmelt during spring. Given that the soil is considerably less saturated and thaws faster after the abrupt decrease in soil moisture, a large fraction of the snowmelt is projected to infiltrate under the drier regime, rather than reach the streams as surface runoff. GEM projections suggest an abrupt decrease of about 62% in surface runoff due to the regime shift (Fig. 4.2a), which implies that the magnitude of the streamflow peak is expected to decrease because the water that infiltrates is released gradually from the soil into the rivers, which also suggests a delay in peak streamflow. These changes point towards a reduction in flood risk during the snowmelt period but, because streamflow is projected to be higher during the warm season (due to the gradual release of snowmelt water from soils), the risk of flooding due to heavy rainfall events will probably increase. Furthermore, the serviceability of ice roads might be abruptly and negatively impacted by the increased groundwater release expected during the cold season because it would result in increased water temperatures and reduced ice cover. The assessment of these changes to streamflow is complicated by the fact that permafrost does not degrade at the same time over an entire river basin, meaning that there is usually a transition period of decades between the two regimes, at least for large basins.

The previously described abrupt decrease in soil moisture is also clearly reflected in the annual cycle of surface soil moisture. Figure 4.2b shows that in the years preceding the abrupt decrease, surface soil moisture stays near saturation during the cold season, decreasing to about two-thirds of saturation during the warm season, resembling the overall behaviour seen in present-day permafrost regions4. The year of the abrupt decrease is characterized by surface soil moisture that stays below saturation after the warm season is over. This pattern persists for the years after the decrease, with the yearly cycle of surface soil moisture characterized by a peak during snowmelt, followed by a much more pronounced decrease during the warm season and a slow recovery during autumn and winter. In both regimes, there is a gradual increase in the duration and magnitude of the warm-season decrease driven by increasing evapotranspiration as temperatures increase.

During the warm season surface soil moisture controls the partitioning of the turbulent heat flux between sensible heat and latent heat, modifies the surface thermal conductivity and can also influence surface albedo. Figure 4.3a shows that the abrupt decrease in surface soil moisture during summer is about 29% for the median grid cell (IQR: 23–32%). In the eastern part of northern Canada, where mineral soils predominate, this abrupt decrease in surface soil moisture results in an increase to surface albedo, leading to cooler near-surface temperatures and reduced turbulent fluxes after permafrost degrades. In all other regions, an abrupt decrease in summer ground heat flux due to the lower thermal conductivity of drier organic soils is the dominant process (Fig. 4.3b), resulting in warmer near-surface soils and an increase in the sensible heat flux (Fig. 4.3c).

In regions where regime change favours warmer near-surface soils, atmospheric stability abruptly decreases due to the warmer surface layer. This results in increased convective precipitation during the summer months (10% for the median grid cell showing an increase), and is accompanied by a decrease in large-scale precipitation, which appears to indicate a shift in precipitation producing processes. This shift from large-scale to convective precipitation results in an increase in intense short-duration precipitation events (Fig. 4.3d).

This abrupt increase in convective precipitation is expected to result in an abrupt increase in lightning frequency (Fig. 4.3e), based on previously found relationships between lightning and other thunderstorm-related variables, such as convective precipitation and mass flux (Magi, 2015). In sparsely populated regions, such as the Arctic, cloud-to-ground lightning is the process responsible for the ignition of most wildfires (Stocks et al., 2002), which are a major concern for the safety of northern communities and infrastructure (McGee et al., 2015). An abrupt increase in ignition events would further endanger northern ecosystems and development.

In addition to lightning, combustibility of available fuel is an essential condition for the ignition and growth of wildfires. The Canadian Forest Fire Weather Index (FWI; Van Wagner, 1987) uses daily weather observations to model the combustibility of different types of forest fuels and has been shown to be successful in estimating wildfire intensity—if ignition occurs. Here the FWI and its associated daily severity rating (DSR) are computed from GEM outputs. Results show that the abrupt decrease in soil moisture has a strong influence on the combustibility of fuels, which undergoes an abrupt increase that results in similarly abrupt increases in the FWI and DSR (Fig. 4.3f).

One region where the increase in fire danger is projected to be particularly large is northwestern Canada (Fig. 4.4a). This region of approximately 220,000 km^2 is projected to experience an abrupt ~100% increase in potential fire severity as permafrost degrades (Fig. 4.4b). This region is characterized by one of the largest abrupt decreases in summer relative humidity (3%) due to permafrost degradation (Fig. 4.4c), which appears to be the main driver for the abrupt increase in the DSR, given that the rest of the FWI variables only show modest changes (temperature, Fig. 4.4d) or no abrupt change at all (precipitation and wind speed, Fig. 4.4e,f). This is consistent with previous studies (Lawson and Armitage, 2008) that show that the FWI is most sensitive to changes in humidity.

Permafrost hydrology is complex and a number of processes are not yet included in climate models, including lateral soil heat and moisture transport, soil subsidence, erosion, subpermafrost aquifers and evolving water bodies (for example, thermokarst lakes). In addition to the uncertainties introduced by these unresolved processes, projected changes to the vegetative cover and its water-use efficiency are also likely to influence soil moisture. Due to the large influence that geomorphology has on the occurrence, timing and consequences of the abrupt changes described earlier, it is essential to obtain reliable estimates of geomorphological parameters (for example, depth to bedrock), which are currently poorly constrained by observations. To provide actionable information on abrupt changes to the climate adaptation and engineering communities, climate simulations will need to be performed at convection-permitting scales (Prein et al., 2015). Additional benefits obtained from high-resolution simulations would include a better understanding of changes to intense short-duration rainfall events because the convective processes involved would be resolved rather than parameterized.

The implications of the abrupt changes identified in the present study are important for northern communities and engineering projects. For example, the abrupt changes in soil moisture presented in this study have major implications for the stability of structures and roads. These changes are also expected to influence flooding hazards through changes in river flow regimes. Diverse feedback processes result in permafrost degradation abruptly increasing the risk of intense precipitation, lightning frequency and fire severity, each of which poses unique threats to vulnerable northern ecosystems and human activities. This study highlights the importance of going beyond mean projected changes and smooth trends when making decisions on climate change adaptation, given the potential of abrupt climatic shifts occurring throughout the twenty-first century.

It is important to highlight that the occurrence of these abrupt changes in GEM (see Methods) is conditional on permafrost degradation, which could be prevented by limiting global warming. For example, by the time global warming reaches the 2.0 °C threshold(Schleussner et al., 2016) in the driving climate model (around the year 2031), only 42% of the permafrost degradation leading to abrupt changes is projected to occur. Also significant is the fact that the likelihood of abrupt changes depends on the rate of temperature increase (that is, the RCP followed), meaning that a slower rate of warming would probably result in transition periods longer than those shown in Fig. 4.1d, allowing for additional time for adaptation and mitigation measures. However, it should be noted that this study explores abrupt changes until the year 2070, which corresponds to about 4.0 °C global warming in the driving climate model. If global warming crosses this threshold, an additional 2.2 million km2 of the Arctic (shown dark blue in Fig. 4.1b) would be at risk of experiencing abrupt changes linked to permafrost degradation and their consequences.

4.2. Methods

4.2.1. Model

This study is based on the limited area version of the GEM model, which is used for numerical weather prediction at Environment and Climate Change Canada (Côté et al., 1998). A description of the parameterizations used is provided in a previous study (Teufel et al., 2017). The land surface scheme used is CLASS v.3.6 (Verseghy, 2011), which makes a distinction between permeable and impermeable soil (not present in most other land surface models), meaning that hydrological calculations are performed only for the permeable soil layers. To accurately represent permafrost extent, a 60-m deep soil profile is used (Teufel et al., 2018). The thickness of the soil layers in this profile is distributed as follows, starting from the surface: 0.1, 0.2, 0.3, 0.4, 0.5 m (10 layers), 1.0, 3.0 and 5.0 m (10 layers). To obtain initial conditions for the state of the soil, a 500-year spin-up is performed using CLASS driven by repeating atmospheric fields for the 1979–1988 period from the ERA-Interim reanalysis (Dee et al., 2011).

In CLASS, the percentages of sand and clay in each soil layer determine their hydraulic and thermal properties. For this study, soil composition is obtained by upscaling the high-resolution Harmonized World Soil Database (HWSD; Nachtergaele et al., 2012). Depth to the bedrock is also obtained from a high-resolution dataset (Pelletier et al., 2016). Due to the distinct thermal and hydraulic properties of organic soils, these are treated differently from mineral soils in CLASS. This enables the model to represent the rapid decrease of hydraulic conductivity with depth in organic soils (Letts et al., 2000). For grid cells covered mostly by histosols in the HWSD, all soil layers above the bedrock are considered organic. To account for organic matter within mineral soils, soil carbon density from the HWSD is used to classify each soil type into having zero, one (10 cm) or two layers (30 cm) of organic matter at the surface. Each grid cell is then assigned its most representative number of organic soil layers (Teufel et al., 2018).

An ensemble of five GEM simulations were performed for the 1950–2099 period over a pan-Arctic domain at 0.5° resolution covering all areas north of 49° N. The vertical discretization is set at 56 vertical levels and the model top is near 10 hPa. Each of these simulations is driven at the boundaries by the corresponding member of the second-generation Canadian Earth System Model (CanESM2) ensemble for the RCP8.5, which allows the signal-to-noise ratio to be maximized and represents a realistic 'business as usual' scenario for recent trends in greenhouse gas emissions.

4.2.2. Change point detection

Many techniques for discontinuity detection (for example, the Pettitt change point test (Pettitt, 1979)) make the implicit (but often erroneous) assumption that any long-term change must be attributed to a discontinuity. Change point analysis in the present work is inspired by a recently developed method (Bowman et al., 2006), which allows for the presence of both smooth trends and abrupt changes in a timeseries, enabling discrimination between the two. This data-driven approach evaluates the evidence for discontinuities without assuming that the underlying regression function takes a specific functional form (for example, linearity, piecewise linearity or step functions) (Bates et al., 2012).

The detection of change points in the chosen approach rests on the comparison of two smooth estimates of the regression function, one constructed from data before the time of interest and the other constructed from data after the time of interest. If there is a discontinuity in the regression function near the time of interest then this difference will be large; however, if the function is continuous near the time of interest the difference will be small. The parameter controlling the smoothness of the regression function is selected using a version of the Akaike information criterion (Hurvich et al., 1998). To assess whether there is enough evidence to support the existence of a change point, the corrected Akaike information criterion is compared to one of a regression function constructed from the entirety of the data (that is, without change point).

The first 20 years (1950–1969) of each GEM realization are discarded to allow for spin-up. Change point analysis is first limited to grid cells with the presence of permafrost in any of the hydrologically active soil layers at any point in the simulation. Permafrost is defined here as soil layer temperatures remaining at or below 0 °C for at least two consecutive years. Each of the grid cells described above is screened for the presence of a period of at least 30 consecutive years (starting in 1970) where permafrost acts as a hydraulic barrier. Grid cells where permafrost degradation causes the first disappearance of this hydraulic barrier at the latest by 2070 (to allow for a second 30-year period) are the final candidates for change point analysis. Grid cells with perennial snow cover are eliminated by considering only cells where the annual minimum snow mass is zero for each of the 30 years preceding the change point. The above procedure is performed separately for each GEM simulation.

Although change points can be reliably detected at the grid cell level for some variables, such as vertically integrated soil moisture, most variables exhibit considerable interannual variability (noise for the purposes of this analysis), which masks the presence of change points (signal). To increase the signal-to-noise ratio, data are aggregated across GEM realizations and neighbouring grid cells using an 11 × 11 grid centred on the grid cell of interest. Averaging is performed for 60 consecutive years (the 30 years before and after permafrost degradation for each grid cell and realization) and each grid cell is weighed by the fraction of land area it contributes to the total. Change point analysis is performed on the resulting 60-year timeseries for each grid cell.

Given that the year in which permafrost degrades is generally characterized by warm and wet conditions during summer (see Appendix A), it often constitutes an outlier with the potential to introduce bias in the magnitude of the abrupt change estimates. For this reason, data for the year of permafrost degradation are excluded from the construction of these estimates.

Acknowledgements

This research was funded by the Natural Sciences and Engineering Research Council of Canada (grant no. RGPIN-2019-05238), the Trottier Institute for Sustainability in Engineering and Design and the McGill Sustainability Systems Initiative. The GEM simulations in this study were performed on supercomputers managed by Calcul Québec and Compute Canada.

Contributions

B.T. and L.S. designed the study and analysis. B.T. performed the climate model simulations, analysed the data and wrote the manuscript. Both authors contributed to interpreting the results and made substantial improvements to the manuscript.

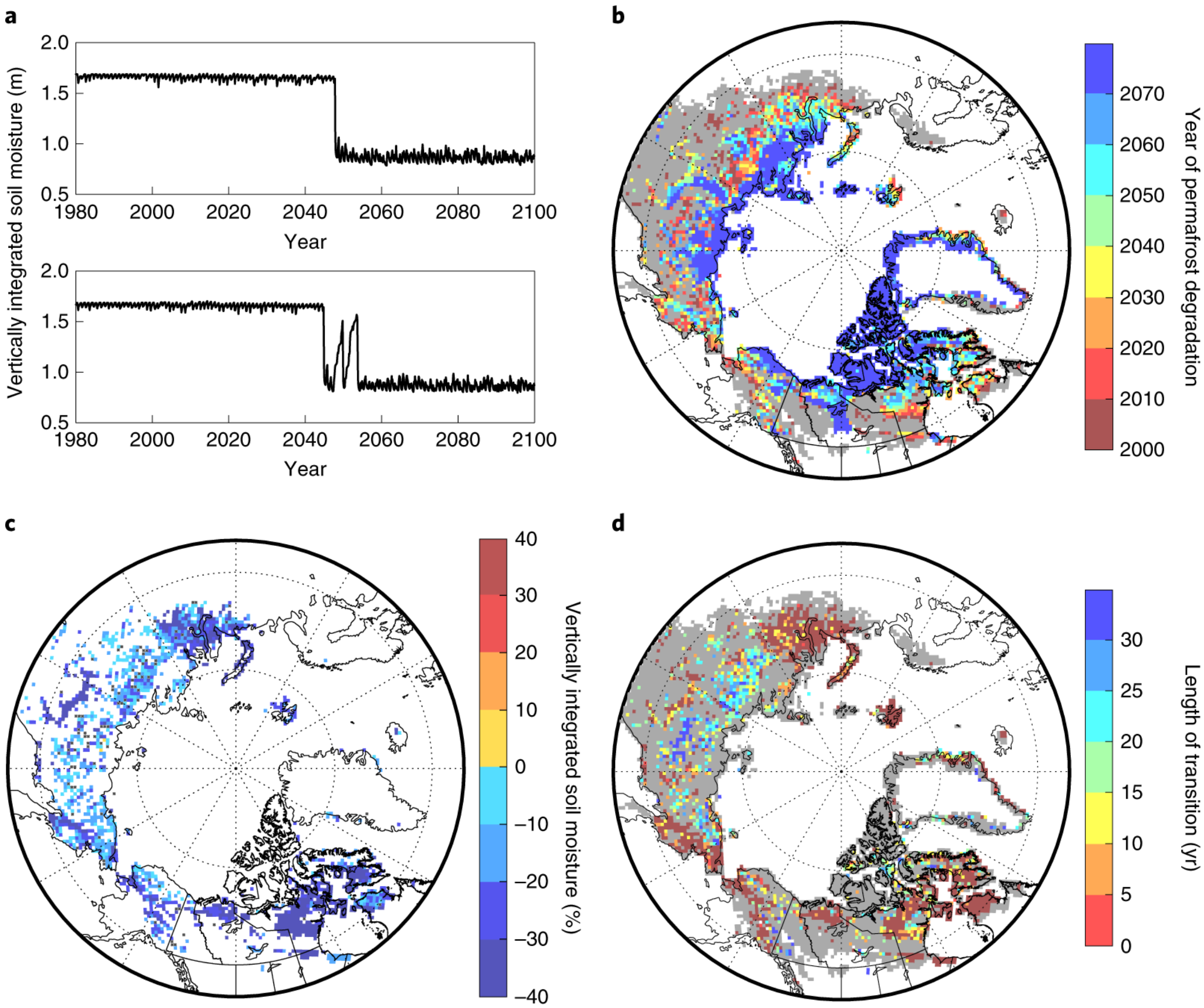

Figure 4.1: Timing and magnitude of abrupt changes in soil moisture. a, Monthly evolution of vertically integrated soil moisture for a typical grid cell undergoing abrupt changes. Regime shifts with both short and long transitions are shown. b, Median year in which permafrost first stops acting as a hydraulic barrier, if before 2070. c, Relative magnitude of abrupt changes in summer (June, July, August, JJA) vertically integrated soil moisture. d, Median length of the transition between the frozen and thawed regimes. Grey shading in b and d indicates the modelled maximum near-surface (5 m) permafrost extent. Grey markers in c are used where there is no evidence of an abrupt change (see Methods).

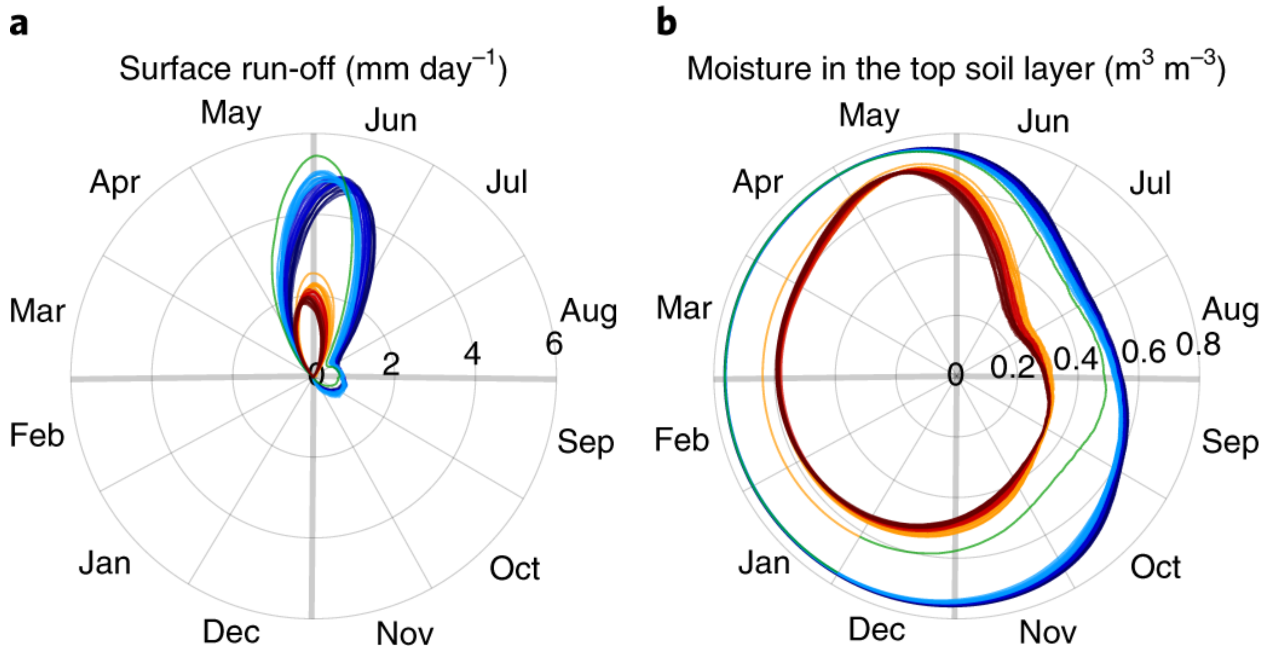

Figure 4.2: Abrupt changes in annual cycles. a,b, Evolution of the annual cycle of 15-d surface runoff (a) and 3-hourly moisture in the top soil layer (0–10 cm, b) aggregated across all grid cells where the hydraulic barrier associated with permafrost degraded abruptly during the 2000–2070 period. The 30 years preceding permafrost degradation are shown in blue, with the darkest blue corresponding to the earliest decade. The year of permafrost degradation is shown in green and the 29 years after permafrost degradation are shown in red, with the darkest red corresponding to the latest decade.

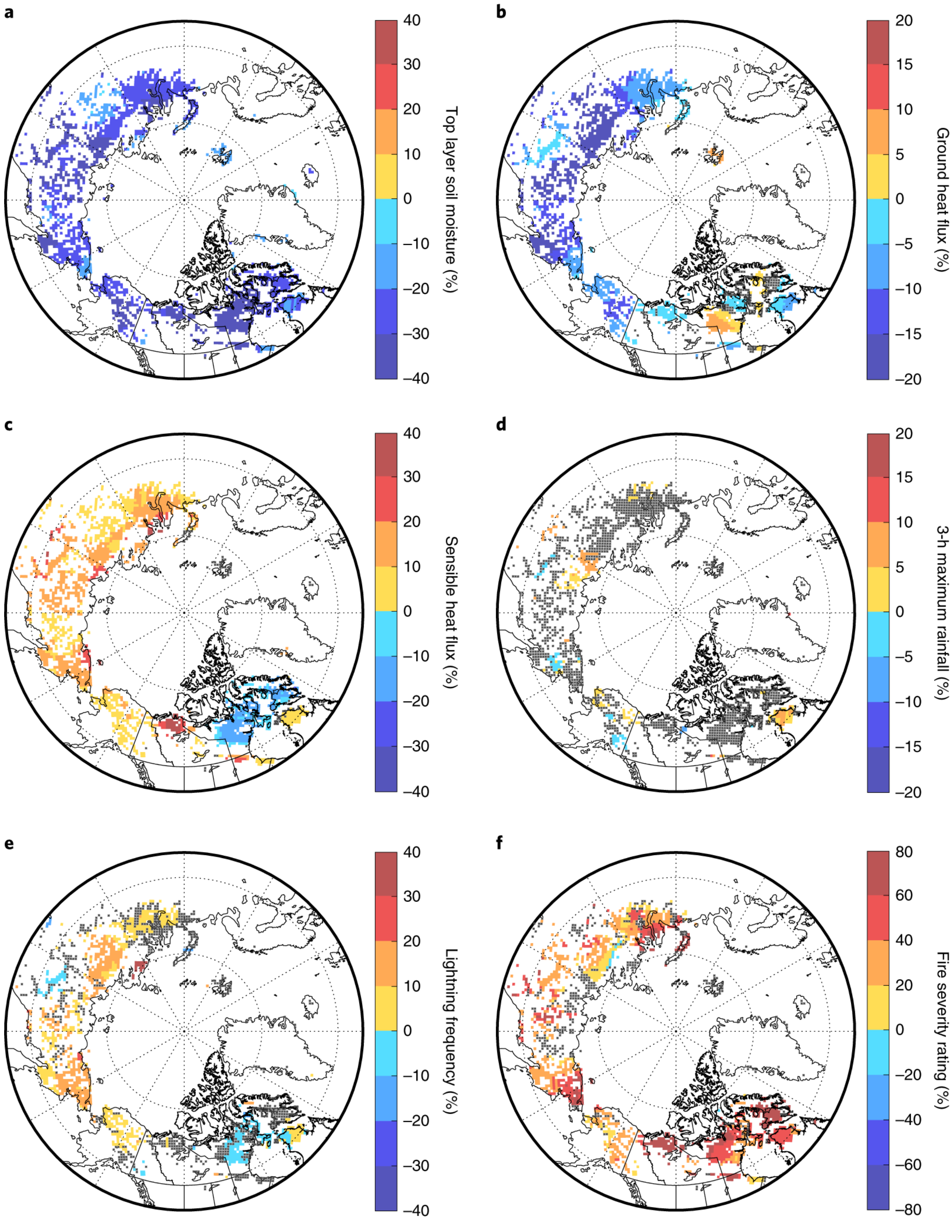
a
Top layer soil moisture (%)
40
30
20
10
0
−10
−20
−30
−40
b
Ground heat flux (%)
20
15
10
5
0
−5
−10
−15
−20
c
Sensible heat flux (%)
40
30
20
10
0
−10
−20
−30
−40
d
3-h maximum rainfall (%)
20
15
10
5
0
−5
−10
−15
−20
e
Lightning frequency (%)
40
30
20
10
0
−10
−20
−30
−40
f
Fire severity rating (%)
80
60
40
20
0
−20
−40
−60
−80

Figure 4.3: Abrupt changes in land and atmosphere processes. a–f, Relative magnitude of abrupt changes due to permafrost degradation in summer (JJA) moisture in the top soil layer (0–10 cm, a), summer ground heat flux (downwards, b), summer sensible heat flux (upwards, c), annual maximum 3-h rainfall (d), summer lightning frequency (e) and annual fire severity rating (f). Changes are shown as percentages with respect to the regression estimate before the abrupt change. Grey markers are used when there is no evidence of an abrupt change (see Methods).

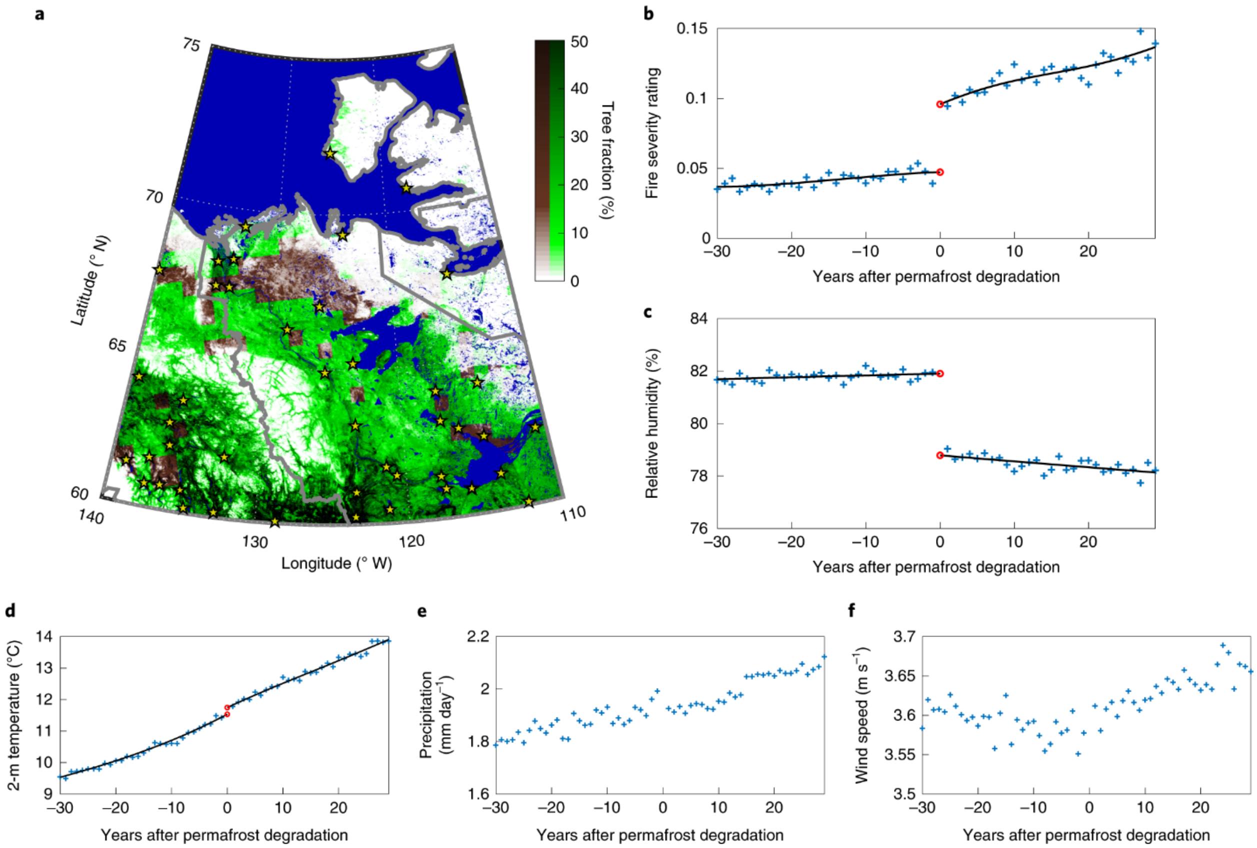

Figure 4.4: Abrupt changes in fire severity and its drivers. a, Tree fraction from MODIS (Moderate Resolution Imaging Spectroradiometer) over northwestern Canada, shown in brown where abrupt increases in fire severity are projected to occur and green otherwise. Communities are shown with yellow stars and water bodies in blue. b–f, Evolution of fire weather variables aggregated across grid cells shown in brown in a; annual fire severity rating (b), summer average (JJA) relative humidity at noon (c), JJA 2-m temperature at noon (d), JJA total precipitation (e) and JJA wind speed at noon (f). Modelled values are shown with blue markers and regression estimates with black lines, while red markers indicate abrupt changes.

Preface to Chapter 5

The research in Chapters 3 and 4 resulted in novel discoveries which addressed significant knowledge gaps, but was in some aspects limited by the relatively coarse resolution of the climate simulations analyzed. Chapter 5 is based on high-resolution simulations and projections, which were developed for the first time over northern Canada. Given the novelty of these simulations, the first part of Chapter 5 focuses on assessing their performance against observations and coarser resolution simulations. The second part of Chapter 5 analyzes projected changes to various hazards to northern transportation, for the first time at engineering-relevant scales.

One of these hazards is fog, which is a complex variable that has been proven to be difficult to accurately simulate. Chapter 5 also presents the development, validation and application of a novel machine learning-based framework to diagnose this complex variable, using outputs from high-resolution climate simulations, with the goal of allowing fog occurrence to be estimated at unobserved locations and also in future climate.

Chapter 5: High-resolution modelling of climatic hazards relevant for the northern transportation sector

Bernardo Teufel and Laxmi Sushama

Abstract

Infrastructure and transportation systems on which northern communities rely are exposed to a variety of climatic hazards over a broad range of scales. Efforts to adapt these systems to the rapidly warming Arctic climate require high-quality climate projections. Here, a state-of-the-art regional climate model is used to perform simulations at 4-km resolution over the eastern and central Canadian Arctic. These include, for the first time over this region, high-resolution climate projections extending to the year 2040. Validation shows that the model adequately simulates base climate variables, as well as variables hazardous to northern engineering and transportation systems, such as degrading permafrost, extreme rainfall, and extreme wind gust. Added value is found against coarser resolution simulations. A novel approach integrating climate model output and machine learning is used for deriving fog – an important, but complex hazard. Hotspots of change to climatic hazards over the next two decades (2021-2040) are identified. These include increases to short-duration rainfall intensity extremes exceeding 50%, suggesting Super–Clausius–Clapeyron scaling. Increases to extreme wind gust pressure are projected to reach 25% over some regions, while widespread increases in active layer thickness and ground temperature are expected. Overall fog frequency is projected to increase by around 10% over most of the study region by 2040, due to increasing frequency of high humidity conditions. Given that these changes are projected to be already underway, urgent action is required to successfully adapt northern transportation and engineering systems located in regions where the magnitude of hazards is projected to increase.

5.1. Introduction

Northern communities are feeling the pressures of climate change, as temperatures in the Arctic have markedly increased in recent decades, impacting the built and natural environments. Since the Arctic is expected to continue to warm at more than twice the global average rate and considering the vulnerability of the infrastructure and transportation systems on which northern communities rely, efforts to adapt these systems to the changing climate require high-quality climate projections.

The horizontal resolution of most existing climate projections from global and regional climate models (GCMs and RCMs) is insufficiently fine (e.g., Jacob et al., 2014) to describe important processes that rarely extend beyond a few kilometres (e.g., convective cloud systems), which are consequently approximated using parameterizations. These approximations are the main source of errors and uncertainties in climate simulations (Dai, 2006; Hohenegger and Brockhaus, 2008; Zhang and Song, 2010; Ban et al., 2014; Palmer, 2014; Prein et al., 2015), and lead to limited confidence in model projections of precipitation extremes and other local phenomena, which are crucial in local planning and decision-making processes.

Shorter time scale extreme events are often associated with smaller scale spatial structures and are expected to be better represented as model resolution increases. For example, it is known from sensitivity studies that simulated extreme precipitation is strongly dependent on model resolution. Growing evidence has shown that high-resolution models perform better at reproducing the observed intensity of extreme precipitation (Wehner et al., 2010; Endo et al., 2012; Sakamoto et al., 2012).

Decreasing the size of grid cells of the climate model to kilometre scale allows major convective cloud systems to be resolved explicitly and is consequently termed as convection-permitting model (CPM). Besides explicitly resolving deep convection, CPMs also offer the advantage of further improving the representation of fine-scale orography and surface heterogeneity when compared to coarser RCMs (e.g., Lauwaet et al., 2012; Prein et al., 2013a; Prein et al., 2013b; Trusilova et al., 2013). Limited-area modelling is the approach most frequently used for CPM climate simulations. This approach telescopically nests limited-area domains at decreasing horizontal resolution until convection-permitting scales are reached (e.g., Prein et al., 2013b). CPM climate simulations are able to provide spatial data on scales that are small enough to derive impact-relevant information (Zhang et al., 2017).

Diro and Sushama (2019) carried out a five-year simulation for a Canadian Arctic domain covering Nunavut for the first time at 3 km grid spacing (i.e., at convection permitting resolutions) using the limited-area version of the Global Environmental Multiscale model (GEM; Côté et al., 1998). They noted substantial improvements; the representation of extreme precipitation events during summer and the simulation of winter temperatures are better captured at 3 km compared to simulations for example at 12 km grid spacing (Diro and Sushama, 2019). Moreover, the observed temperature–extreme precipitation scaling is realistically reproduced by the higher resolution simulation.

In this study, both reanalysis-driven and GCM-driven CPM simulations are performed at 4 km grid spacing over the eastern and central Canadian Arctic. These include, for the first time over this region, CPM climate projections extending to the year 2040. The analysis focuses on variables that are expected to benefit from high-resolution and are also crucial to northern engineering and transportation systems, such as permafrost, extreme rainfall, extreme wind gust and fog. Given that fog is not directly simulated, a novel approach integrating climate model output and machine learning algorithms is used to diagnose and project fog occurrence.

The paper is organized as follows: Section 2 describes the model, simulations, and methods. Section 3 deals with model evaluation. Projected changes to climate hazards are presented in Section 4. Finally, discussion and conclusions are presented in Section 5.

5.2. Model and methods

5.2.1. Climate model and simulations

GEM solves non-hydrostatic, deep atmosphere dynamics with an implicit, two-time-level semi-Lagrangian numerical scheme. In the horizontal, the model uses a regular latitude–longitude grid with Arakawa C staggering and a rotated pole configuration such that the domain is approximately centered on the equator, in order to minimize changes in grid spacing across the domain. In the vertical coordinate, Charney–Phillips staggering is used, following Girard et al. (2014). The radiation scheme is represented by Correlated K solar and terrestrial radiation of Li and Barker (2005) and the planetary boundary layer scheme follows Benoit et al. (1989) and Delage (1997). The scheme employed for condensation processes is the double-moment microphysics scheme of Milbrandt and Yau (2005). In addition to the large-scale precipitation schemes, the model includes the deep convection scheme of Kain and Fritsch (1990) and the shallow convection based on Belair et al. (2005). It must be noted that the use of convection parameterization for ~3–8 km grid spacing is still a topic of debate and considered a grey zone as convection is neither fully resolved nor can it be assumed to be smaller than the grid box spacing (Gerard et al., 2009). The thresholds used for the convection schemes are those of Diro and Sushama (2019), which account for the high resolution of the simulations.

Land processes in the model are represented using the Canadian Land-Surface Scheme (CLASS) version 3.5 (Verseghy, 2011). This scheme includes prognostic equations for energy and water conservation and allows for a flexible number of ground layers and thicknesses. Given the importance of permafrost in the study domain (Teufel and Sushama, 2019), a 60-m deep configuration is used for all GEM simulations, consisting of 26 layers, which are distributed as follows, starting from the surface: 0.1, 0.2, 0.3, 0.4, 0.5 m (10 layers), 1.0, 3.0 and 5.0 m (10 layers). To obtain adequate initial conditions for the state of the ground, a 500-year spin-up is performed using CLASS driven by repeating atmospheric fields for the 1979–1988 period from the ERA-Interim reanalysis (Dee et al., 2011).

Figure 5.1a shows the model domain, with the inner domain covering Nunavut and the Northwest Territories (NWT), at 4 km grid spacing. The simulation driven by 'perfect boundary conditions', ERA5 reanalysis (Hersbach et al., 2020) in this case, spans the 1989-2010 period, and is hereafter referred to as GEM4_ERA5. The climate change simulation spanning the 1989–2040 period is driven by the Canadian Earth System Model (CanESM2; Arora et al., 2011) for Representative Concentration Pathway 8.5 (RCP8.5; Riahi et al., 2011). When driven by CanESM2, GEM simulations are first performed over the outer 10 km grid spacing domain shown in Figure 5.1a, the outputs of which are used as lateral boundary conditions for the ultra-high resolution GEM simulation over the inner domain at 4 km horizontal grid spacing. The simulation period was chosen to maximize the usefulness of the projections by focusing on hazards in the near-term future and was also constrained by limited computational resources and storage space.

To help assess the added value of high-resolution modelling, an existing reanalysis-driven (i.e., ERA-Interim) GEM simulation at 50 km grid spacing is also considered in this study (hereafter, GEM50_ERA). Though the GEM simulation at 50 km covers a pan-Arctic domain, the analysis is focused over the smaller domain covering Nunavut and NWT (Figure 5.1a), over which the 4 km simulations are performed.

5.2.2. Methods

Comparison of GEM4_ERA5 and GEM50_ERA with available observations will help assess the ability of the model in simulating current climate (1991-2010), and the added value of the high-resolution simulations. Projected changes will be assessed by comparing the future (2021-2040) and current periods of the high-resolution GEM simulations driven by CanESM2. In this study, model validation and assessment of projected changes are undertaken for a set of climate variables related to terrestrial and aerial northern transportation.

The road network in NWT consists of 2,200 km of all-weather roads and at least 2,195 km of winter roads (Palko and Lemmen, 2017). In contrast, no communities in Nunavut are interconnected by road. In both territories, the air sector plays a significant role and serves as the only year-round link between many northern communities and southern Canada (Figure 5.1b). Numerous environmental variables have the potential to impact northern transportation, such as air temperature, frost, freeze-thaw cycles, precipitation (rainfall, snowfall, freezing rain), soil temperature and moisture conditions (including permafrost), wind and visibility. In this study, the focus is on select climatic hazards: (1) extreme rainfall, which can lead to flooding and washing out of roads, bridges, and runways; (2) extreme wind, which can interrupt operations and damage infrastructure; (3) fog, which may impede aircraft take-off and landing; and (4) permafrost degradation, which threatens the structural integrity of roadways and runways. All these hazards are the result of small-scale processes and/or are strongly influenced by local factors, which are expected to be much better represented in high-resolution simulations.

In this study, a two-step process is used for validation. Base variables, such as annual and seasonal air temperature and precipitation, are validated first. Validation then proceeds to transportation related hazards, such as extreme rainfall, extreme wind gust, fog, and permafrost. Validation is achieved by comparing simulations with station observations, gridded observation datasets such as Daymet (Thornton et al., 2016) and reanalysis products such as the Arctic System Reanalysis (Bromwich et al., 2018). To facilitate comparison, higher resolution gridded data is aggregated, while lower resolution gridded data is linearly interpolated to the GEM4_ERA5 grid. Site observations are directly compared to the simulated values for the grid cell in which the observing station is located.

Daymet is a 1 km horizontal resolution dataset derived from daily observations of near-surface maximum and minimum air temperature and precipitation at weather stations. At unobserved locations, the Daymet algorithm uses a combination of interpolation and extrapolation, using inputs from multiple weather stations and weights that reflect the spatial and temporal relationships between a Daymet grid cell and the surrounding weather stations. Daymet also provides station-level cross validation data that offers insights into the regional accuracy of its algorithm. The protocol is to withhold data for one station at a time and generate a prediction for the withheld station using data from neighboring stations. Large deviations from the withheld data suggest poor accuracy for the region, and vice versa.

For extreme rainfall, extreme wind gust and fog, validation is achieved by directly comparing simulation data with station observations, given that they represent the best (and often the only) source of information regarding these variables. Over the analysis domain, a total of 243 sites reported hourly observations during the 1991-2010 period according to the archives kept by Environment and Climate Change Canada (ECCC), although each variable of interest was recorded only at a fraction of these sites – only 17 sites measured rainfall,.71 sites reported fog and 123 sites had wind gust data. For all variables, only those sites with at least 10 years of data were considered.

The GEM model employs a physical approach to estimate wind gusts following Brasseur (2001). This approach assumes that the surface wind gust occurs from the deflection of air particles flowing higher in the boundary layer, which are transported by turbulent eddies to the surface. At ECCC stations, wind gust is the maximum instantaneous reading from the anemometer. The duration of a gust typically corresponds to an elapsed time of 3 to 5 seconds. Stations only report wind gusts exceeding 30 km/h.

Some of the physical processes leading to fog formation are difficult to capture by climate models, and thus statistical techniques have been used for diagnosing the occurrence of fog (Bocchieri et al., 1974; Pasini et al., 2001; Fabbian et al., 2007; Menut et al., 2014). In this study, fog is diagnosed using decision trees – a predictive machine learning algorithm that is able to learn the complex relationships between observed fog occurrence and associated meteorological conditions, here modelled by GEM4_ERA5. Hourly fog occurrence (yes or no) observations from the 71 stations in the domain reporting fog for at least 10 years in the 1991-2010 period are used to train the model. The training dataset consists of 7,287,115 observations of which 373,728 are positive for fog, resulting in an average fog occurrence rate close to 5%.

Fog can form due to radiative cooling, advection, and strong vertical heat and moisture fluxes. Climatologically, fog in Arctic Canada is characterized by highly variable seasonal occurrence and strong local influences by terrain and proximity to open water (Hanesiak and Wang, 2005). To capture the various mechanisms of fog formation, the following GEM variables are included in the training dataset as predictors at the time and location of each observation: 2-m relative humidity, 2-m temperature, snowpack mass, 10-m wind components (u and v) and 10-m wind gust speed. In addition, 10-m wind components computed along the NW-SE and the NE-SW axes are included to allow for advection along further directions. The minimum 2-m relative humidity on a 3x3 grid centered on the location of interest is included to provide additional differentiation during near-saturation conditions. Local solar time (0 to 23 h) and the month of the year (1 to 12) are included as well.

Given the importance of surface conditions, terrain and open water, the time-invariant site characteristics considered are elevation above sea level, elevation with respect to the surrounding 3x3 grid, soil depth, soil organic matter (yes or no), ocean fraction, lake fraction, water fraction (ocean plus lake) and glacier fraction. The water fraction of each neighbouring cell (for advection) and the maximum glacier, ocean and water fraction on the surrounding 3x3 grid are also included in the training dataset. In summary, a total of 30 predictors are considered, of which 19 are time-invariant, but serve the purpose of allowing the estimation of fog at unobserved locations.

Starting from the full set of observations, the decision tree (DT) algorithm recursively splits the observations into groups, considering all possible values for each predictor and selecting the split that maximizes the reduction in mean square error (MSE) at each step. If the number of observations per group gets too small, overfitting due to spurious splits tends to occur. To avoid overfitting, cross-validation is performed by randomly dividing the training dataset into 10 folds and then repeatedly using 90% of the data for training models that predict each of the remaining 10%. The choice of minimum observations per group (i.e., leaf size) that achieves the lowest Brier score (i.e., MSE) during cross-validation is selected to train the model used for climate projections (for this study, the optimal minimum leaf size is 192). The relative importance of each predictor is shown on Figure B3.

Estimates of permafrost extent are generally obtained from field surveys. For this study, the map from Brown et al. (1997) is used to validate the modelled permafrost extent. In this map, permafrost is categorized as continuous (> 90% coverage), discontinuous (50–90% coverage), sporadic (10–50% coverage) and isolated (< 10% coverage). In this study, a grid cell is said to contain near-surface permafrost when the modelled temperature of at least one soil layer in the top 5 m remains at or below 0 °C for 24 consecutive months. Further validation is performed by comparing simulated and observed values of active layer thickness (ALT), where ALT is defined as the maximum annual thaw depth. The circumpolar active layer monitoring (CALM) dataset from Brown et al. (2000) contains yearly observations of ALT at specific sites, starting from 1990. ALT is estimated in the field using a variety of methods, including mechanical probing with steel rods, thaw tubes and interpolation from ground temperature measurements at different depths. In the model, the ALT for a particular year is assumed to be the depth to the top of the soil layer closest to the surface with maximum temperature at or below 0 °C during the year under consideration. Observed permafrost temperatures for select locations in Nunavut are available in the database by Smith et al. (2013), and are compared to GEM-simulated permafrost temperatures.

5.3. Validation

5.3.1. Air temperature

During the summer season, average 2-m air temperatures over most of the study domain vary between 0 and 20 °C, while during winter, average temperatures of -15 to -35 °C are the norm. Figure 5.2 shows that GEM4_ERA5 captures the diurnal and seasonal temperature variability in the Daymet dataset and the underlying station data. For daily maximum temperature, GEM has little to no bias on the annual scale, except for a slight cold bias (1-2 °C) over parts of the NWT. For winter, most of the domain has close to zero bias, except for a warm bias of around 2 °C over the high Arctic, while for summer, GEM has a cold bias of 2 to 4 °C over most of the domain. This bias is similar to the one found by Diro and Sushama (2019) in their 5-year 3-km resolution GEM simulation over Nunavut.

The performance for daily minimum temperature is even better, again with little (< 2 °C) to no bias on the annual scale for most of the domain. During the winter season, warm bias is present for the high Arctic and cold bias is present for parts of Baffin Island. During the summer season, slight cold bias (1-2 °C) occurs over Nunavut, while the southwestern corner of the domain presents some warm bias. In summary, GEM temperatures are close to those of Daymet, which itself performs well (i.e., biases below 2 °C) at estimating temperatures at most stations in the domain during cross-validation (see Section 2.2 for details). When compared directly to site observations, while summer daily maximum temperature is underestimated by GEM, all other biases at most stations are below 2 °C. Additionally, GEM4_ERA5 improves on GEM50_ERA (Figure B1) in terms of the magnitude and spatial extent of temperature biases on both annual and seasonal scales, and for both maximum and minimum temperatures. This represents a first example of the added value of the high-resolution simulations.

5.3.2. Precipitation

Precipitation has much greater spatiotemporal variability than air temperature and is consequently more challenging to accurately estimate at unobserved locations. For example, a significant number of stations in Daymet exhibit relatively large biases (> 20%) during cross-validation, implying that Daymet is likely to have large biases at some unobserved locations and is thus not an ideal reference dataset. To improve the assessment of precipitation in GEM, the Arctic System Reanalysis (ASR) at 15 km horizontal resolution is considered as an alternative reference.

In both Daymet and ASR, regions near the western, eastern, and southern boundaries of the domain receive more precipitation than interior and northern regions (Figure 5.3). In both datasets, precipitation is significantly more abundant during summer than during winter. These features are well captured by GEM4_ERA5, despite the presence of some biases. During all seasons, GEM presents a wet bias over the high Arctic, which is more moderate against ASR than Daymet. It should be noted that Daymet exhibits large biases during cross-validation at most stations over this region, suggesting that ASR might be a more suitable reference. In particular, the extension of the wet bias towards the interior NWT-Nunavut border in Daymet is not supported by site observations nor ASR.

GEM also presents some moderate dry biases against both references towards the western and southern boundaries of the domain. These occur due to the difference in horizontal resolution between the driving dataset (ERA5) and GEM, as air parcels entering the domain at the western boundary are too homogeneous in terms of water vapour saturation, resulting in less precipitation being produced near the edge of the domain. Once far enough (~200 km) from the edge, this effect disappears, and GEM presents little to no bias. This explanation is supported by the absence of this effect along the southern edge during the winter season, as the predominant flow is from the north, meaning that few parcels enter from the south.

GEM-simulated precipitation is also directly compared to site observations (Figure 5.3), with most stations in Nunavut suggesting a moderate wet bias in accordance with ASR, while most stations in NWT indicate excellent performance of GEM, with little to no bias over this region for all seasons. Added value of GEM4_ERA5 over GEM50_ERA (Figure B2) can be noted over southeastern Nunavut in winter and near the Arctic coast in summer.

5.3.3. Extreme short-duration rainfall

At each observation site (Figure 5.4, top panel), the annual maximum rainfall intensity for durations from 1 to 24 hours is fitted by the GEV distribution using the method of L-moments, and the intensity of the 1 in 10-year event is calculated. The observed and modelled maximum hourly rainfall intensities range from below 10 mm/h (over northern regions) to over 20 mm/h (over southern regions). For all observation sites in the analysis domain, GEM4_ERA5 significantly outperforms GEM50_ERA in simulating extreme rainfall intensity (Figure 5.4, bottom panel), especially at shorter durations (3 hours and below) associated with the heaviest rainfall rates. This is a very clear example of the added value of high-resolution simulations, which allow for improved representation of shorter time scale extreme events, as they are generally associated with smaller scale spatial structures, which cannot be adequately captured by low-resolution simulations.

5.3.4. Extreme wind gust speed

At each observation site (Figure 5.5, left panel), annual maximum wind gust speed is fitted by the GEV distribution using the method of L-moments, and the wind gust speed of the 1 in 2-year event is calculated. Observed and modelled wind gust speeds are in good agreement, with the lowest speeds (around 50 km/h) occurring over the Mackenzie valley in NWT, and the highest speeds (near 120 km/h) over the eastern part of Baffin Island (Figure 5.5). Small-scale features are also well captured by GEM4_ERA5, such as the two observed clusters of higher wind gust speeds near the coast of the Arctic Ocean – one near the Yukon-NWT border, and the other near the NWT-Nunavut border.

5.3.5. Fog

Observations show that fog is highly variable in both space and time over the domain, with fog frequency peaking during different seasons depending on the location, due to the different physical processes leading to fog formation. The novel fog diagnostic described in Section 2.2 correctly captures the complex daily and annual cycles of fog at all 16 reference sites when applied to GEM4_ERA5 (Figure 5.6, bottom panel), with only small differences from observed behaviour. Additional insights obtained by training the diagnostic for each reference site separately show that relative humidity is the most important predictor of fog, as expected. While temperature has little importance during summer, it is an important predictor during winter for sites in the NWT and western provinces. Wind is an important predictor at all sites for at least part of the year and it is important during most of the year for sites in Nunavut and sites near Great Slave Lake, suggesting that advection is an important factor for fog formation at these sites.

When applied over the entire domain, the diagnostic produces a detailed representation of the estimated spatial distribution of fog occurrence rates (Figure 5.6, top panel), which suggest lower fog frequency over most of NWT and the southern part of the domain (few hundred hours per year), and higher fog frequency over the high Arctic (exceeding 1,000 hours per year), in excellent agreement with observations.

5.3.6. Permafrost

Permafrost extent is reasonably modelled by the GEM4_ERA5 simulation, which fully captures the continuous permafrost region, along with a fraction of the discontinuous permafrost region (Figure 5.7). At locations where active layer thickness (ALT) observations are available from the CALM dataset, the values modelled by GEM are close to those observed. Permafrost temperatures are also adequately captured by GEM4_ERA5 at most locations where observations are available (Figure 5.7). The underestimation of permafrost extent in GEM is comparable to previous studies at coarser resolution (e.g., Teufel and Sushama, 2019), and is linked to insufficient thermal inertia in CLASS, which does not yet include an excess ground ice parameterization and considers bedrock to be completely ice-free. High-resolution datasets of permeable soil depth are also expected to aid towards improving the performance of GEM.

5.4. Projected changes

Given that the simulation driven by reanalysis (GEM4_ERA5) and the simulation driven by CanESM2 differ by the addition of boundary forcing errors, it is important to confirm that the GCM-driven simulation performs reasonably for current climate. The performance of the GCM-driven simulation when compared to reference datasets is very similar to the performance of GEM4_ERA5 (discussed extensively in Section 3), implying that boundary forcing errors are small and that the performance of GEM4_ERA5 is an accurate indicator of the reliability of the projections presented here.

5.4.1. Extreme short-duration rainfall

Extreme short-duration rainfall is generally expected to increase due to warmer temperatures favouring convective events during summer. GEM projects an increase in extreme rainfall intensity during the 2021-2040 period when compared to the 1991-2010 reference over many locations in the domain (Figure 5.8). Due to the relatively short time horizon of the projections (until 2040), statistical significance is only achieved over a fraction of the domain. Nonetheless, certain regions, such as the surroundings of Grays Bay, eastern Baffin Island and parts of Nunavik are projected to experience significant changes to the 2-year return levels of annual maximum rainfall at durations from 15 minutes to 4 hours (Figure 5.8). The projected increases to short-duration rainfall intensity exceed 50% over some parts of these regions, which is well above the baseline ~7% increase per degree of warming from the Clausius–Clapeyron (CC) relation. This implies super–CC scaling, which has been widely observed for short-duration precipitation extremes (e.g., Lenderink et al., 2017; Oh and Sushama, 2020) and is linked to positive feedbacks from latent heat release during convective events (e.g., Trenberth et al., 2003), although changes to atmospheric stability and large-scale circulation also need to be considered. The large magnitude of these projected changes could result in significant impacts on engineering and transportation systems designed for the lower rainfall rates of observed climate. For instance, loss of friction and flooding of roads and runways can cause road closures and flight cancellations, while excessive short-duration rainfall can lead to severe flooding and washing out of roads, bridges, and runways.

5.4.2. Extreme wind gust speed

Projected changes to the 2-year return level of wind gust speed indicate that extreme wind gusts are projected to remain within ±10% of their reference 1991-2010 values. Larger changes are projected for 10-year return level of wind gust speed, with decreases projected for the NWT (especially near the coast) and increases over eastern Baffin Island and parts of northern Alberta and the high Arctic (Figure 5.9). It is important to note that small increases in extreme wind speed could still have significant impacts on the design and management of structures, as design wind pressure is directly proportional to the square of the design wind speed. Applying this relationship to the modelled wind gust speeds results in larger increases, which are projected to exceed 25% over the aforementioned regions and could pose a hazard to structures and operations. For instance, high winds can reduce road vehicle stability, cause damage to road and aerodrome structures and result in road obstructions (e.g., fallen trees) and bridge closures.

5.4.3. Fog

Fog frequency is projected to increase by around 10% over most of the domain by 2040 (Figure 5.10). Over some southerly regions, increases exceeding 20% are possible, while over small parts of the high Arctic, decreases are projected. Distinct spatial patterns of increases and decreases are projected for each season, with spring dominated by decreases, autumn exhibiting mostly increases, and summer and winter presenting mixed patterns (Figure 5.10). These changes to fog frequency patterns are linked to changes in the frequency of high relative humidity values, which is by far the most important predictor of fog. These projected changes to fog patterns have significant implications for northern transportation (aerial, marine and terrestrial) due to the direct effects of fog on visibility. This study is the first to produce fog projections over the region, and this is only possible due to the novel integration of high-resolution modelling with machine learning algorithms (see Section 2.2 for details).

5.4.4. Permafrost

As a result of warmer temperatures, the active layer thickness (ALT) is projected to deepen over the permafrost domain, with increases of 0.5 to 3 m over southern regions for the 2021-2040 period, with respect to 1991-2010 (Figure 5.11). Permafrost temperature at 5 m depth is projected to increase between 0.5 and 3 °C over most of the present-day permafrost domain, with the largest increases over the middle latitude ranges, as warming is confined to the upper layers in the high Arctic, and phase change results in temperatures remaining close to 0 °C over southern regions, limiting temperature change over both those regions. These increases in ALT and ground temperature are hazardous for northern transportation and engineering systems, as extensively demonstrated by deterioration and failures in recent years (Government of the NWT, 2008). Given that permafrost behaviour at the site scale is controlled by local factors beyond the parameterizations and resolution of climate models, site-specific studies are required for the adaptation of these systems to permafrost degradation.

5.5. Summary and conclusions

The reanalysis-driven 4 km grid spacing GEM simulation is able to well capture the observed behaviour of base climate variables and several climatic hazards over the eastern and central Canadian Arctic. The added value of high-resolution simulations is clearly demonstrated for extreme rainfall intensity at short durations (3 hours and below), when compared to a coarser resolution simulation. Improvements in the simulation of annual and seasonal temperatures and precipitation represent further examples of added value. Observed and modelled wind gust speeds are in good agreement, with GEM being able to capture relatively small-scale features in the observed spatial distribution. Near-surface permafrost extent, active layer thickness and ground temperatures are also adequately captured by GEM. Fog diagnosed using a novel approach integrating climate model output and machine learning algorithms, is in excellent agreement with observations, as its complex daily and annual cycles are well captured at all sites where observations are available.

The good performance of GEM when compared to observed climate lends credibility to high-resolution climate projections extending to the year 2040 – the first time that 4 km grid spacing projections are produced over the study region. Maximum projected increases to short-duration rainfall extremes (of the order of 50%), extreme wind gust pressure (around 25%), fog frequency (near 20%), along with increases in active layer thickness and ground temperature, showcase the variety of hazards to which northern infrastructure and transportation systems are projected to be exposed within the next two decades (2021-2040). Urgent action is thus required for northern transportation and engineering systems to be adapted to the increased magnitude of these various hazards. Additional high-resolution simulations over the region, and climate projections extending beyond 2040 would be very valuable additions to the work presented here, and of very high value to local planning and decision-making processes.

Acknowledgements

This research was funded by Transport Canada (Northern Transportation Adaptation Initiative), Natural Sciences and Engineering Research Council of Canada (NSERC), Trottier Institute for Sustainability in Engineering and Design (TISED) and the McGill Sustainability Systems Initiative (MSSI). The GEM simulations in this study were performed on supercomputers managed by Calcul Québec and Compute Canada.

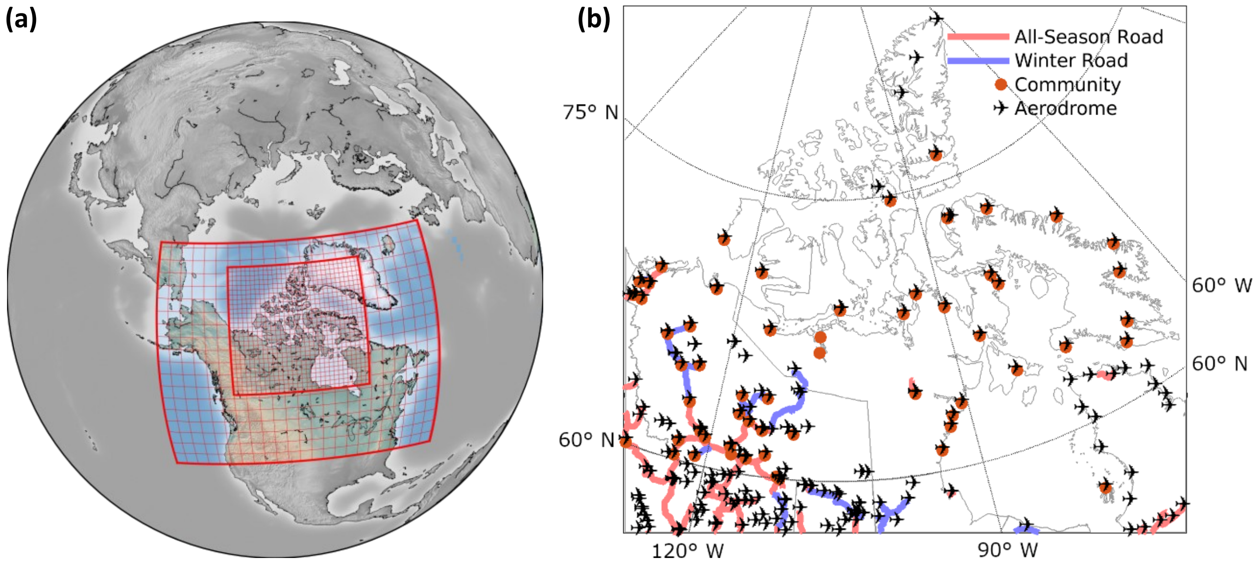

Figure 5.1. (a) Grid telescoping into northern Canada for convection permitting transient climate change simulations at 4 km resolution (inner grid). The outer grid is the 10 km resolution grid. (b) Northern communities and transportation infrastructure in the analysis domain, from the CanVec dataset published by Natural Resources Canada.

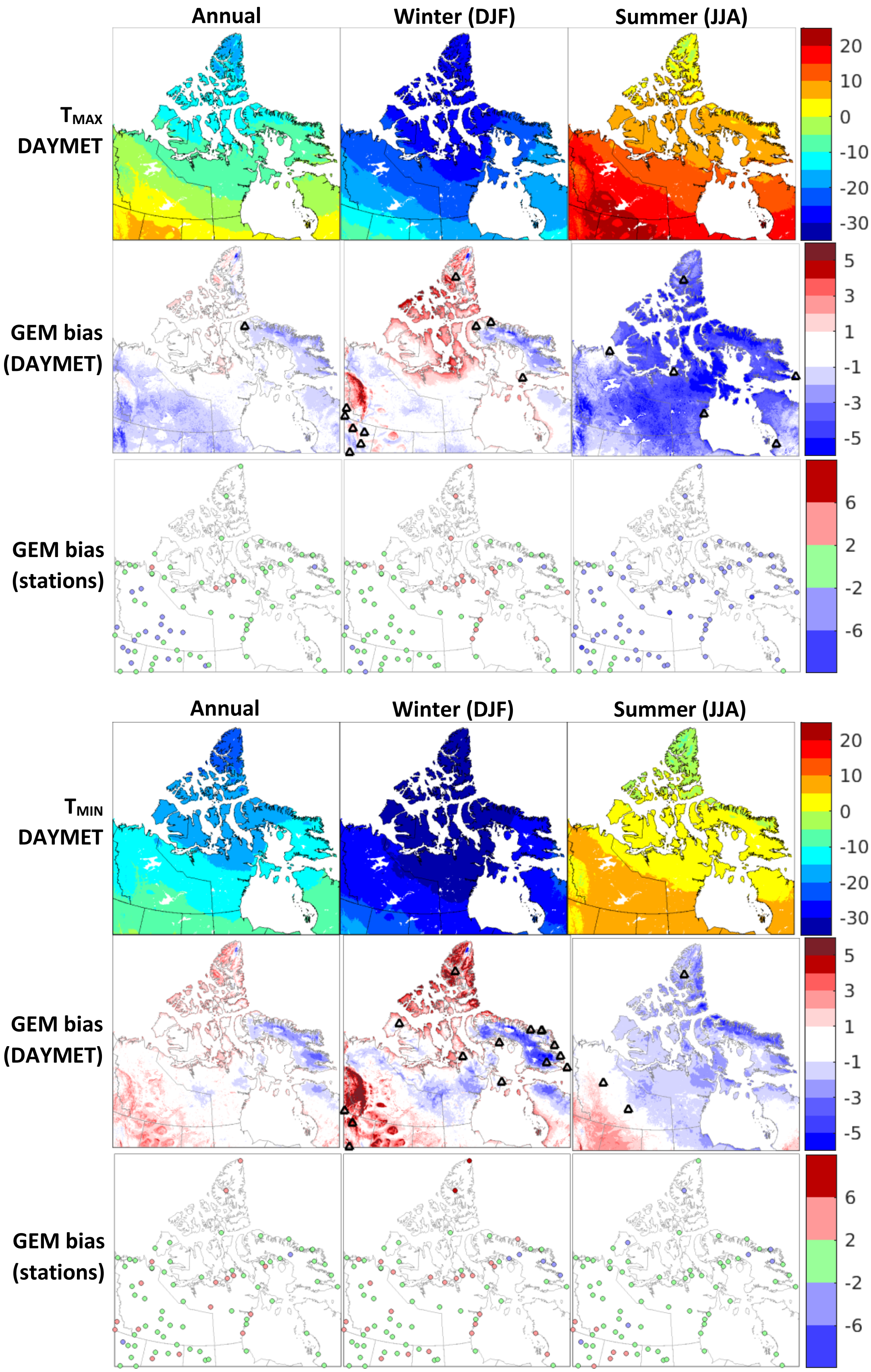

Annual
Winter (DJF)
Summer (JJA)
T_{MAX} DAYMET
20
10
0
-10
-20
-30
GEM bias (DAYMET)
5
3
1
-1
-3
-5
GEM bias (stations)
6
2
-2
-6
Annual
Winter (DJF)
Summer (JJA)
T_{MIN} DAYMET
20
10
0
-10
-20
-30
GEM bias (DAYMET)
5
3
1
-1
-3
-5
GEM bias (stations)
6
2
-2
-6

Figure 5.2. Annual and seasonal averages of daily maximum and minimum 2-m air temperature during the 1991-2010 period, from the DAYMET dataset. Also shown are GEM4_ERA5 biases with respect to DAYMET and to site observations (only sites with at least 10 observations for each day of the year are shown). Black triangles denote sites where cross-validation biases within DAYMET exceed 2 °C, denoting lower reliability of its estimates.

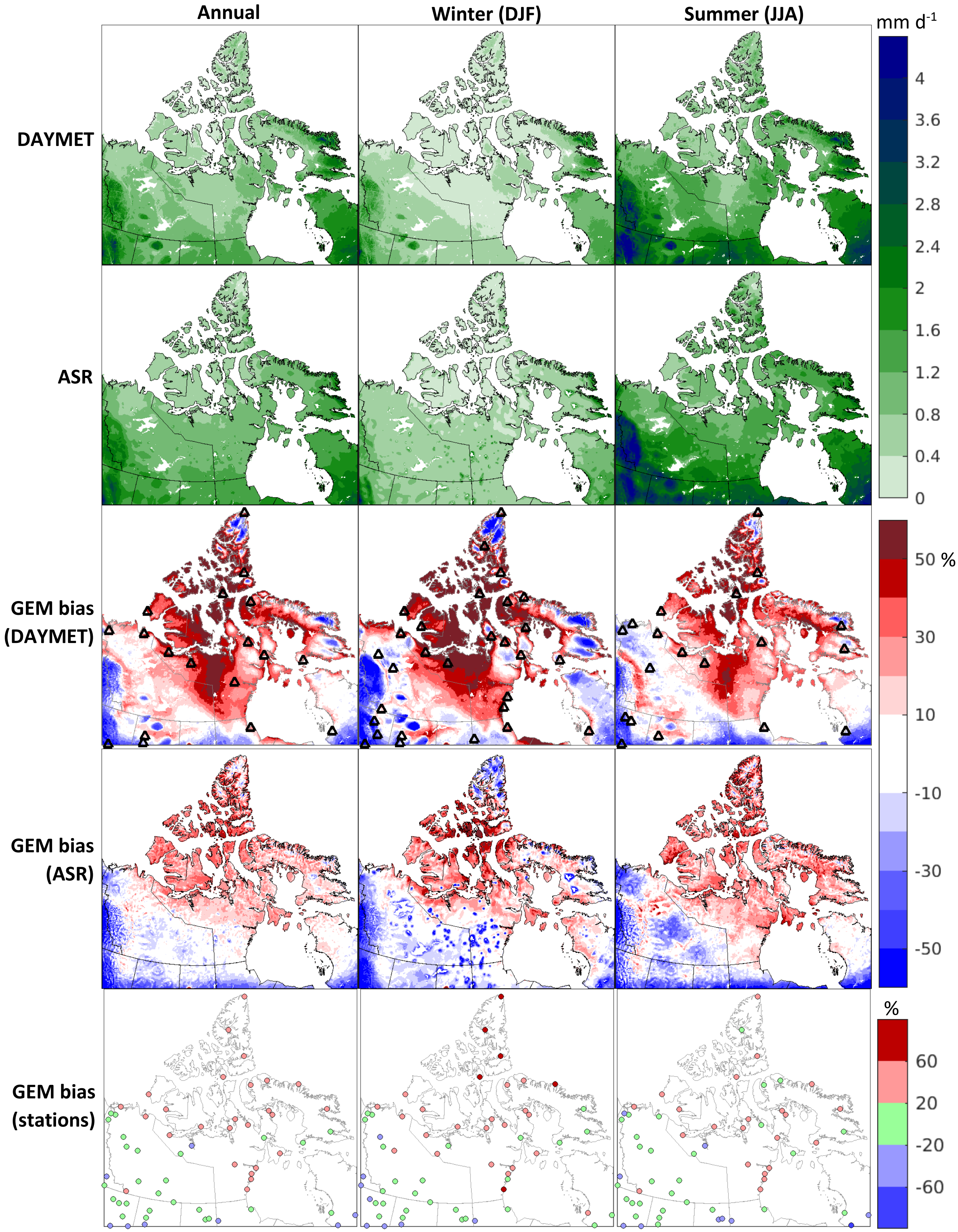

Annual
Winter (DJF)
Summer (JJA)
DAYMET
ASR
GEM bias (DAYMET)
GEM bias (ASR)
GEM bias (stations)
mm d-1
4
3.6
3.2
2.8
2.4
2
1.6
1.2
0.8
0.4
0
50 %
30
10
-10
-30
-50
%
60
20
-20
-60

Figure 5.3. Annual and seasonal averages of precipitation from the DAYMET dataset (1991-2010) and the Arctic System Reanalysis (ASR; 2000-2010). Also shown are GEM4_ERA5 biases with respect to DAYMET, to ASR and to site observations (only sites with at least 10 observations for each day of the year are shown). Black triangles denote sites where cross-validation biases within DAYMET exceed 20%, denoting lower reliability of its estimates.

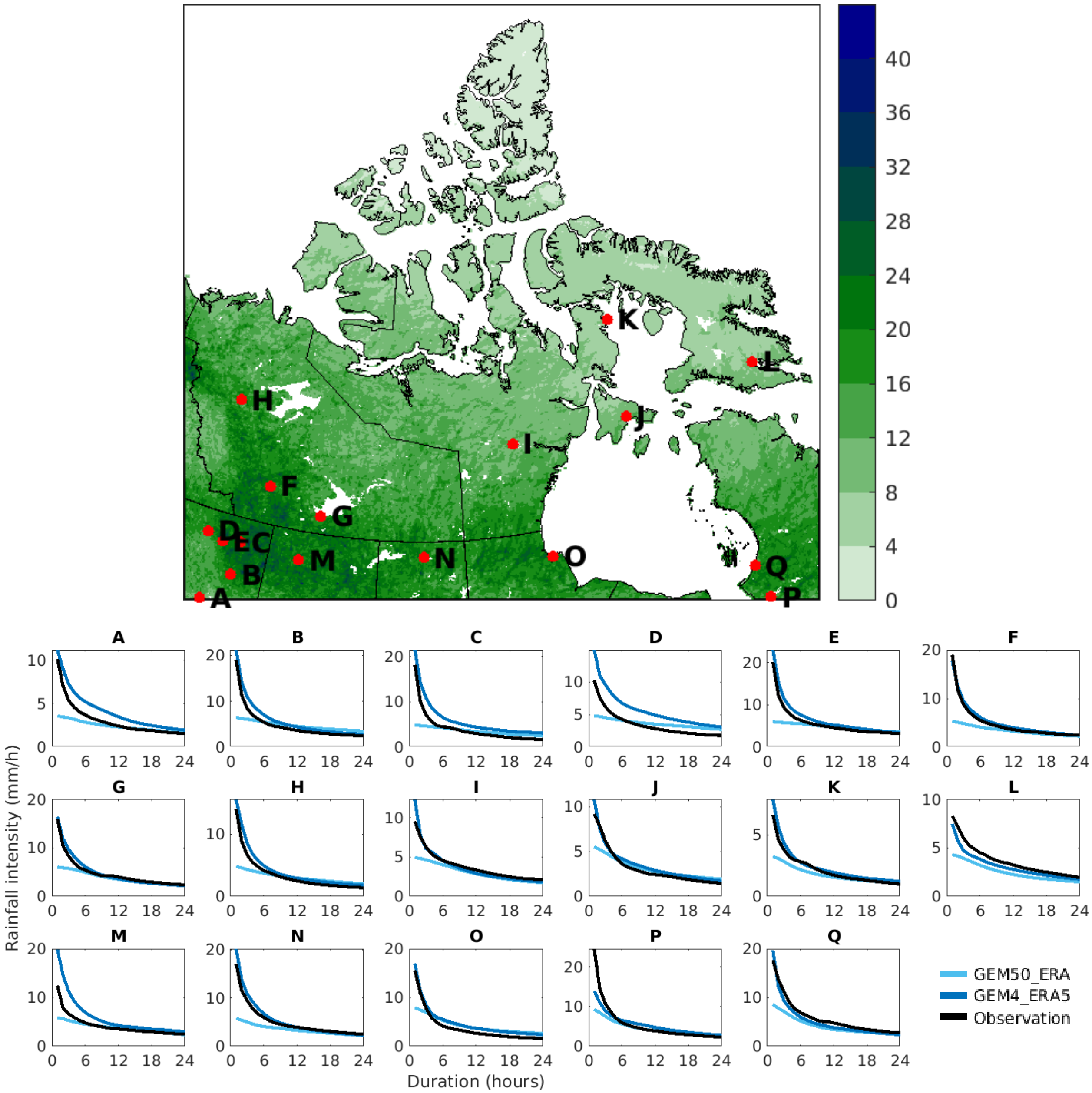

Figure 5.4. One-hour rainfall accumulation (mm) for the 1 in 10-year event during the 1991-2010 period, as modelled by GEM4_ERA5 (top panel). Lettered red dots mark the location of observing sites with at least 10 years of rainfall data. Also shown is the rainfall intensity of the 1 in 10-year event at each site shown in the top panel, for the 1991-2010 period, for durations ranging from 1 to 24 hours, from observations (black lines), GEM4_ERA5 (dark blue lines) and GEM50_ERA (light blue lines).

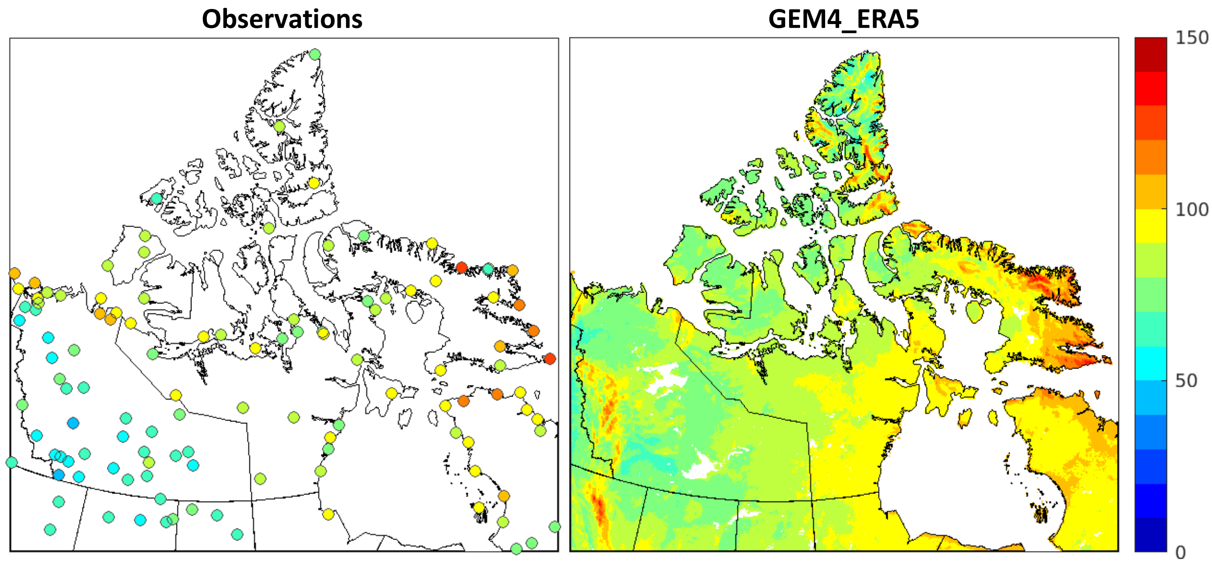

Figure 5.5. Observed and GEM4_ERA5 modelled two-year return level of annual maximum wind gust (km h^{-1}) during the 1991-2010 period. Only observing sites with at least 10 years of data are shown.

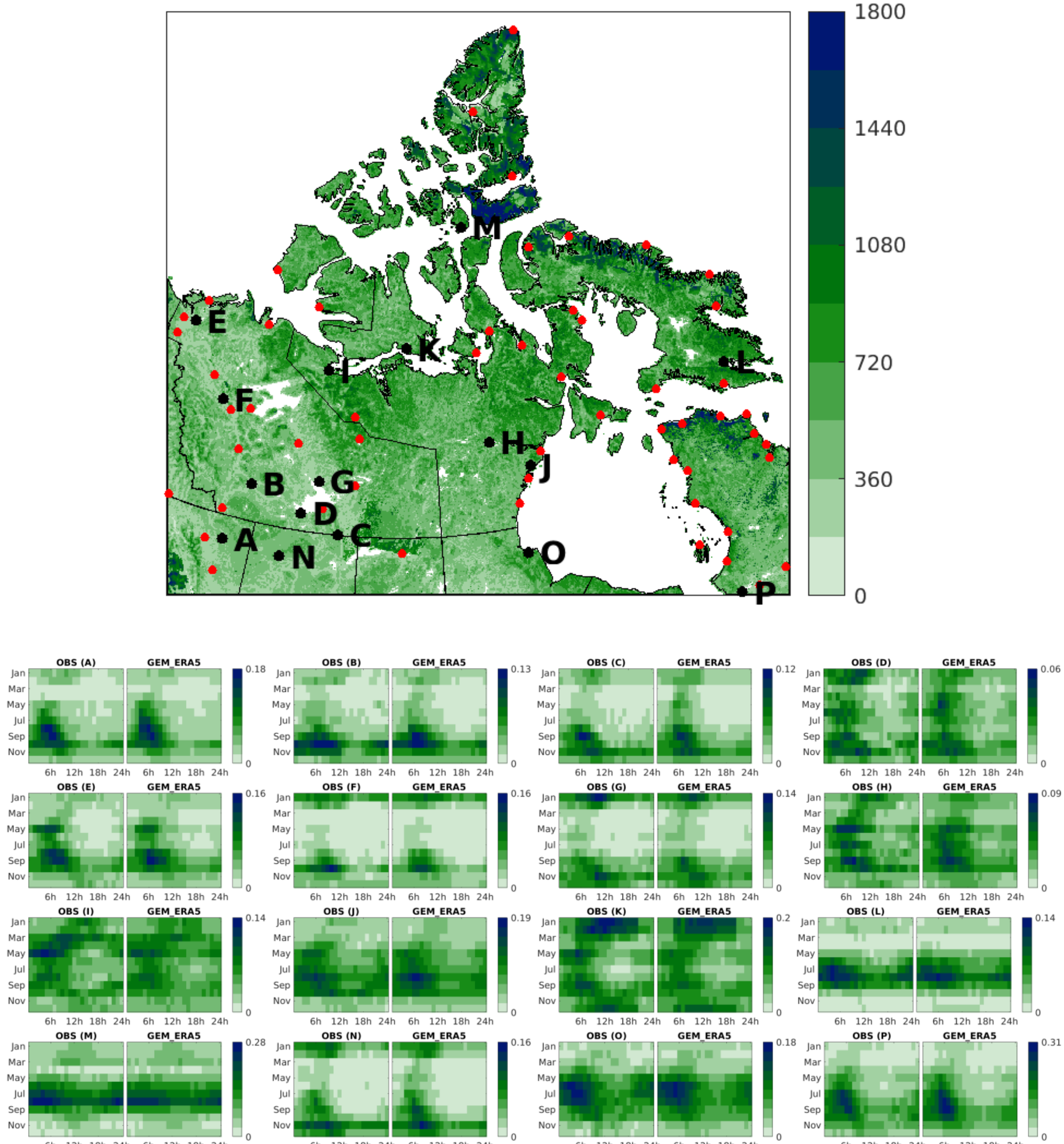

Figure 5.6. Average number of hours with fog per year during the 1991-2010 period, as modelled by GEM4_ERA5. Lettered black dots mark the location of reference observing sites (fog data >95% complete), while red dots mark the location of other observing sites with at least 10 years of fog data. Daily and annual cycles of fog frequency are shown for each reference site.

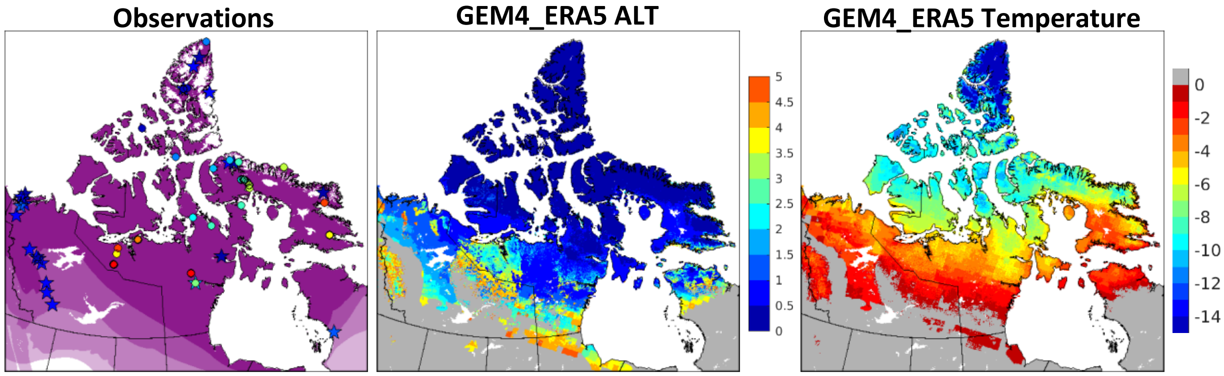

Figure 5.7. Permafrost extent (left panel) from the circum-Arctic permafrost map. Different shades of purple, from dark to light, indicate continuous, discontinuous, sporadic and isolated permafrost regions. Coloured stars with black borders show observed mean active layer thickness (m) at the CALM sites for the 1991-2010 period, while colored dots with black borders show observed ground temperatures near the depth of zero annual amplitude. Also shown are the GEM4_ERA5 simulated active layer thickness (center panel) and deep ground temperature (°C) for the 1991-2010 period.

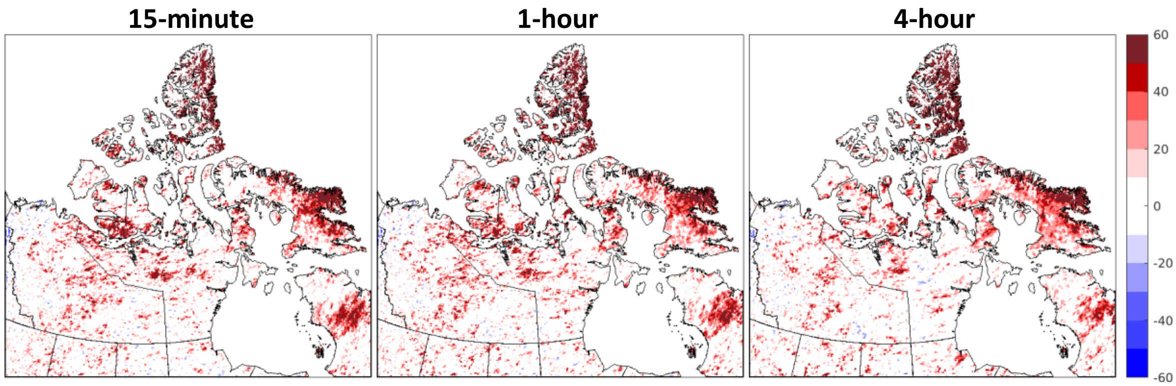

Figure 5.8. Relative projected changes to 2-yr return levels of annual maximum 15-minute (left), 1-hour (center) and 4-hour (right) rainfall for the 2021-2040 period, with respect to the 1991-2010 reference. Only changes exceeding the 10% statistical significance level are shown.

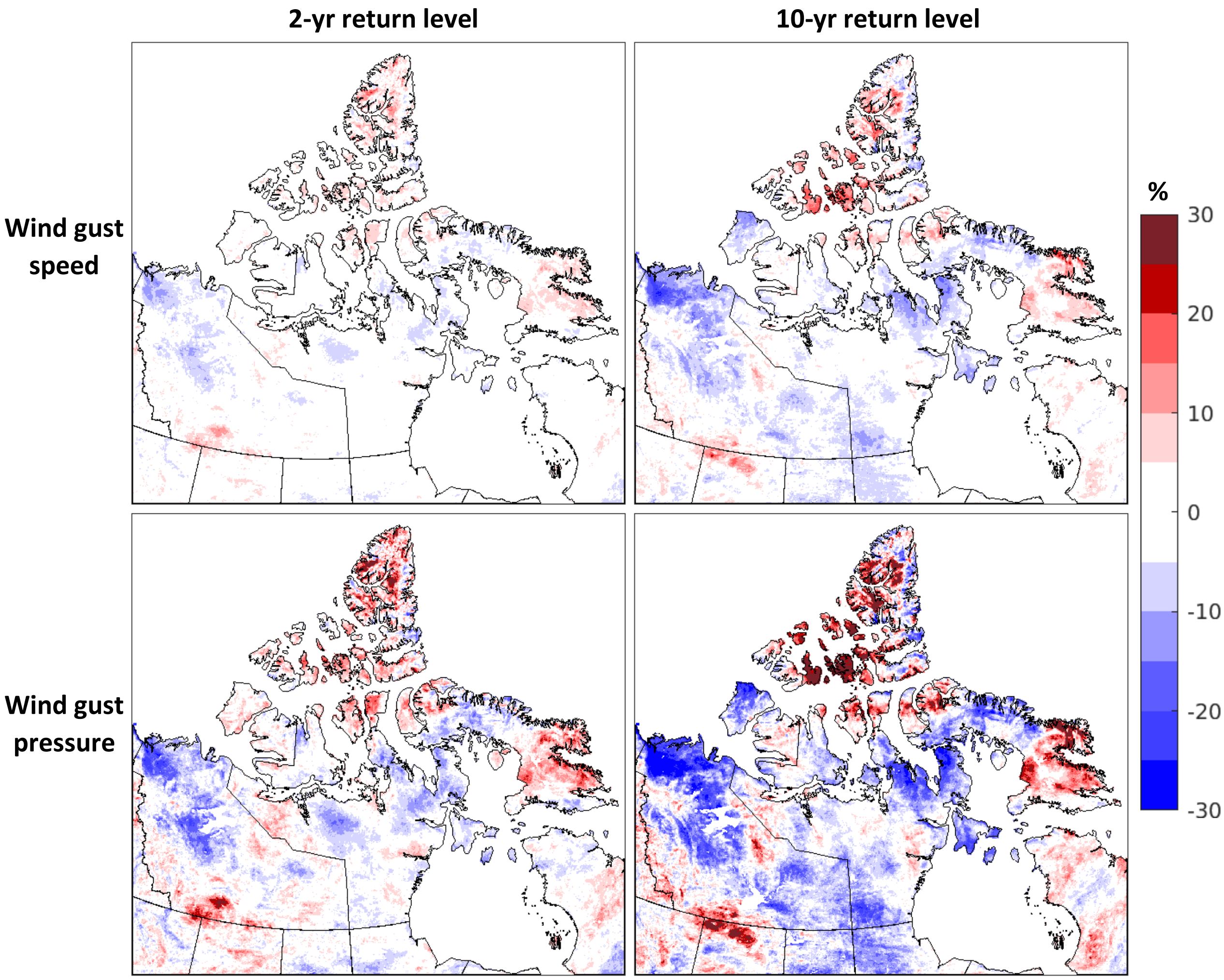

Figure 5.9. Relative projected changes to 2-yr and 10-yr return levels of annual maximum wind gust speed and pressure for the 2021-2040 period, with respect to the 1991-2010 reference.

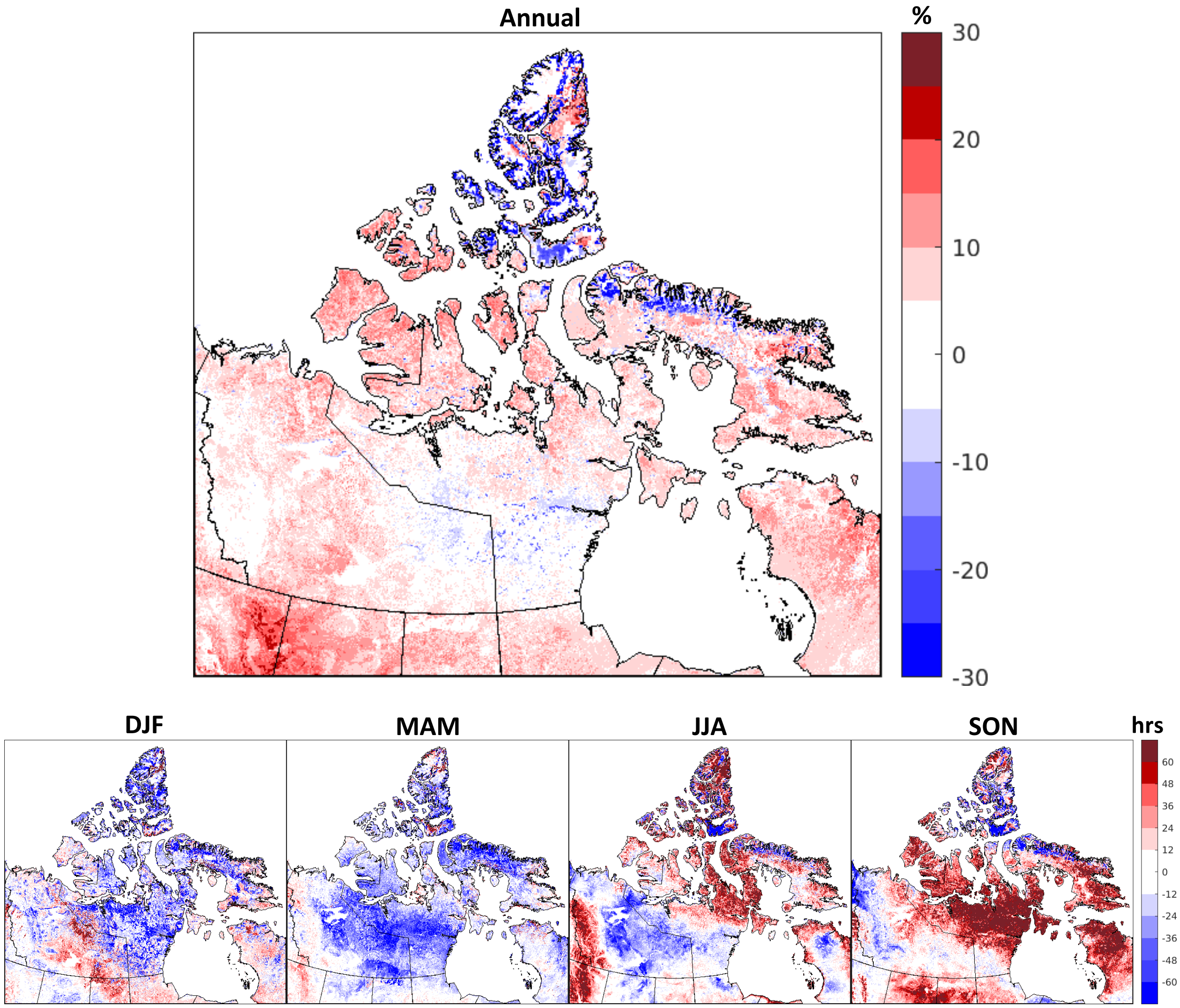

Figure 5.10. Relative projected changes to the average number of hours with fog per year for the 2021-2040 period, with respect to the 1991-2010 reference. Projected changes to the average number of hours with fog are also shown for each season.

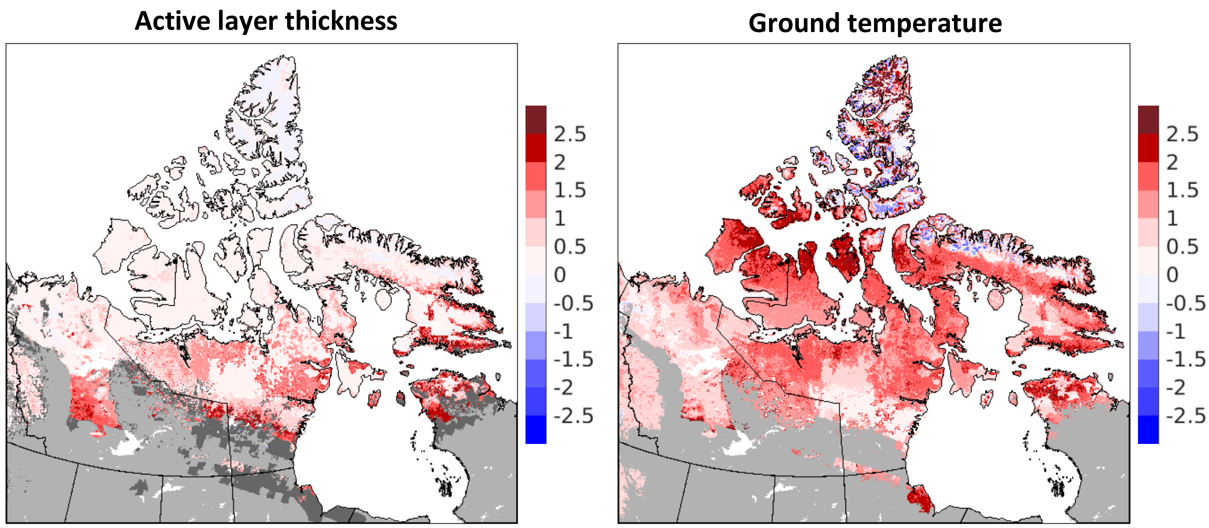

Figure 5.11. Projected changes to mean active layer thickness (m) of near-surface permafrost (left) and projected changes to mean ground temperature (°C) at 5 m depth (right) for the 2021-2040 period, with respect to the 1991-2010 reference. Dark grey is used for regions where near-surface permafrost was modelled to be present during the 1991-2010 period, but not during the 2021-2040 period.

Chapter 6: Conclusions

6.1. Contributions to original knowledge

The overall goal of this thesis was to generate high-quality actionable climate change information for the adaptation of engineering systems in cold environments, which was accomplished through the development and advanced analysis of medium- and high-resolution climate projections. The following knowledge gaps were addressed through application of innovative analysis methods to these state-of-the-art climate simulations and represent contributions to original knowledge:

1) In Chapter 3, the relative contributions of snowmelt and rainfall to flood events in both current and future climates were quantified for the first time across Canada. As expected, rainfall contribution is projected to increase over many regions. However, there is significant regional heterogeneity in the projected magnitude of this increase, which led to the identification of potential hotspots of change. In some of these hotspots, along with other regions, rainfall is projected to become the predominant flood-generating mechanism, in contrast with the current regime, where both rainfall and snowmelt are important mechanisms. These changes have significant implications for the management of flood risks and freshwater resources and for the development of flow regulation plans in these regions, given that the projected shift in mechanisms influences both flood magnitude and timing.
2) In Chapter 4, permafrost-related potential abrupt changes to engineering-relevant variables were identified and quantified for the first time. These include abrupt decreases to soil moisture, and abrupt increases to convective precipitation, lightning frequency and wildfire severity. The implications for engineering systems are clear – while rainfall extremes were already projected to increase over northern regions, an abrupt and unexpected additional

increase has significant potential to result in excessive rainfall and thus flooding, damaging northern infrastructure and disrupting operations. An abrupt doubling of wildfire severity, such as projected for some regions in northwestern Canada, could put severe stress on fire-fighting efforts around northern communities and is expected to have significant impacts on the transportation sector, as wildfires often result in the closure of road segments and smoke considerably reduces visibility for planes. In addition, wildfires can promote further permafrost thaw, with the associated implications for the structural integrity of infrastructure. Adaptation strategies for northern infrastructure need to be modified, as they currently do not account for the possibility of abrupt changes.

3) In Chapter 5, high-resolution climate projections were developed for the first time over northern Canada. Comparisons against ground truth demonstrated that these 4-km resolution simulations represent a significant improvement over the 50-km simulations considered in Chapters 3 and 4, especially for critical small-scale phenomena, such as extreme short-duration rainfall. Analysis of projected changes to climatic hazards over the next two decades (2021-2040) revealed significant implications for vital systems in the northern transportation sector. For instance, local increases of over 50% to short-duration rainfall extremes can lead to flooding and washing out of roads, bridges, and runways. Increases of up to 25% to wind pressure extremes can cause damage to road and aerodrome structures and result in road obstructions (e.g., fallen trees) and bridge closures. Continuing permafrost degradation is expected to reduce the structural stability of buildings, roads, and runways. The identification of hotspots of change to these climatic hazards will allow adaptation efforts to focus on the regions and systems with the highest likelihood of being disrupted by climate change.

4) Also in Chapter 5, a novel machine learning-based framework was developed to diagnose fog from high-resolution climate model outputs. The method exhibits excellent agreement with observations, as the complex daily and annual cycles of fog are well captured at all sites where observations are available. The good performance of the method lends credibility to projections of fog in future climate, developed for the first time over the region. Overall fog frequency is projected to increase by around 10% over most of the central and eastern Canadian Arctic by 2040, due to increasing frequency of high humidity conditions, although with important seasonal variations. These projected changes to fog patterns have significant implications for northern transportation (aerial, marine and terrestrial) due to the direct effects of fog on visibility.

The research developed in this thesis will help stakeholders to be prepared and take appropriate climate change adaptation measures. For example, the research presented in Chapter 5 informed the "Engineering Climate Simulations and Thresholds for Nunavut" report prepared for Transport Canada in the context of the Northern Transportation Adaptation Initiative.

This generation of actionable knowledge for adapting engineering systems in cold regions to a changing climate is the first step to increase the service life and performance of engineering systems in these regions, and has the potential to result in long term cost savings, reducing environmental impact and increasing sustainability of communities, industry and government at all levels.

6.2. Insights and recommendations for future research

Future work on floods and their mechanisms will benefit from the identification of potential hotspots of change presented in Chapter 3. High-resolution simulations are urgently required to assess projected impacts and develop adaptation plans on local scales. However, these simulations are also very expensive, especially for extreme floods, which have devastating impacts on infrastructure and society at large, but are by definition very rare occurrences, requiring hundreds of simulation years or more. Knowing which regions are most at risk of experiencing significant changes to flooding (i.e., the hotspots identified here) allows to best take advantage of the limited resources available. High-resolution simulations are also required to assess projected changes to flash flooding – generally triggered by extreme rainfall events, which due to their small-scale nature are much better represented in high-resolution simulations, as demonstrated in Chapter 5.

Another interesting research question that remains open on the topic of floods in cold regions and their mechanisms is the projected evolution of ice jams, which are often the triggering mechanism for extreme flooding in Canadian rivers, but are complex phenomena requiring implementation of river ice and its mechanics into hydrologically-enabled climate models. Due to the small-scale nature of ice jams, it is likely that high-resolution simulations will be required to capture them realistically and to produce credible projections. The amounts of rainfall and snowmelt contribution are expected to have an important influence on the breaking-up of river ice, given that rainfall water has greater ice-melt potential due to its warmer temperature. This suggests that hotspots of increased rainfall contribution might also be hotspots of ice jam change – again allowing for the targeting of specific regions and potential for more efficient use of resources based on the results presented in this thesis.

Recent studies have used hydrodynamic models to bridge the gap between hydrologically-enabled climate models and actionable flood-risk mapping at local scales. Hydrodynamic models explicitly simulate inundation area and flood depths, but require ultra-high resolution elevation data and are expensive to run over large regions due to their fine grid. With the ongoing generation and release of high-quality elevation data (e.g., the High Resolution Digital Elevation Model at 1 m resolution by Natural Resources Canada), along with advances in high-resolution climate modelling and machine learning, the gap between scales has the potential to be closed, resulting in physically-based and consistent flood-risk mapping in current and future climates across large regions.

Future work on permafrost will require ultra high-resolution modelling, at scales even finer than the 4-km resolution simulations presented in Chapter 5. This is due to the very high spatial heterogeneity of near-surface permafrost, controlled by factors such as the local terrain, hydrology, vegetation, geology and disturbances, which sometimes vary in scales of tens of meters. Simulations at those scales would result in locally actionable information on current and future permafrost conditions, but depend on reliable estimates of geomorphological parameters (e.g., depth to bedrock), which are currently poorly constrained by observations over the vast majority of the permafrost region, given that no methods exist to obtain accurate high-resolution estimates of these parameters over large regions, and surveying is both expensive and limited by harsh environmental conditions. In addition to ultra high-resolution, additional processes need to be included in climate models to ensure accurate modelling of permafrost at local scales, such as lateral soil heat and moisture transport, soil subsidence, erosion, sub-permafrost aquifers and evolving water bodies (e.g., thermokarst lakes). Including these processes might also enable models to reproduce the complex process of abrupt permafrost thaw, which may be the norm for many parts of the Arctic landscape. Abrupt permafrost thaw is a completely different process from the abrupt changes due to permafrost thaw explored in Chapter 4, but both are important to understand the future evolution of permafrost and its impact on engineering systems in the Arctic.

The research leading to Chapter 4 presented statistical challenges, given that large year-to-year variability and long-term trends in climate make detecting and quantifying abrupt (i.e., step) changes very difficult. These challenges were only overcome due to the ensemble approach employed, which pooled information from five climate simulations and allowed separating signal (i.e., abrupt changes) from noise (i.e., internal variability). The ensemble approach was also very beneficial in Chapter 3, as it allowed to consider five times more flood events than analysis based on a single simulation, resulting in significantly more robust estimates of the projected changes to rainfall/snowmelt contribution. In Chapter 5, pursuing an ensemble approach was not feasible, due to the high cost of 4-km resolution simulations. An ensemble would have likely allowed achieving statistical significance over more regions and would have resulted in better delineation of hotspots of change, improving the efficiency of adaptation efforts.

The machine learning-based framework developed in Chapter 5 to generate projections of fog has the potential to be directly applied to diagnose other complex climatic hazards, such as blizzard conditions, which also cause disruptions to transportation systems. Successfully applying machine learning algorithms to high-resolution climate model outputs is an example of the potential synergy between physical modelling and data-driven approaches, a field of research which is very likely to expand in coming years, as advances in machine learning allow researchers to fully exploit the rapidly growing volume of climate simulation data, paving the way for numerous discoveries.

References

Arora, V. K., Scinocca, J. F., Boer, G. J., Christian, J. R., Denman, K. L., Flato, G. M., Kharin, V. V., Lee, W. G., and Merryfield, W. J. (2011). Carbon emission limits required to satisfy future representative concentration pathways of greenhouse gases. *Geophysical Research Letters, 38*, L05805. doi:10.1029/2010gl046270

Ashley, S. T., and Ashley, W. S. (2008). Flood Fatalities in the United States. *Journal of Applied Meteorology and Climatology, 47*(3), 805-818. doi:10.1175/2007jamc1611.1

Avis, C. A., Weaver, A. J., and Meissner, K. J. (2011). Reduction in areal extent of high-latitude wetlands in response to permafrost thaw. *Nature Geoscience, 4*(7), 444-448. doi:10.1038/Ngeo1160

Ban, N., Schmidli, J., and Schär, C. (2014). Evaluation of the convection-resolving regional climate modeling approach in decade-long simulations. *Journal of Geophysical Research: Atmospheres, 119*(13), 7889-7907. doi:https://doi.org/10.1002/2014JD021478

Bates, B. C., Chandler, R. E., and Bowman, A. W. (2012). Trend estimation and change point detection in individual climatic series using flexible regression methods. *Journal of Geophysical Research-Atmospheres, 117*. doi:10.1029/2011jd017077

Belair, S., Mailhot, J., Girard, C., and Vaillancourt, P. (2005). Boundary layer and shallow cumulus clouds in a medium-range forecast of a large-scale weather system. *Monthly Weather Review, 133*(7), 1938-1960. doi:Doi 10.1175/Mwr2958.1

Beltaos, S. (2002). Effects of climate on mid-winter ice jams. *Hydrological Processes, 16*(4), 789-804. doi:https://doi.org/10.1002/hyp.370

Beltaos, S., Ismail, S., and Burrell, B. C. (2003). Midwinter breakup and jamming on the upper Saint John River: a case study. *Canadian Journal of Civil Engineering, 30*(1), 77-88. doi:10.1139/l02-062

Beniston, M., and Stoffel, M. (2016). Rain-on-snow events, floods and climate change in the Alps: Events may increase with warming up to 4°C and decrease thereafter. *Science of The Total Environment, 571*, 228-236. doi:https://doi.org/10.1016/j.scitotenv.2016.07.146

Benoit, R., Cote, J., and Mailhot, J. (1989). Inclusion of a Tke Boundary-Layer Parameterization in the Canadian Regional Finite-Element Model. *Monthly Weather Review, 117*(8), 1726-1750. doi:Doi 10.1175/1520-0493(1989)117<1726:Ioatbl>2.0.Co;2

Bocchieri, J. R., Crisci, R. L., Glahn, H. R., Lewis, F., and Globokar, F. T. (1974). Recent developments in automated prediction of ceiling and visibility. *Journal of Applied Meteorology and Climatology, 13*(2), 277-288.

Bowman, A. W., Pope, A., and Ismail, B. (2006). Detecting discontinuities in nonparametric regression curves and surfaces. *Statistics and Computing, 16*(4), 377-390. doi:10.1007/s11222-006-9618-y

Brasseur, O. (2001). Development and application of a physical approach to estimating wind gusts. *Monthly Weather Review, 129*(1), 5-25.

Bromwich, D., Wilson, A., Bai, L., Liu, Z., Barlage, M., Shih, C.-F., Maldonado, S., Hines, K., Wang, S.-H., and Woollen, J. (2018). The arctic system reanalysis, version 2. *Bulletin of the American Meteorological Society, 99*(4), 805-828.

Brown, D. R. N., Jorgenson, M. T., Douglas, T. A., Romanovsky, V. E., Kielland, K., Hiemstra, C., Euskirchen, E. S., and Ruess, R. W. (2015). Interactive effects of wildfire and climate on permafrost degradation in Alaskan lowland forests. *Journal of Geophysical Research: Biogeosciences, 120*(8), 1619-1637. doi:10.1002/2015jg003033

Brown, J., Ferrians Jr, O. J., Heginbottom, J. A., and Melnikov, E. S. (1997). *Circum-Arctic map of permafrost and ground-ice conditions*. Retrieved from

Brown, J., Hinkel, K. M., and Nelson, F. E. (2000). The circumpolar active layer monitoring (calm) program: Research designs and initial results. *Polar Geography, 24*(3), 166-258. doi:10.1080/10889370009377698

Burn, D. H., and Whitfield, P. H. (2016). Changes in floods and flood regimes in Canada. *Canadian Water Resources Journal / Revue canadienne des ressources hydriques, 41*(1-2), 139-150. doi:10.1080/07011784.2015.1026844

Bush, E. J., Loder, J., James, T., Mortsch, L., and Cohen, S. (2014). An overview of Canada's changing climate. *Canada in a changing climate: Sector perspectives on impacts and adaptation*, 23-64.

Clavet-Gaumont, J., Sushama, L., Khaliq, M. N., Huziy, O., and Roy, R. (2013). Canadian RCM projected changes to high flows for Québec watersheds using regional frequency analysis. *International Journal of Climatology, 33*(14), 2940-2955. doi:doi:10.1002/joc.3641

Côté, J., Gravel, S., Méthot, A., Patoine, A., Roch, M., and Staniforth, A. (1998). The Operational CMC–MRB Global Environmental Multiscale (GEM) Model. Part I: Design Considerations and Formulation. *Monthly Weather Review, 126*(6), 1373-1395. doi:10.1175/1520-0493(1998)126<1373:tocmge>2.0.co;2

Dai, A. (2006). Precipitation characteristics in eighteen coupled climate models. *Journal of Climate, 19*(18), 4605-4630.

de Groot, W. J., Flannigan, M. D., and Cantin, A. S. (2013). Climate change impacts on future boreal fire regimes. *Forest Ecology and Management, 294*, 35-44. doi:10.1016/j.foreco.2012.09.027

de Rham, L., Dibike, Y., Beltaos, S., Peters, D., Bonsal, B., and Prowse, T. (2020). A Canadian River Ice Database from the National Hydrometric Program Archives. *Earth Syst. Sci. Data, 12*(3), 1835-1860. doi:10.5194/essd-12-1835-2020

Dee, D. P., Uppala, S. M., Simmons, A. J., Berrisford, P., Poli, P., Kobayashi, S., Andrae, U., Balmaseda, M. A., Balsamo, G., Bauer, P., Bechtold, P., Beljaars, A. C. M., van de Berg, L., Bidlot, J., Bormann, N., Delsol, C., Dragani, R., Fuentes, M., Geer, A. J., Haimberger, L., Healy, S. B., Hersbach, H., Holm, E. V., Isaksen, L., Kallberg, P., Kohler, M., Matricardi, M., McNally, A. P., Monge-Sanz, B. M., Morcrette, J. J., Park, B. K., Peubey, C., de Rosnay, P., Tavolato, C., Thepaut, J. N., and Vitart, F. (2011). The ERA-Interim reanalysis: configuration and performance of the data assimilation system. *Quarterly Journal of the Royal Meteorological Society, 137*(656), 553-597. doi:10.1002/qj.828

Delage, Y. (1997). Parameterising sub-grid scale vertical transport in atmospheric models under statically stable conditions. *Boundary-Layer Meteorology, 82*(1), 23-48. doi:Doi 10.1023/A:1000132524077

Delage, Y., and Girard, C. (1992). Stability Functions Correct at the Free-Convection Limit and Consistent for Both the Surface and Ekman Layers. *Boundary-Layer Meteorology, 58*(1-2), 19-31. doi:Doi 10.1007/Bf00120749

Delisle, G. (2007). Near-surface permafrost degradation: How severe during the 21st century? *Geophysical Research Letters, 34*(9). doi:10.1029/2007gl029323

Deton' Cho Stantec. (2013). *Change and Challenge: Climate Change Adaptation Plan for the GNWT Department of Transportation*. Yellowknife, NT: Government of the Northwest Territories.

Diro, G. T., and Sushama, L. (2019). Simulating Canadian Arctic Climate at Convection-Permitting Resolution. *Atmosphere, 10*(8), 430.

Diro, G. T., Sushama, L., and Huziy, O. (2018). Snow-atmosphere coupling and its impact on temperature variability and extremes over North America. *Climate Dynamics, 50*(7), 2993-3007. doi:10.1007/s00382-017-3788-5

Diro, G. T., Sushama, L., Martynov, A., Jeong, D. I., Verseghy, D., and Winger, K. (2014). Land-atmosphere coupling over North America in CRCM5. *Journal of Geophysical Research: Atmospheres, 119*(21), 11,955-911,972. doi:doi:10.1002/2014JD021677

Drijfhout, S., Bathiany, S., Beaulieu, C., Brovkin, V., Claussen, M., Huntingford, C., Scheffer, M., Sgubin, G., and Swingedouw, D. (2015). Catalogue of abrupt shifts in Intergovernmental Panel on Climate Change climate models. *Proceedings of the National Academy of Sciences*. doi:10.1073/pnas.1511451112

Duchesne, C., Smith, S., Ednie, M., and Bonnaventure, P. (2015). *Active layer variability and change in the Mackenzie Valley, Northwest Territories.* Paper presented at the GEOQuebec 2015, Proceedings, 68th Canadian Geotechnical Conference and 7th Canadian Conference on Permafrost, Quebec, Quebec.

ECCC. (2019). *Manual of Surface Weather Observations (MANOBS)*. Environment and Climate Change Canada.

Endo, H., Kitoh, A., Ose, T., Mizuta, R., and Kusunoki, S. (2012). Future changes and uncertainties in Asian precipitation simulated by multiphysics and multi-sea surface temperature ensemble experiments with high-resolution Meteorological Research Institute atmospheric general circulation models (MRI-AGCMs). *Journal of Geophysical Research-Atmospheres, 117*, D16118. doi:10.1029/2012jd017874

Fabbian, D., De Dear, R., and Lellyett, S. (2007). Application of artificial neural network forecasts to predict fog at Canberra International Airport. *Weather and Forecasting, 22*(2), 372-381.

Feser, F., Rockel, B., von Storch, H., Winterfeldt, J., and Zahn, M. (2011). Regional Climate Models Add Value to Global Model Data: A Review and Selected Examples. *Bulletin of the American Meteorological Society, 92*(9), 1181-1192. doi:10.1175/2011BAMS3061.1

Flannigan, M., Cantin, A. S., de Groot, W. J., Wotton, M., Newbery, A., and Gowman, L. M. (2013). Global wildland fire season severity in the 21st century. *Forest Ecology and Management, 294*, 54-61. doi:10.1016/j.foreco.2012.10.022

Garnaud, C., and Sushama, L. (2015). Biosphere-climate interactions in a changing climate over North America. *Journal of Geophysical Research-Atmospheres, 120*(3), 1091-1108. doi:10.1002/2014jd022055

Gerard, L., Piriou, J.-M., Brožková, R., Geleyn, J.-F., and Banciu, D. (2009). Cloud and precipitation parameterization in a meso-gamma-scale operational weather prediction model. *Monthly Weather Review, 137*(11), 3960-3977.

Girard, C., Plante, A., Desgagné, M., McTaggart-Cowan, R., Côté, J., Charron, M., Gravel, S., Lee, V., Patoine, A., Qaddouri, A., Roch, M., Spacek, L., Tanguay, M., Vaillancourt, P. A., and Zadra, A. (2014). Staggered Vertical Discretization of the Canadian Environmental Multiscale (GEM) Model Using a Coordinate of the Log-Hydrostatic-Pressure Type. *Monthly Weather Review, 142*(3), 1183-1196. doi:10.1175/mwr-d-13-00255.1

Government of the NTW. (2008). *NWT climate change impacts and adaptation report*. Yellowknife, NWT: Government of the Northwest Territories.

Hamlet, A. F., Elsner, M. M., Mauger, G. S., Lee, S.-Y., Tohver, I., and Norheim, R. A. (2013). An Overview of the Columbia Basin Climate Change Scenarios Project: Approach,

Methods, and Summary of Key Results. *Atmosphere-Ocean, 51*(4), 392-415. doi:10.1080/07055900.2013.819555
Hanesiak, J. M., and Wang, X. L. (2005). Adverse-weather trends in the Canadian Arctic. *Journal of Climate, 18*(16), 3140-3156.
Harris, I., Osborn, T. J., Jones, P., and Lister, D. (2020). Version 4 of the CRU TS monthly high-resolution gridded multivariate climate dataset. *Scientific Data, 7*(1), 109. doi:10.1038/s41597-020-0453-3
Hersbach, H., Bell, B., Berrisford, P., Hirahara, S., Horányi, A., Muñoz-Sabater, J., Nicolas, J., Peubey, C., Radu, R., Schepers, D., Simmons, A., Soci, C., Abdalla, S., Abellan, X., Balsamo, G., Bechtold, P., Biavati, G., Bidlot, J., Bonavita, M., De Chiara, G., Dahlgren, P., Dee, D., Diamantakis, M., Dragani, R., Flemming, J., Forbes, R., Fuentes, M., Geer, A., Haimberger, L., Healy, S., Hogan, R. J., Hólm, E., Janisková, M., Keeley, S., Laloyaux, P., Lopez, P., Lupu, C., Radnoti, G., de Rosnay, P., Rozum, I., Vamborg, F., Villaume, S., and Thépaut, J.-N. (2020). The ERA5 global reanalysis. *Quarterly Journal of the Royal Meteorological Society, 146*(730), 1999-2049. doi:10.1002/qj.3803
Hohenegger, C., and Brockhaus, P. (2008). Towards climate simulations at cloud-resolving scales. *Meteorologische Zeitschrift, 17*(4), 383-394.
Hu, Z. Z., Kumar, A., Jha, B., and Huang, B. H. (2012). An analysis of forced and internal variability in a warmer climate in CCSM3. *Journal of Climate, 25*(7), 2356-2373. doi:10.1175/jcli-d-11-00323.1
Huntington, H. P., Hamilton, L. C., Nicolson, C., Brunner, R., Lynch, A., Ogilvie, A. E. J., and Voinov, A. (2007). Toward understanding the human dimensions of the rapidly changing arctic system: insights and approaches from five HARC projects. *Regional Environmental Change, 7*(4), 173-186. doi:10.1007/s10113-007-0038-0
Hurvich, C. M., Simonoff, J. S., and Tsai, C. L. (1998). Smoothing parameter selection in nonparametric regression using an improved Akaike information criterion. *Journal of the Royal Statistical Society Series B-Statistical Methodology, 60*, 271-293. doi:Doi 10.1111/1467-9868.00125
Hutchinson, M. F., McKenney, D. W., Lawrence, K., Pedlar, J. H., Hopkinson, R. F., Milewska, E., and Papadopol, P. (2009). Development and Testing of Canada-Wide Interpolated Spatial Models of Daily Minimum–Maximum Temperature and Precipitation for 1961–2003. *Journal of Applied Meteorology and Climatology, 48*(4), 725-741. doi:10.1175/2008jamc1979.1
Huziy, O., and Sushama, L. (2017a). Impact of lake–river connectivity and interflow on the Canadian RCM simulated regional climate and hydrology for Northeast Canada. *Climate Dynamics, 48*(3), 709-725. doi:10.1007/s00382-016-3104-9
Huziy, O., and Sushama, L. (2017b). Lake–river and lake–atmosphere interactions in a changing climate over Northeast Canada. *Climate Dynamics, 48*(9), 3227-3246. doi:10.1007/s00382-016-3260-y
Huziy, O., Sushama, L., Khaliq, M. N., Laprise, R., Lehner, B., and Roy, R. (2013). Analysis of streamflow characteristics over Northeastern Canada in a changing climate. *Climate Dynamics, 40*(7), 1879-1901. doi:10.1007/s00382-012-1406-0
IPCC. (2012). *Managing the Risks of Extreme Events and Disasters to Advance Climate Change Adaptation. A Special Report of Working Groups I and II of the Intergovernmental Panel on Climate Change (IPCC) [Field, C. B., V. Barros, T. F. Stocker, D. Qin, D. J. Dokken, K. L. Ebi, M. D. Mastrandrea, K. J. Mach, G.-K. PLattner, S. K. Allen, M. Tignor, and P.*

M. Midgley (eds.)]. Cambridge, United Kingdom and New York, NY, USA: Cambridge University Press.

IPCC. (2013). *Climate Change 2013: The Physical Science Basis. Contribution of Working Group I to the Fifth Assessment Report of the Intergovernmental Panel on Climate Change* (T. F. Stocker, D. Qin, G.-K. Plattner, M. Tignor, S. K. Allen, J. Boschung, A. Nauels, Y. Xia, V. Bex, & P. M. Midgley Eds.). Cambridge, United Kingdom and New York, NY, USA: Cambridge University Press.

Jacob, D., Petersen, J., Eggert, B., Alias, A., Christensen, O. B., Bouwer, L. M., Braun, A., Colette, A., Déqué, M., Georgievski, G., Georgopoulou, E., Gobiet, A., Menut, L., Nikulin, G., Haensler, A., Hempelmann, N., Jones, C., Keuler, K., Kovats, S., Kröner, N., Kotlarski, S., Kriegsmann, A., Martin, E., van Meijgaard, E., Moseley, C., Pfeifer, S., Preuschmann, S., Radermacher, C., Radtke, K., Rechid, D., Rounsevell, M., Samuelsson, P., Somot, S., Soussana, J.-F., Teichmann, C., Valentini, R., Vautard, R., Weber, B., and Yiou, P. (2014). EURO-CORDEX: new high-resolution climate change projections for European impact research. *Regional Environmental Change, 14*(2), 563-578. doi:10.1007/s10113-013-0499-2

Javelle, P., Ouarda, T. B. M. J., Lang, M., Bobée, B., Galéa, G., and Grésillon, J.-M. (2002). Development of regional flood-duration–frequency curves based on the index-flood method. *Journal of Hydrology, 258*(1), 249-259. doi:https://doi.org/10.1016/S0022-1694(01)00577-7

Jeong, D. I., and Sushama, L. (2018a). Projected changes to extreme wind and snow environmental loads for buildings and infrastructure across Canada. *Sustainable Cities and Society, 36*, 225-236. doi:10.1016/j.scs.2017.10.004

Jeong, D. I., and Sushama, L. (2018b). Rain-on-snow events over North America based on two Canadian regional climate models. *Climate Dynamics, 50*(1), 303-316. doi:10.1007/s00382-017-3609-x

Jeong, D. I., Sushama, L., Khaliq, M. N., and Roy, R. (2014). A copula-based multivariate analysis of Canadian RCM projected changes to flood characteristics for northeastern Canada. *Climate Dynamics, 42*(7), 2045-2066. doi:10.1007/s00382-013-1851-4

Jongman, B., Ward, P. J., and Aerts, J. C. J. H. (2012). Global exposure to river and coastal flooding: Long term trends and changes. *Global Environmental Change, 22*(4), 823-835. doi:https://doi.org/10.1016/j.gloenvcha.2012.07.004

Jorgenson, M. T., Harden, J., Kanevskiy, M., O'Donnell, J., Wickland, K., Ewing, S., Manies, K., Zhuang, Q. L., Shur, Y., Striegl, R., and Koch, J. (2013). Reorganization of vegetation, hydrology and soil carbon after permafrost degradation across heterogeneous boreal landscapes. *Environmental Research Letters, 8*(3). doi:10.1088/1748-9326/8/3/035017

Kain, J. S., and Fritsch, J. M. (1990). A One-Dimensional Entraining Detraining Plume Model and Its Application in Convective Parameterization. *Journal of the Atmospheric Sciences, 47*(23), 2784-2802. doi:Doi 10.1175/1520-0469(1990)047<2784:Aodepm>2.0.Co;2

Kaufman, D. S., Schneider, D. P., McKay, N. P., Ammann, C. M., Bradley, R. S., Briffa, K. R., Miller, G. H., Otto-Bliesner, B. L., Overpeck, J. T., and Vinther, B. M. (2009). Recent warming reverses long-term arctic cooling. *Science, 325*(5945), 1236-1239. doi:10.1126/science.1173983

Kay, A. L., Reynard, N. S., and Jones, R. G. (2006). RCM rainfall for UK flood frequency estimation. I. Method and validation. *Journal of Hydrology, 318*(1), 151-162. doi:https://doi.org/10.1016/j.jhydrol.2005.06.012

Khaliq, M. N., Sushama, L., Monette, A., and Wheater, H. (2015). Seasonal and extreme precipitation characteristics for the watersheds of the Canadian Prairie Provinces as simulated by the NARCCAP multi-RCM ensemble. *Climate Dynamics, 44*(1), 255-277. doi:10.1007/s00382-014-2235-0

Koven, C. D., Riley, W. J., and Stern, A. (2013). Analysis of Permafrost Thermal Dynamics and Response to Climate Change in the CMIP5 Earth System Models. *Journal of Climate, 26*(6), 1877-1900. doi:10.1175/Jcli-D-12-00228.1

Krause, A., Kloster, S., Wilkenskjeld, S., and Paeth, H. (2014). The sensitivity of global wildfires to simulated past, present, and future lightning frequency. *Journal of Geophysical Research-Biogeosciences, 119*(3), 312-322. doi:10.1002/2013jg002502

Kuo, H. L. (1965). On Formation and Intensification of Tropical Cyclones through Latent Heat Release by Cumulus Convection. *Journal of the Atmospheric Sciences, 22*(1), 40-&. doi:Doi 10.1175/1520-0469(1965)022<0040:Ofaiot>2.0.Co;2

Laprise, R. (1992). The Euler Equations of Motion with Hydrostatic Pressure as an Independent Variable. *Monthly Weather Review, 120*(1), 197-207. doi:10.1175/1520-0493(1992)120<0197:teeomw>2.0.co;2

Lauwaet, D., van Lipzig, N. P. M., Van Weverberg, K., De Ridder, K., and Goyens, C. (2012). The precipitation response to the desiccation of Lake Chad. *Quarterly Journal of the Royal Meteorological Society, 138*(664), 707-719. doi:https://doi.org/10.1002/qj.942

Lawrence, D. M., Koven, C. D., Swenson, S. C., Riley, W. J., and Slater, A. G. (2015). Permafrost thaw and resulting soil moisture changes regulate projected high-latitude CO 2 and CH 4 emissions. *Environmental Research Letters, 10*(9), 094011.

Lawson, B. D., and Armitage, O. (2008). *Weather guide for the Canadian forest fire danger rating system*. (0831-8247). Canadian Forest Service.

Lehner, B., Verdin, K., and Jarvis, A. (2008). New Global Hydrography Derived From Spaceborne Elevation Data. *Eos, Transactions American Geophysical Union, 89*(10), 93-94. doi:https://doi.org/10.1029/2008EO100001

Lenderink, G., Barbero, R., Loriaux, J., and Fowler, H. (2017). Super-Clausius–Clapeyron scaling of extreme hourly convective precipitation and its relation to large-scale atmospheric conditions. *Journal of Climate, 30*(15), 6037-6052.

Lenton, T. M. (2012). Arctic climate tipping points. *Ambio, 41*(1), 10-22. doi:10.1007/s13280-011-0221-x

Letson, F., Pryor, S. C., Barthelmie, R. J., and Hu, W. (2018). Observed gust wind speeds in the coterminous United States, and their relationship to local and regional drivers. *Journal of Wind Engineering and Industrial Aerodynamics, 173*, 199-209. doi:https://doi.org/10.1016/j.jweia.2017.12.008

Letts, M. G., Roulet, N. T., Comer, N. T., Skarupa, M. R., and Verseghy, D. L. (2000). Parametrization of peatland hydraulic properties for the Canadian Land Surface Scheme. *Atmosphere-Ocean, 38*(1), 141-160. doi:10.1080/07055900.2000.9649643

Li, H. W., Lai, Y. M., Wang, L. Z., Yang, X. S., Jiang, N. S., Li, L., Wang, C., and Yang, B. C. (2019). Review of the state of the art: interactions between a buried pipeline and frozen soil. *Cold Regions Science and Technology, 157*, 171-186. doi:10.1016/j.coldregions.2018.10.014

Li, J., and Barker, H. W. (2005). A radiation algorithm with correlated-k distribution. Part I: Local thermal equilibrium. *Journal of the Atmospheric Sciences, 62*(2), 286-309. doi:Doi 10.1175/Jas-3396.1

Liljedahl, A. K., Boike, J., Daanen, R. P., Fedorov, A. N., Frost, G. V., Grosse, G., Hinzman, L. D., Iijma, Y., Jorgenson, J. C., Matveyeva, N., Necsoiu, M., Raynolds, M. K., Romanovsky, V. E., Schulla, J., Tape, K. D., Walker, D. A., Wilson, C. J., Yabuki, H., and Zona, D. (2016). Pan-Arctic ice-wedge degradation in warming permafrost and its influence on tundra hydrology. *Nature Geoscience, 9*(4), 312-318. doi:10.1038/Ngeo2674

Magi, B. I. (2015). Global Lightning Parameterization from CMIP5 Climate Model Output. *Journal of Atmospheric and Oceanic Technology, 32*(3), 434-452. doi:10.1175/Jtech-D-13-00261.1

Mcfarlane, N. A. (1987). The Effect of Orographically Excited Gravity-Wave Drag on the General-Circulation of the Lower Stratosphere and Troposphere. *Journal of the Atmospheric Sciences, 44*(14), 1775-1800. doi:Doi 10.1175/1520-0469(1987)044<1775:Teooeg>2.0.Co;2

McGee, T., McFarlane, B., and Tymstra, C. (2015). Chapter 3 - Wildfire: A Canadian Perspective. In J. F. Shroder & D. Paton (Eds.), *Wildfire Hazards, Risks and Disasters* (pp. 35-58). Oxford: Elsevier.

Menut, L., Mailler, S., Dupont, J.-C., Haeffelin, M., and Elias, T. (2014). Predictability of the Meteorological Conditions Favourable to Radiative Fog Formation During the 2011 ParisFog Campaign. *Boundary-Layer Meteorology, 150*(2), 277-297. doi:10.1007/s10546-013-9875-1

Mesinger, F., DiMego, G., Kalnay, E., Mitchell, K., Shafran, P. C., Ebisuzaki, W., Jovi?, D. a., Woollen, J., Rogers, E., Berbery, E. H., Ek, M. B., Fan, Y., Grumbine, R., Higgins, W., Li, H., Lin, Y., Manikin, G., Parrish, D., and Shi, W. (2006). North American Regional Reanalysis. *Bulletin of the American Meteorological Society, 87*(3), 343-360. doi:10.1175/bams-87-3-343

Milbrandt, J. A., and Yau, M. K. (2005). A Multimoment Bulk Microphysics Parameterization. Part I: Analysis of the Role of the Spectral Shape Parameter. *Journal of the Atmospheric Sciences, 62*(9), 3051-3064. doi:10.1175/jas3534.1

Miller, G. H., Alley, R. B., Brigham-Grette, J., Fitzpatrick, J. J., Polyak, L., Serreze, M. C., and White, J. W. C. (2010). Arctic amplification: can the past constrain the future? *Quaternary Science Reviews, 29*(15-16), 1779-1790. doi:10.1016/j.quascirev.2010.02.008

Mironov, D. V. (2008). Parameterization of lakes in numerical weather prediction. Part 1: Description of a lake model.

Mladjic, B., Sushama, L., Khaliq, M. N., Laprise, R., Caya, D., and Roy, R. (2011). Canadian RCM Projected Changes to Extreme Precipitation Characteristics over Canada. *Journal of Climate, 24*(10), 2565-2584. doi:10.1175/2010jcli3937.1

Mohanty, M. P., and Simonovic, S. P. (2021). Understanding dynamics of population flood exposure in Canada with multiple high-resolution population datasets. *Science of The Total Environment, 759*, 143559. doi:https://doi.org/10.1016/j.scitotenv.2020.143559

Monette, A., Sushama, L., Khaliq, M. N., Laprise, R., and Roy, R. (2012). Projected changes to precipitation extremes for northeast Canadian watersheds using a multi-RCM ensemble. *Journal of Geophysical Research: Atmospheres, 117*(D13). doi:doi:10.1029/2012JD017543

Musselman, K. N., Clark, M. P., Liu, C., Ikeda, K., and Rasmussen, R. (2017). Slower snowmelt in a warmer world. *Nature Climate Change, 7*, 214. doi:10.1038/nclimate3225

Nachtergaele, F. O., van Velthuizen, H., Verelst, L., Wiberg, D., Batjes, N. H., Dijkshoorn, J. A., van Engelen, V. W. P., Fischer, G., Jones, A., Montanarella, L., Petri, M., Prieler, S., Teixeira, E., and Shi, X. (2012). *Harmonized World Soil Database (version 1.2)*. Laxenburg, Austria: Food and Agriculture Organization of the UN, International Institute for Applied Systems Analysis, ISRIC - World Soil Information, Institute of Soil Science - Chinese Academy of Sciences, Joint Research Centre of the EC.

NRCC. (2015). *National building code of Canada*. Ottawa, Ontario: National Research Council of Canada.

Oh, S.-G., and Sushama, L. (2020). Short-duration precipitation extremes over Canada in a warmer climate. *Climate Dynamics, 54*(3), 2493-2509. doi:10.1007/s00382-020-05126-4

Osterkamp, T. E. (2007). Characteristics of the recent warming of permafrost in Alaska. *Journal of Geophysical Research: Earth Surface, 112*(F2), n/a-n/a. doi:10.1029/2006JF000578

Palko, K., and Lemmen, D. S. (2017). Climate risks and adaptation practices for the Canadian transportation sector 2016.

Palmer, T. (2014). Climate forecasting: Build high-resolution global climate models. *Nature, 515*(7527), 338-339. doi:10.1038/515338a

Paquin, J. P., and Sushama, L. (2014). On the Arctic near-surface permafrost and climate sensitivities to soil and snow model formulations in climate models. *Climate Dynamics, 44*(1-2), 203-228. doi:10.1007/s00382-014-2185-6

Pasini, A., Pelino, V., and Potestà, S. (2001). A neural network model for visibility nowcasting from surface observations: Results and sensitivity to physical input variables. *Journal of Geophysical Research: Atmospheres, 106*(D14), 14951-14959. doi:https://doi.org/10.1029/2001JD900134

Pelletier, J. D., Broxton, P. D., Hazenberg, P., Zeng, X., Troch, P. A., Niu, G., Williams, Z. C., Brunke, M. A., and Gochis, D. (2016). *Global 1-km Gridded Thickness of Soil, Regolith, and Sedimentary Deposit Layers*. ORNL Distributed Active Archive Center Retrieved from http://daac.ornl.gov/cgi-bin/dsviewer.pl?ds_id=1304.

Perreault, N., Levesque, E., Fortier, D., and Lamarque, L. J. (2016). Thermo-erosion gullies boost the transition from wet to mesic tundra vegetation. *Biogeosciences, 13*(4), 1237-1253. doi:10.5194/bg-13-1237-2016

Perrin, A., Dion, J., Eng, S., Sawyer, D., Nodelman, J. R., Comer, N., Auld, H., Sparling, E., Harris, M., Nodelman, J. Y. H., and Kinnear, L. (2015). *Economic Implications of Climate Change Adaptations for Mine Access Roads in Northern Canada*. Northern Climate ExChange, Yukon Research Centre, Yukon College.

Pettitt, A. N. (1979). A Non-Parametric Approach to the Change-Point Problem. *Journal of the Royal Statistical Society: Series C (Applied Statistics), 28*(2), 126-135. doi:10.2307/2346729

Poitras, V., Sushama, L., Seglenieks, F., Khaliq, M. N., and Soulis, E. (2011). Projected Changes to Streamflow Characteristics over Western Canada as Simulated by the Canadian RCM. *Journal of Hydrometeorology, 12*(6), 1395-1413. doi:10.1175/jhm-d-10-05002.1

Prein, A. F., Gobiet, A., Suklitsch, M., Truhetz, H., Awan, N. K., Keuler, K., and Georgievski, G. (2013a). Added value of convection permitting seasonal simulations. *Climate Dynamics, 41*(9), 2655-2677. doi:10.1007/s00382-013-1744-6

Prein, A. F., Holland, G. J., Rasmussen, R. M., Done, J., Ikeda, K., Clark, M. P., and Liu, C. H. (2013b). Importance of regional climate model grid spacing for the simulation of heavy precipitation in the Colorado headwaters. *Journal of Climate, 26*(13), 4848-4857.

Prein, A. F., Langhans, W., Fosser, G., Ferrone, A., Ban, N., Goergen, K., Keller, M., Tölle, M., Gutjahr, O., Feser, F., Brisson, E., Kollet, S., Schmidli, J., van Lipzig, N. P. M., and Leung,

R. (2015). A review on regional convection-permitting climate modeling: Demonstrations, prospects, and challenges. *Reviews of Geophysics, 53*(2), 323-361. doi:https://doi.org/10.1002/2014RG000475

Pryor, S., Nikulin, G., and Jones, C. (2012). Influence of spatial resolution on regional climate model derived wind climates. *Journal of Geophysical Research-Atmospheres, 117*, D03117. doi:10.1029/2011JD016822

Rasmussen, P. F. (2016). Assessing the impact of climate change on the frequency of floods in the Red River basin. *Canadian Water Resources Journal / Revue canadienne des ressources hydriques, 41*(1-2), 331-342. doi:10.1080/07011784.2015.1025101

Riahi, K., Rao, S., Krey, V., Cho, C., Chirkov, V., Fischer, G., Kindermann, G., Nakicenovic, N., and Rafaj, P. (2011). RCP 8.5—A scenario of comparatively high greenhouse gas emissions. *Climatic Change, 109*(1), 33. doi:10.1007/s10584-011-0149-y

Rienecker, M. M., Suarez, M.J., Gelaro, R., Todling, R., Bacmeister, J., Liu, E., Bosilovich, M.G., Schubert, S.D., Takacs, L., Kim, G.-K., Bloom, S., Chen, J., Collins, D., Conaty, A., da Silva, A., Gu, W., Joiner, J., Koster, R.D., Lucchesi, R., Molod, A., Owens, T., Pawson, S., Pegion, P., Redder, C. R., Reichle, R., Robertson, F. R., Ruddick, A. G., Sienkiewicz, M., Woollen, J. (2011). MERRA: NASA's Modern-Era Retrospective Analysis for Research and Applications. *J. Climate, in press*.

Rummukainen, M. (2010). State-of-the-art with regional climate models. *Wiley Interdisciplinary Reviews: Climate Change, 1*(1), 82-96. doi:10.1002/wcc.8

Saha, S., Moorthi, S., Pan, H.-L., Wu, X., Wang, J., Nadiga, S., Tripp, P., Kistler, R., Woollen, J., Behringer, D., Liu, H., Stokes, D., Grumbine, R., Gayno, G., Wang, J., Hou, Y.-T., Chuang, H.-Y., Juang, H.-M. H., Sela, J., Iredell, M., Treadon, R., Kleist, D., Van Delst, P., Keyser, D., Derber, J., Ek, M., Meng, J., Wei, H., Yang, R., Lord, S., Van den Dool, H., Kumar, A., Wang, W., Long, C., Chelliah, M., Xue, Y., Huang, B., Schemm, J.-K., Ebisuzaki, W., Lin, R., Xie, P., Chen, M., Zhou, S., Higgins, W., Zou, C.-Z., Liu, Q., Chen, Y., Han, Y., Cucurull, L., Reynolds, R. W., Rutledge, G., and Goldberg, M. (2010). The NCEP Climate Forecast System Reanalysis. *Bulletin of the American Meteorological Society, 91*(8), 1015-1105. doi:10.1175/2010bams3001.1

Sakamoto, T. T., Komuro, Y., Nishimura, T., Ishii, M., Tatebe, H., Shiogama, H., Hasegawa, A., Toyoda, T., Mori, M., Suzuki, T., Imada, Y., Nozawa, T., Takata, K., Mochizuki, T., Ogochi, K., Emori, S., Hasumi, H., and Kimoto, M. (2012). MIROC4h – a new high-resolution atmosphere-ocean coupled general circulation model. *Journal of Meteorological Society of Japan, 90*(3), 325-359. doi:10.2151/jmsj.2012-301

Schleussner, C.-F., Rogelj, J., Schaeffer, M., Lissner, T., Licker, R., Fischer, E. M., Knutti, R., Levermann, A., Frieler, K., and Hare, W. (2016). Science and policy characteristics of the Paris Agreement temperature goal. *Nature Climate Change, 6*(9), 827-835. doi:10.1038/nclimate3096

Schuur, E. A. G., Abbott, B. W., Bowden, W. B., Brovkin, V., Camill, P., Canadell, J. G., Chanton, J. P., Chapin, F. S., Christensen, T. R., Ciais, P., Crosby, B. T., Czimczik, C. I., Grosse, G., Harden, J., Hayes, D. J., Hugelius, G., Jastrow, J. D., Jones, J. B., Kleinen, T., Koven, C. D., Krinner, G., Kuhry, P., Lawrence, D. M., McGuire, A. D., Natali, S. M., O'Donnell, J. A., Ping, C. L., Riley, W. J., Rinke, A., Romanovsky, V. E., Sannel, A. B. K., Schadel, C., Schaefer, K., Sky, J., Subin, Z. M., Tarnocai, C., Turetsky, M. R., Waldrop, M. P., Anthony, K. M. W., Wickland, K. P., Wilson, C. J., and Zimov, S. A. (2013). Expert assessment of vulnerability of permafrost carbon to climate change. *Climatic Change, 119*(2), 359-374. doi:10.1007/s10584-013-0730-7

Slater, A. G., and Lawrence, D. M. (2013). Diagnosing Present and Future Permafrost from Climate Models. *Journal of Climate, 26*(15), 5608-5623. doi:10.1175/Jcli-D-12-00341.1

Smith, L. C., Sheng, Y., MacDonald, G. M., and Hinzman, L. D. (2005). Disappearing Arctic lakes. *Science, 308*(5727), 1429. doi:10.1126/science.1108142

Smith, S., Chartrand, J., Duchesne, C., and Ednie, M. (2017). *Report on 2016 field activities and collection of ground thermal and active layer data in the Mackenzie Corridor, Northwest Territories*. Geological Survey of Canada.

Smith, S., Riseborough, D., Ednie, M., and Chartrand, J. (2013). A map and summary database of permafrost temperatures in Nunavut, Canada. *Geological Survey of Canada, Ottawa, Ont., Open File, 7393*(20), 10.4095.

Soulis, E. D., Snelgrove, K. R., Kouwen, N., Seglenieks, F., and Verseghy, D. L. (2000). Towards closing the vertical water balance in Canadian atmospheric models: Coupling of the land surface scheme class with the distributed hydrological model watflood. *Atmosphere-Ocean, 38*(1), 251-269. doi:10.1080/07055900.2000.9649648

Stocks, B. J., Mason, J. A., Todd, J. B., Bosch, E. M., Wotton, B. M., Amiro, B. D., Flannigan, M. D., Hirsch, K. G., Logan, K. A., Martell, D. L., and Skinner, W. R. (2002). Large forest fires in Canada, 1959-1997. *Journal of Geophysical Research-Atmospheres, 108*(D1). doi:10.1029/2001jd000484

Streletskiy, D. A., Shiklomanov, N. I., and Nelson, F. E. (2012). Permafrost, Infrastructure, and Climate Change: a GIS-Based Landscape Approach to Geotechnical Modeling. *Arctic Antarctic and Alpine Research, 44*(3), 368-380. doi:10.1657/1938-4246-44.3.368

Sundqvist, H., Berge, E., and Kristjansson, J. E. (1989). Condensation and Cloud Parameterization Studies with a Mesoscale Numerical Weather Prediction Model. *Monthly Weather Review, 117*(8), 1641-1657. doi:Doi 10.1175/1520-0493(1989)117<1641:Cacpsw>2.0.Co;2

Sushama, L., Laprise, R., Caya, D., Frigon, A., and Slivitzky, M. (2006). Canadian RCM projected climate-change signal and its sensitivity to model errors. *International Journal of Climatology, 26*(15), 2141-2159. doi:https://doi.org/10.1002/joc.1362

Teng, J., Jakeman, A. J., Vaze, J., Croke, B. F. W., Dutta, D., and Kim, S. (2017). Flood inundation modelling: A review of methods, recent advances and uncertainty analysis. *Environmental Modelling & Software, 90*, 201-216. doi:https://doi.org/10.1016/j.envsoft.2017.01.006

Teufel, B., Diro, G. T., Whan, K., Milrad, S. M., Jeong, D. I., Ganji, A., Huziy, O., Winger, K., Gyakum, J. R., de Elia, R., Zwiers, F. W., and Sushama, L. (2017). Investigation of the 2013 Alberta flood from weather and climate perspectives. *Climate Dynamics, 48*(9), 2881-2899. doi:10.1007/s00382-016-3239-8

Teufel, B., and Sushama, L. (2019). Abrupt changes across the Arctic permafrost region endanger northern development. *Nature Climate Change, 9*(11), 858-862. doi:10.1038/s41558-019-0614-6

Teufel, B., Sushama, L., Arora, V. K., and Verseghy, D. (2018). Impact of dynamic vegetation phenology on the simulated pan-Arctic land surface state. *Climate Dynamics*. doi:10.1007/s00382-018-4142-2

Teufel, B., Sushama, L., Huziy, O., Diro, G. T., Jeong, D. I., Winger, K., Garnaud, C., de Elia, R., Zwiers, F. W., Matthews, H. D., and Nguyen, V. T. V. (2019). Investigation of the mechanisms leading to the 2017 Montreal flood. *Climate Dynamics, 52*(7), 4193-4206. doi:10.1007/s00382-018-4375-0

Thornton, P. E., Thornton, M. M., Mayer, B. W., Wei, Y., Devarakonda, R., Vose, R. S., and Cook, R. B. (2016). Daymet: Daily Surface Weather Data on a 1-km Grid for North America, Version 3: ORNL Distributed Active Archive Center.

Trenberth, K. E., Dai, A., Rasmussen, R. M., and Parsons, D. B. (2003). The changing character of precipitation. *Bulletin of the American Meteorological Society, 84*(9), 1205-1218.

Trusilova, K., Früh, B., Brienen, S., Walter, A., Masson, V., Pigeon, G., and Becker, P. (2013). Implementation of an urban parameterization scheme into the regional climate model COSMO-CLM. *Journal of Applied Meteorology and Climatology, 52*(10), 2296-2311.

Turetsky, M. R., Kane, E. S., Harden, J. W., Ottmar, R. D., Manies, K. L., Hoy, E., and Kasischke, E. S. (2010). Recent acceleration of biomass burning and carbon losses in Alaskan forests and peatlands. *Nature Geoscience, 4*(1), 27-31. doi:10.1038/ngeo1027

van Vuuren, D., Edmonds, J., Kainuma, M., Riahi, K., Thomson, A., Hibbard, K., Hurtt, G., Kram, T., Krey, V., Lamarque, J., Masui, T., Meinshausen, M., Nakicenovic, N., Smith, S., and Rose, S. (2011). The representative concentration pathways: an overview. *Climatic Change, 109*(1-2), 5-31. doi:10.1007/s10584-011-0148-z

Van Wagner, C. (1987). *Development and structure of the Canadian Forest Fire Weather Index System*. (0662151984). Ottawa: Canadian Forestry Service.

Veraverbeke, S., Rogers, B. M., Goulden, M. L., Jandt, R. R., Miller, C. E., Wiggins, E. B., and Randerson, J. T. (2017). Lightning as a major driver of recent large fire years in North American boreal forests. *Nature Climate Change, 7*, 529. doi:10.1038/nclimate3329

Verseghy, D. L. (2011). CLASS–The Canadian Land Surface Scheme (Version 3.5), Technical Documentation (Version 1). *Climate Research Division, Science and Technology Branch, Environment Canada*.

Vormoor, K., Lawrence, D., Heistermann, M., and Bronstert, A. (2015). Climate change impacts on the seasonality and generation processes of floods – projections and uncertainties for catchments with mixed snowmelt/rainfall regimes. *Hydrol. Earth Syst. Sci., 19*(2), 913-931. doi:10.5194/hess-19-913-2015

Warren, F., and Lulham, N. (2021). *Canada in a Changing Climate: National Issues Report*. Ottawa, Ontario: Government of Canada.

Wehner, M. F., Smith, R. L., Bala, G., and Duffy, P. (2010). The effect of horizontal resolution on simulation of very extreme US precipitation events in a global atmosphere model. *Climate Dynamics, 34*(2-3), 241-247. doi:10.1007/s00382-009-0656-y

Westra, S., Alexander, L., and Zwiers, F. (2013). Global increasing trends in annual maximum daily precipitation. *Journal of Climate, in press*.

White, D., Hinzman, L., Alessa, L., Cassano, J., Chambers, M., Falkner, K., Francis, J., Gutowski, W. J., Holland, M., Holmes, R. M., Huntington, H., Kane, D., Kliskey, A., Lee, C., McClelland, J., Peterson, B., Rupp, T. S., Straneo, F., Steele, M., Woodgate, R., Yang, D., Yoshikawa, K., and Zhang, T. (2007). The arctic freshwater system: Changes and impacts. *Journal of Geophysical Research-Biogeosciences, 112*(G4). doi:10.1029/2006jg000353

Whitfield, P. H. (2012). Floods in future climates: a review. *Journal of Flood Risk Management, 5*(4), 336-365. doi:https://doi.org/10.1111/j.1753-318X.2012.01150.x

Winsemius, H. C., Aerts, Jeroen C. J. H., van Beek, Ludovicus P. H., Bierkens, Marc F. P., Bouwman, A., Jongman, B., Kwadijk, Jaap C. J., Ligtvoet, W., Lucas, Paul L., van Vuuren, Detlef P., and Ward, Philip J. (2016). Global drivers of future river flood risk. *Nature Climate Change, 6*(4), 381-385. doi:10.1038/nclimate2893

Woo, M. K., Kane, D. L., Carey, S. K., and Yang, D. Q. (2008). Progress in permafrost hydrology in the new millennium. *Permafrost and Periglacial Processes, 19*(2), 237-254. doi:10.1002/ppp.613

Wrona, F. J., Johansson, M., Culp, J. M., Jenkins, A., Mard, J., Myers-Smith, I. H., Prowse, T. D., Vincent, W. F., and Wookey, P. A. (2016). Transitions in Arctic ecosystems: Ecological implications of a changing hydrological regime. *Journal of Geophysical Research-Biogeosciences, 121*(3), 650-674. doi:10.1002/2015jg003133

Yeh, K.-S., Côté, J., Gravel, S., Méthot, A., Patoine, A., Roch, M., and Staniforth, A. (2002). The CMC–MRB Global Environmental Multiscale (GEM) Model. Part III: Nonhydrostatic Formulation. *Monthly Weather Review, 130*(2), 339-356. doi:10.1175/1520-0493(2002)130<0339:tcmgem>2.0.co;2

Zadra, A., Roch, M., Laroche, S., and Charron, M. (2003). The subgrid-scale orographic blocking parametrization of the GEM model. *Atmosphere-Ocean, 41*(2), 155-170. doi:DOI 10.3137/ao.410204

Zhang, G. J., and Song, X. (2010). Convection parameterization, tropical Pacific double ITCZ, and upper-ocean biases in the NCAR CCSM3. Part II: Coupled feedback and the role of ocean heat transport. *Journal of Climate, 23*(3), 800-812.

Zhang, X., Zwiers, F. W., Li, G., Wan, H., and Cannon, A. J. (2017). Complexity in estimating past and future extreme short-duration rainfall. *Nature Geoscience, 10*(4), 255-259. doi:10.1038/ngeo2911

Appendix A: Supplementary material for Chapter 4

A.1. Abrupt changes to near-surface temperature

One of the most direct implications of the abrupt decrease in soil moisture is a reduction in the thermal inertia of the soil. Due to this, near-surface soil temperatures after the abrupt change follow a more extreme yearly cycle, being warmer during summer (Figure A3) and colder during winter. The decreased soil moisture also results in shorter freezing and thawing periods during the transition seasons, as less mass undergoes phase transitions.

Soil moisture plays a role in attenuating temperature extremes, meaning that their frequency and intensity might increase under drier surface conditions. During the warm season, analysis shows that the abrupt warming is stronger for daily maximum temperatures than for daily minimum temperatures, i.e. there is an increase in the daily temperature range (Figure A3). While the magnitude of abrupt changes to near-surface temperature (generally below 1 °C) appear modest in the context of the large warming expected over northern regions (close to 1 °C per decade), they have the potential to cause disruptions to systems highly sensitive to temperature.

A.2. Processes leading to permafrost degradation

Analysis of the years surrounding permafrost degradation allows insight into the processes behind the permafrost degradation itself. For example, the year that near-surface permafrost degrades is generally characterized by warm and wet conditions during summer. Warmth is transferred downwards into permafrost by thermal conduction and also by the movement of soil moisture, which is greater during abnormally wet years.

A.3. Validation of near-surface climate and permafrost conditions

The ability of GEM to reproduce near-surface climate characteristics is assessed by comparing simulated fields with various observation and reanalysis datasets. For seasonal 2-m temperature, GEM is compared to the CRU TS v4.03 dataset (Harris et al., 2014) and the ERA5 reanalysis (Copernicus Climate Change Service, 2017). Figure A5 shows that GEM performs reasonably well in capturing the spatial and seasonal variations of 2-m temperature, as biases are generally small. For seasonal precipitation, GEM is compared to the ERA5 reanalysis and to the Arctic System Reanalysis v2 (Bromwich et al., 2018). Figure A6 shows that GEM is able to reproduce the spatial and seasonal variations of precipitation without excessive bias.

The circum-Arctic map of permafrost and ground-ice conditions (Brown et al., 2002) is used to validate the modelled permafrost extent. In this map, permafrost is categorized as continuous (> 90% coverage), discontinuous (50–90% coverage), sporadic (10–50% coverage) and isolated (< 10% coverage). In GEM, a grid cell is underlain by near-surface permafrost when the modelled temperature of at least one soil layer in the top 5 m remains at or below 0 °C for 2 consecutive years. Figure A7a shows that the spatial extent of near-surface permafrost is captured realistically in GEM.

Further validation is performed by comparing simulated and observed values of active layer thickness (ALT), which is defined as the maximum annual thaw depth. The observed values used are those from the circumpolar active layer monitoring (CALM) dataset (Brown et al., 2000), which contains yearly observations of ALT at specific sites, from 1990 to present. ALT is estimated in the field using a variety of methods, including mechanical probing with steel rods, thaw tubes and interpolation from ground temperature measurements at different depths. In GEM, the ALT for a particular year is assumed to be the depth to the bottom of the soil layer closest to the surface with maximum temperature above 0 °C during the year under consideration. When comparing simulated and observed ALT, it is important to consider that observations are only representative of a small area within a much larger grid cell, because of complex terrain and heterogeneity of soil properties within the grid cell. Figure A7b shows that the level of agreement between the simulated and observed ALT is generally high.

In addition, previous climate modelling studies have shown that the GEM model can reasonably well reproduce processes such as land-atmosphere coupling (Diro et al., 2014), lake-atmosphere interactions (Huziy and Sushama, 2017b) and snow-atmosphere coupling (Diro et al., 2018), as well as permafrost extent (Paquin and Sushama, 2015), rain-on-snow events (Jeong and Sushama, 2018b) and wind/snow loads (Jeong and Sushama, 2018a).

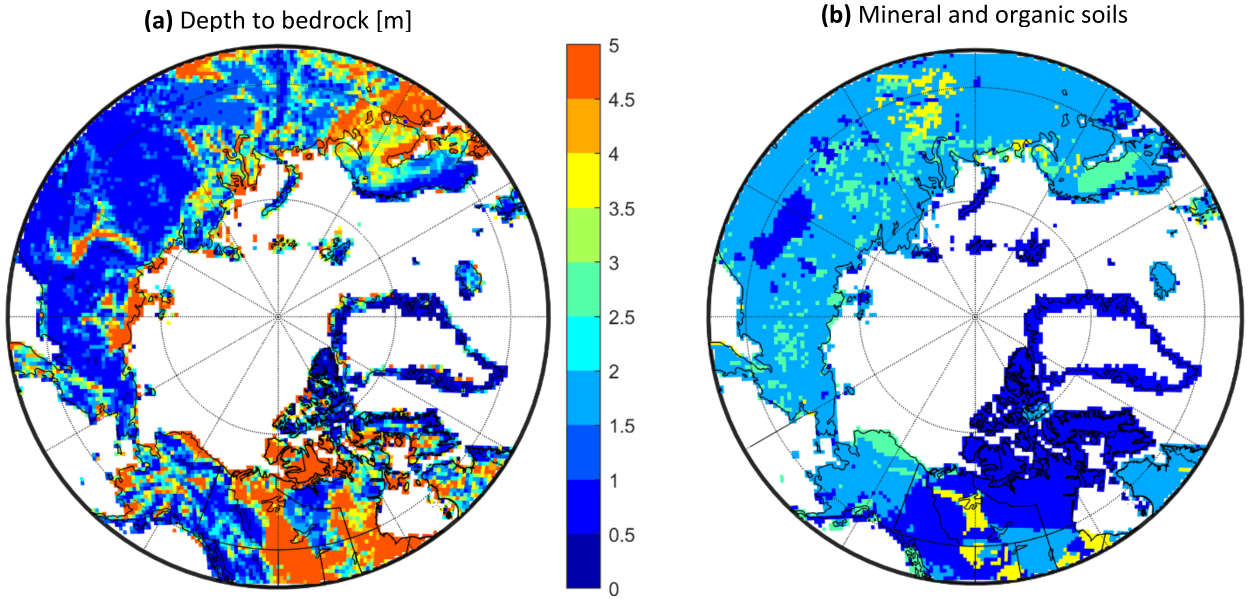

Figure A1. (a) Permeable soil depth. (b) Mineral soils are shown in dark blue, organic soils are shown in yellow. Light blue is used for mineral soils overlain by 10 cm of organic soil and green is used for mineral soils overlain by 30 cm of organic soil.

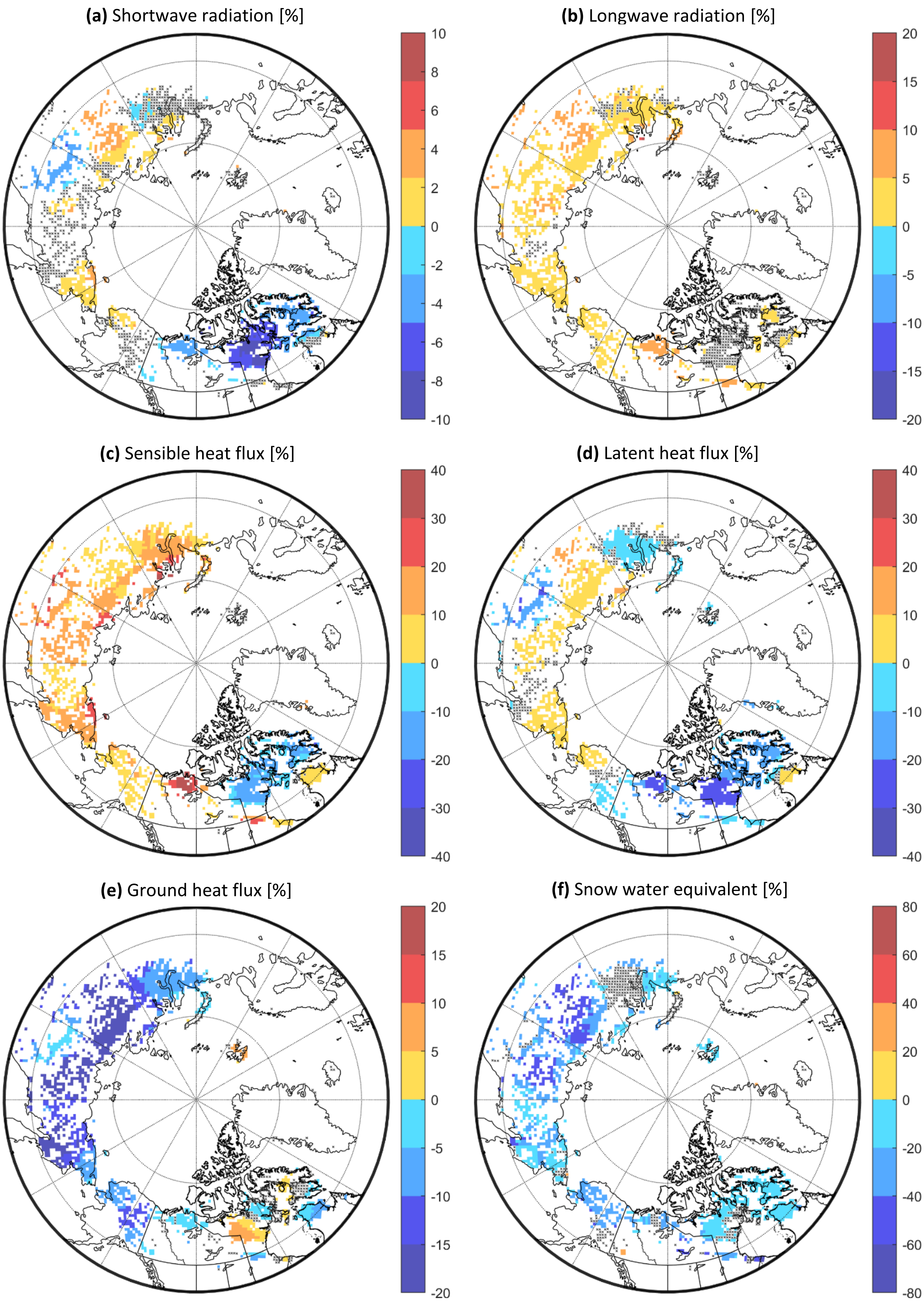
(a) Shortwave radiation [%]
10
8
6
4
2
0
-2
-4
-6
-8
-10
(b) Longwave radiation [%]
20
15
10
5
0
-5
-10
-15
-20
(c) Sensible heat flux [%]
40
30
20
10
0
-10
-20
-30
-40
(d) Latent heat flux [%]
40
30
20
10
0
-10
-20
-30
-40
(e) Ground heat flux [%]
20
15
10
5
0
-5
-10
-15
-20
(f) Snow water equivalent [%]
80
60
40
20
0
-20
-40
-60
-80

Figure A2. Relative magnitude of abrupt changes due to permafrost degradation in (a) summer (JJA) net shortwave radiation (downwards), (b) JJA net longwave radiation (upwards), (c) JJA sensible heat flux (upwards), (d) JJA latent heat flux (upwards), (e) JJA ground heat flux (downwards) and (f) JJA snow water equivalent. Changes are shown as percentages with respect to the regression estimate before the abrupt change. Grey markers are used when there is no evidence of an abrupt change (see Methods).

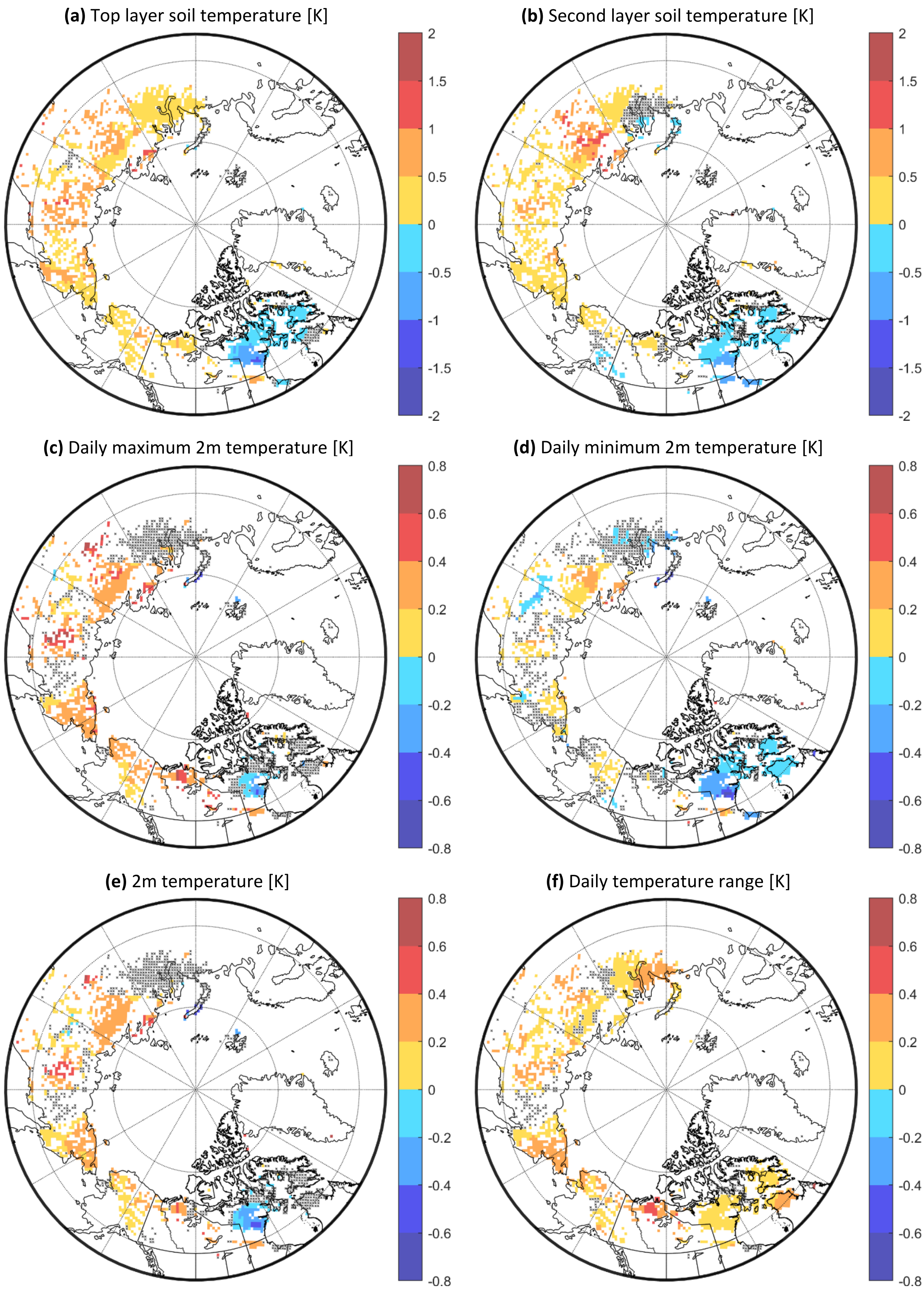
(a) Top layer soil temperature [K]
2
1.5
1
0.5
0
-0.5
-1
-1.5
-2
(b) Second layer soil temperature [K]
2
1.5
1
0.5
0
-0.5
-1
-1.5
-2
(c) Daily maximum 2m temperature [K]
0.8
0.6
0.4
0.2
0
-0.2
-0.4
-0.6
-0.8
(d) Daily minimum 2m temperature [K]
0.8
0.6
0.4
0.2
0
-0.2
-0.4
-0.6
-0.8
(e) 2m temperature [K]
0.8
0.6
0.4
0.2
0
-0.2
-0.4
-0.6
-0.8
(f) Daily temperature range [K]
0.8
0.6
0.4
0.2
0
-0.2
-0.4
-0.6
-0.8

Figure A3. Magnitude of abrupt changes due to permafrost degradation in (a) summer (JJA) top layer (0-10 cm) soil temperature, (b) JJA second layer (10-30 cm) soil temperature, (c) JJA daily maximum 2m temperature, (d) JJA daily minimum 2m temperature, (e) JJA 2m temperature and (f) JJA daily temperature range. Grey markers are used when there is no evidence of an abrupt change (see Methods).

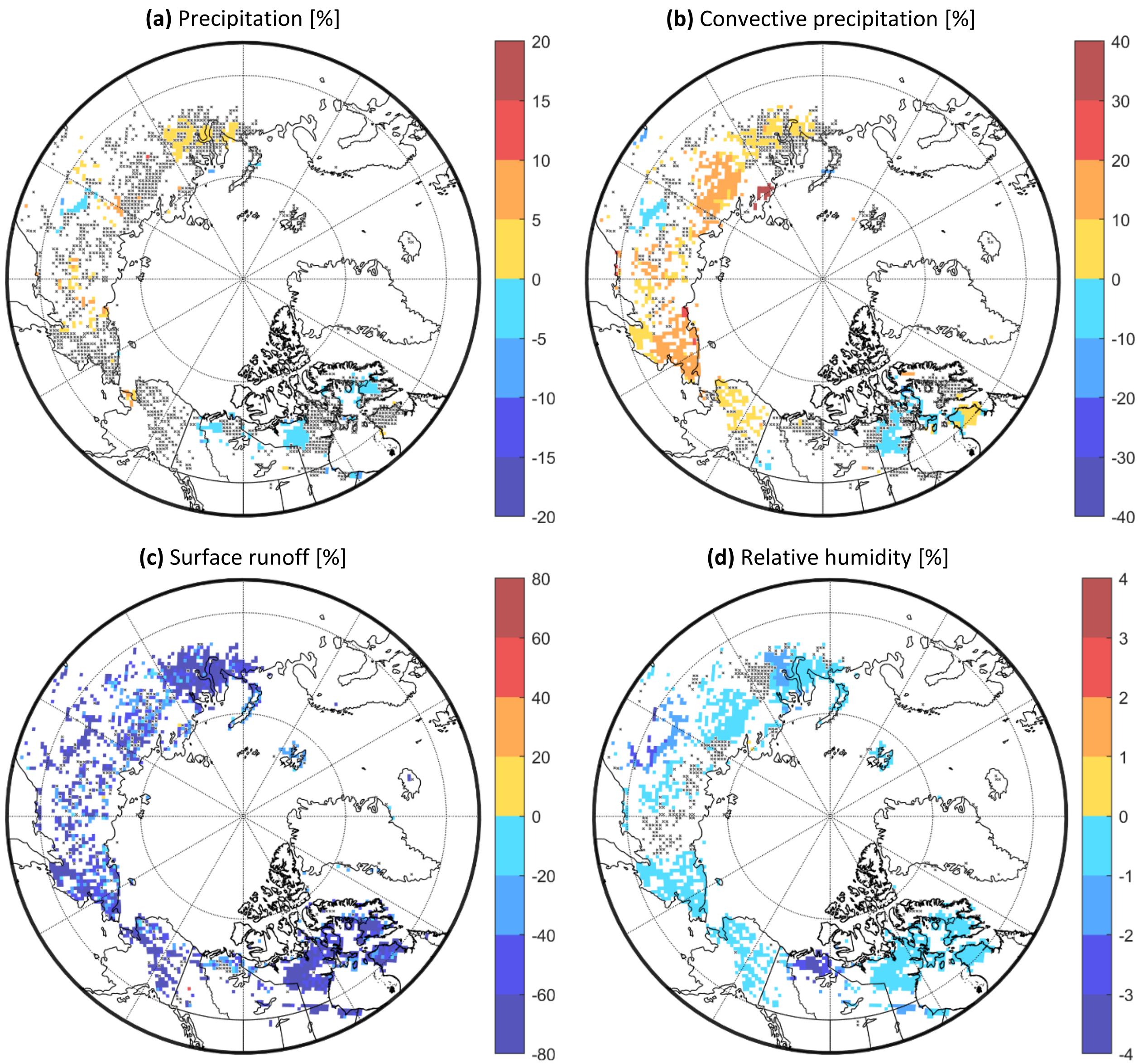

Figure A4. Magnitude of abrupt changes due to permafrost degradation in (a) summer (JJA) precipitation, (b) JJA convective precipitation, (c) annual surface runoff, (d) JJA relative humidity. In (a-c), changes are shown as percentages with respect to the regression estimate before the abrupt change. Grey markers are used when there is no evidence of an abrupt change (see Methods).

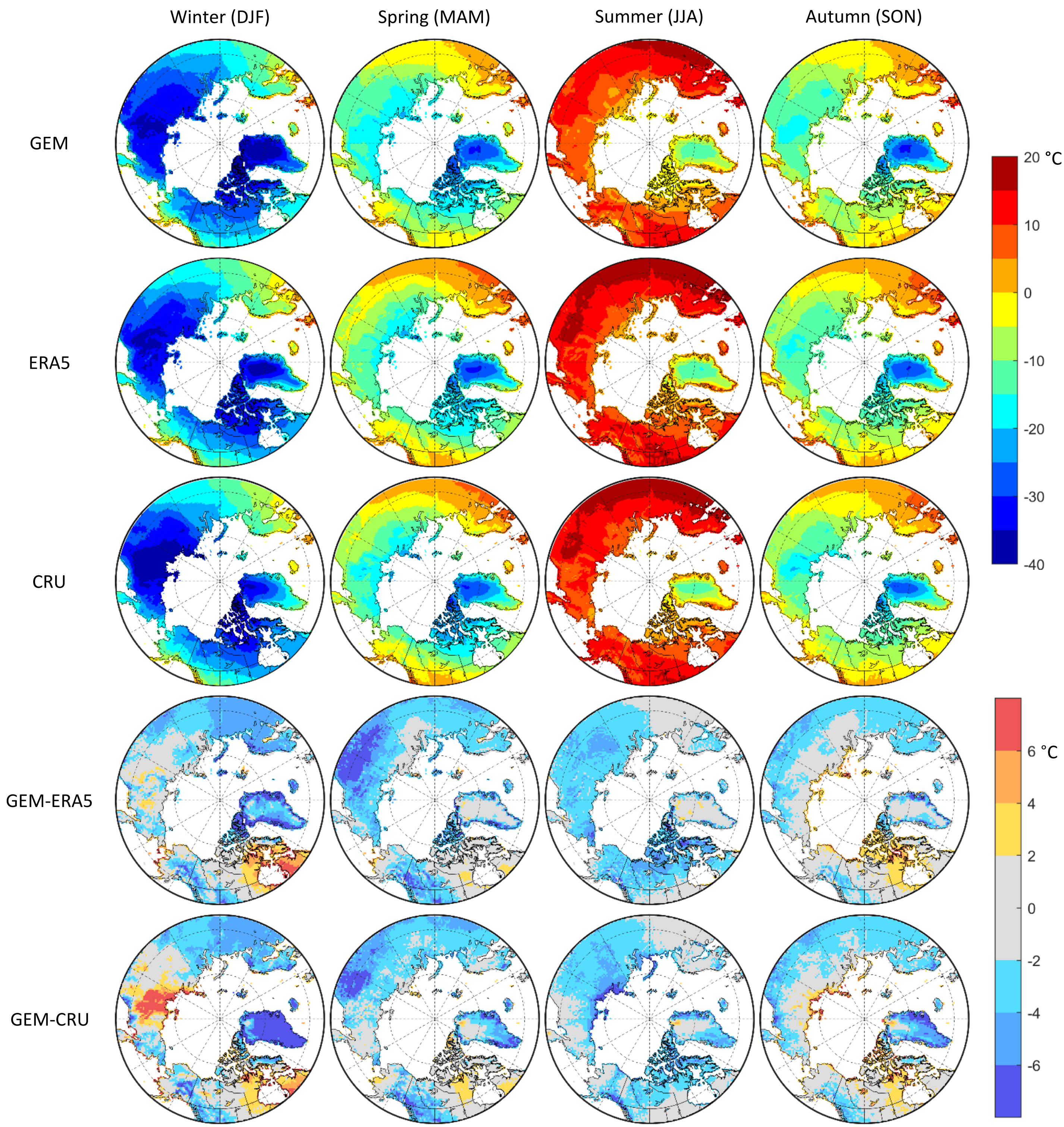

Figure A5. Seasonal mean temperature for the 1981-2010 period from the GEM ensemble (first row), the ERA5 reanalysis (second row) and the CRU dataset (third row). Seasonal temperature differences between GEM and ERA5 (fourth row) and between GEM and CRU (fifth row) are also shown. Non-land areas are shown in white.

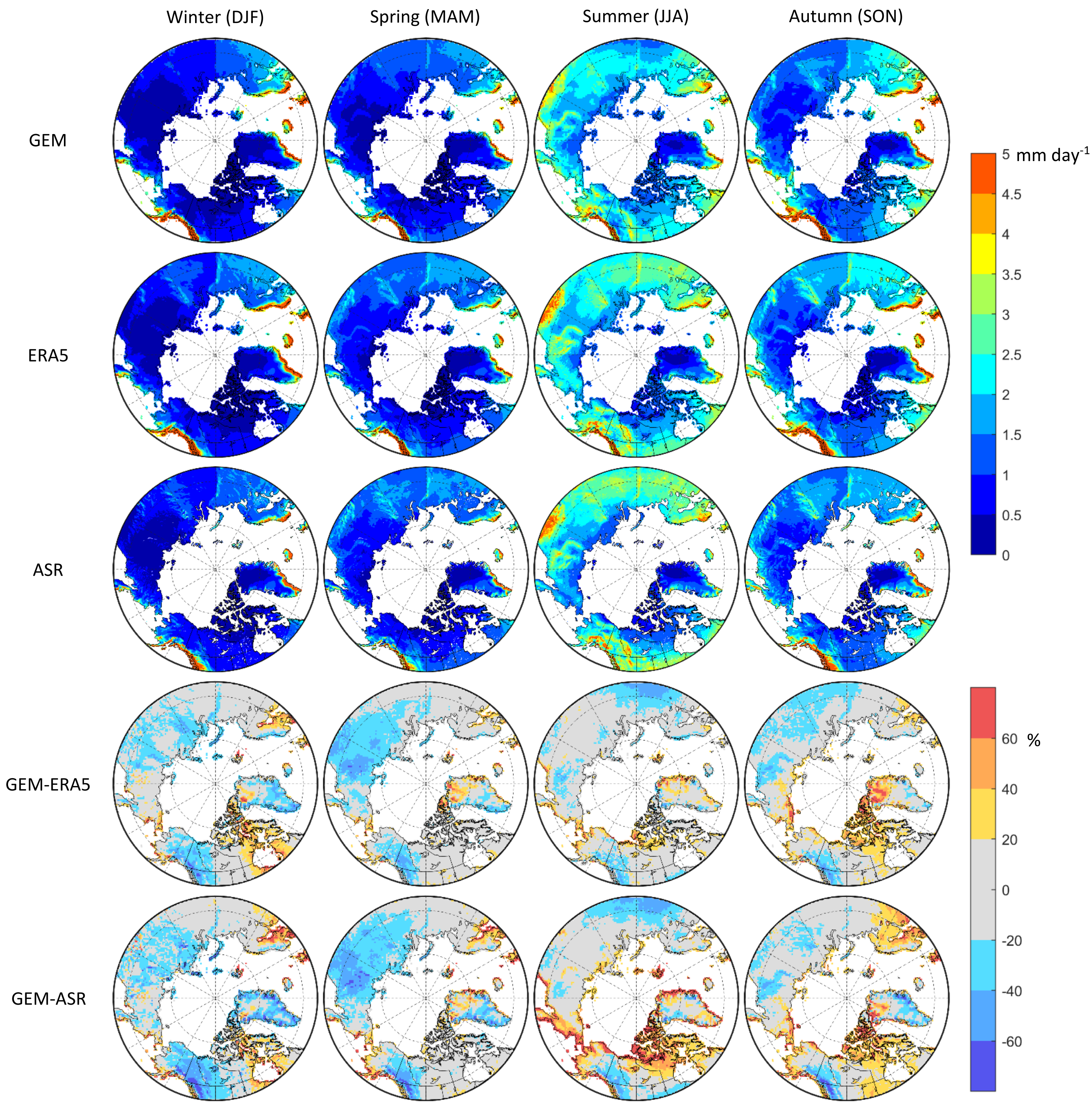

Figure A6. Seasonal mean precipitation for the 1981-2010 period from the GEM ensemble (first row), the ERA5 reanalysis (second row) and the ASR (third row; 2000-2016 period). Relative seasonal precipitation differences between GEM and ERA5 (fourth row) and between GEM and ASR (fifth row) are also shown. Percentages are computed with respect to the reanalysis. Non-land areas are shown in white.

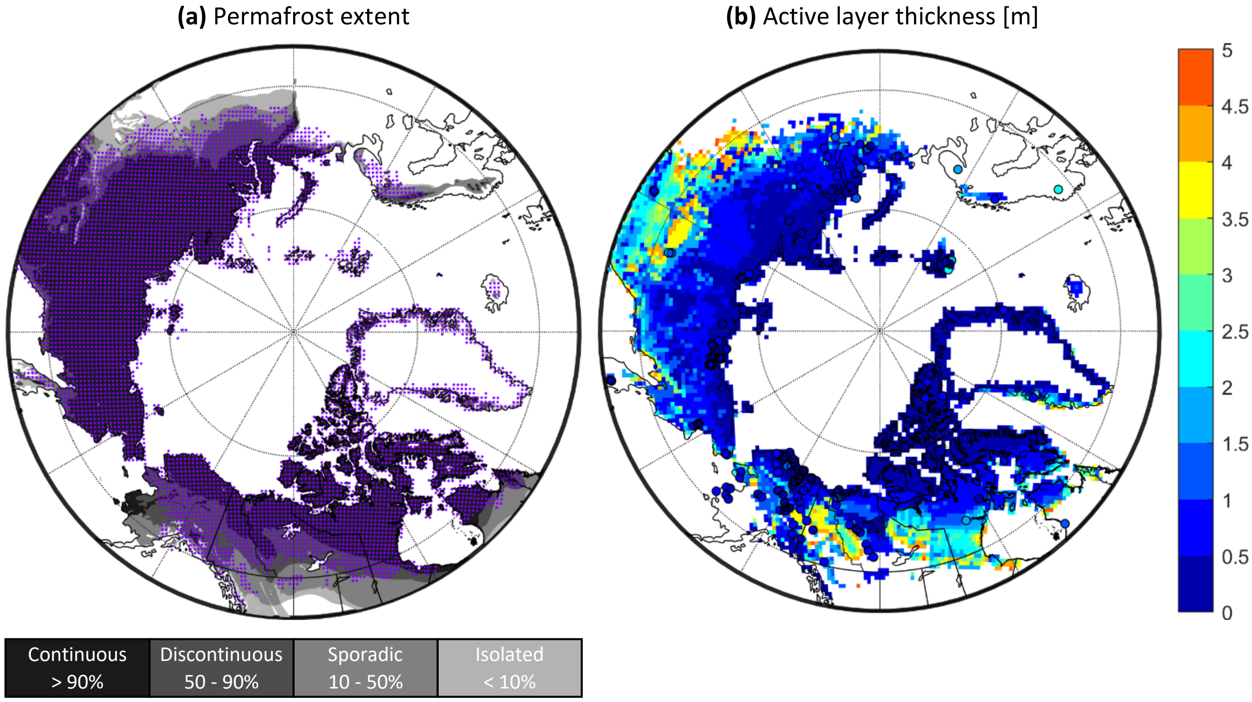

Figure A7. (a) Permafrost extent from the circum-Arctic map of permafrost (grey shading) and from the GEM ensemble for the 1971-2000 period (purple dots mark the center of grid cells with near-surface permafrost). (b) Mean active layer thickness of near-surface permafrost for the 1990-2018 period from the GEM ensemble (shading) and from the sites of the CALM program (coloured circles with black borders).

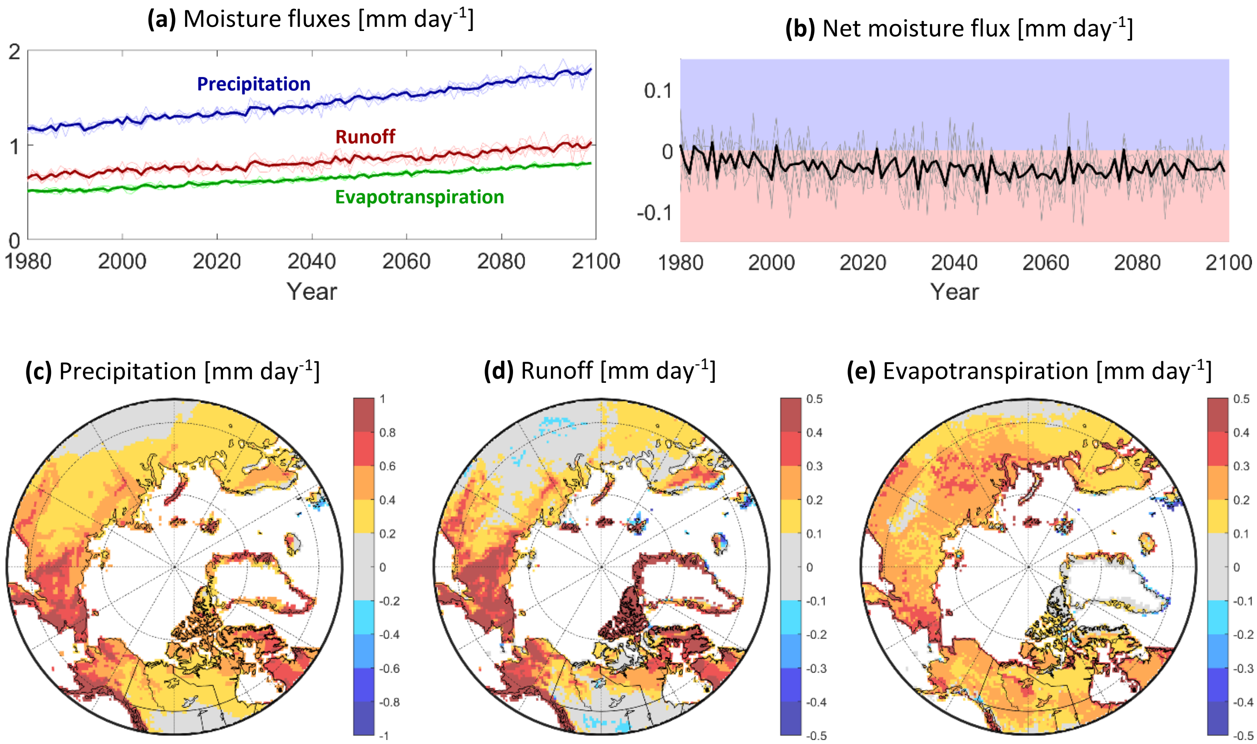

Figure A8. (a) Area-averaged annual moisture fluxes over the 1971-2000 near-surface permafrost region (see Fig. A7). The thick lines correspond to the ensemble mean and the thin lines to each ensemble member. (b) As in (a), but for the downwards net moisture flux at the surface. Also shown are projected changes (2070-2099 minus 1981-2010) in ensemble mean annual (c) precipitation, (d) runoff and (e) evapotranspiration.

Appendix B: Supplementary material for Chapter 5

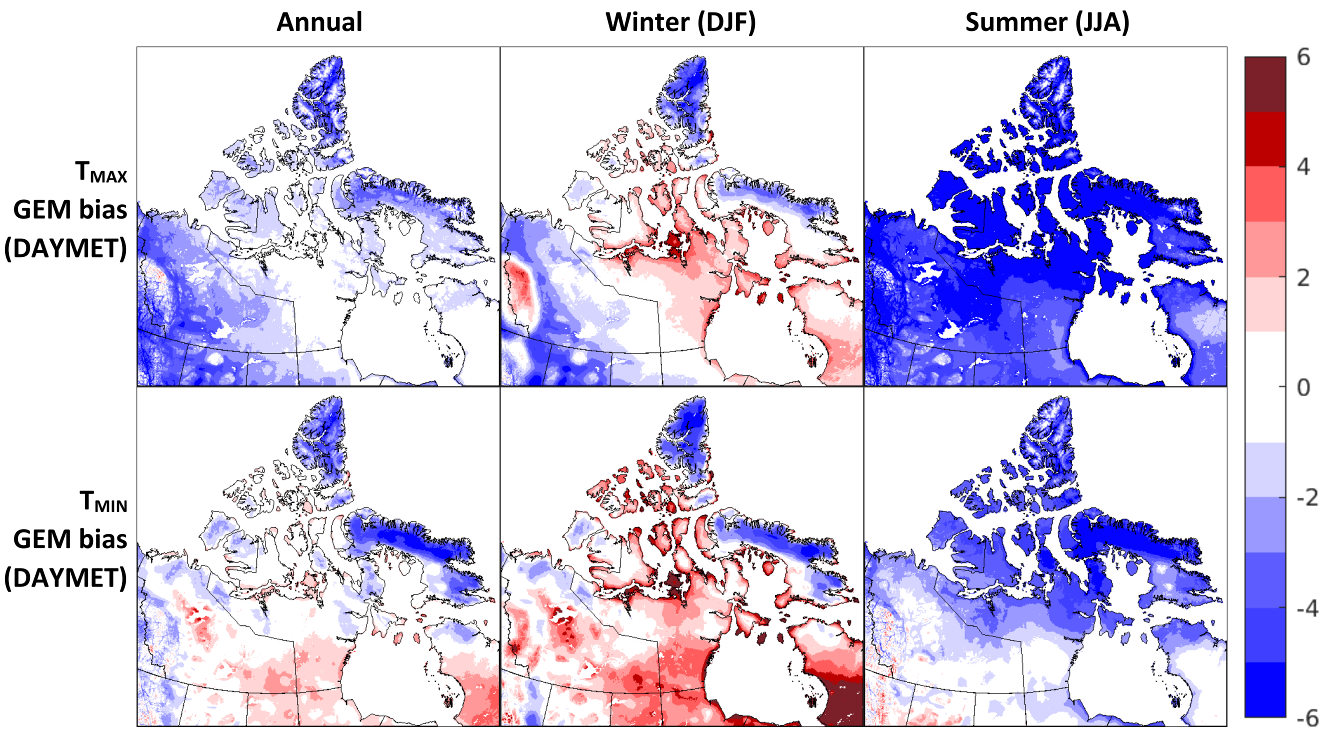

Figure B1. GEM50_ERA biases (°C) with respect to DAYMET for annual and seasonal averages of daily maximum and minimum 2-m air temperature during the 1991-2010 period.

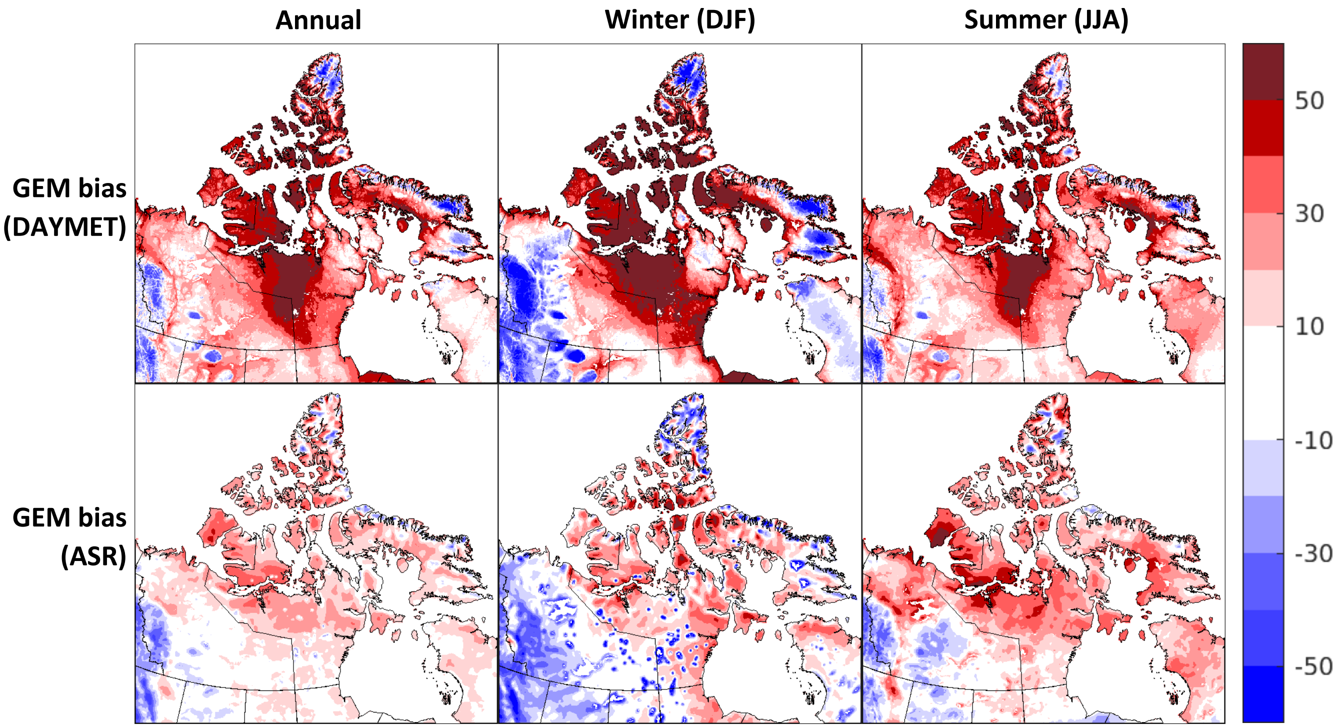

Figure B2. GEM50_ERA biases (%) with respect to DAYMET and ASR for annual and seasonal averages of precipitation during the 1991-2010 period (2000-2010 for ASR).

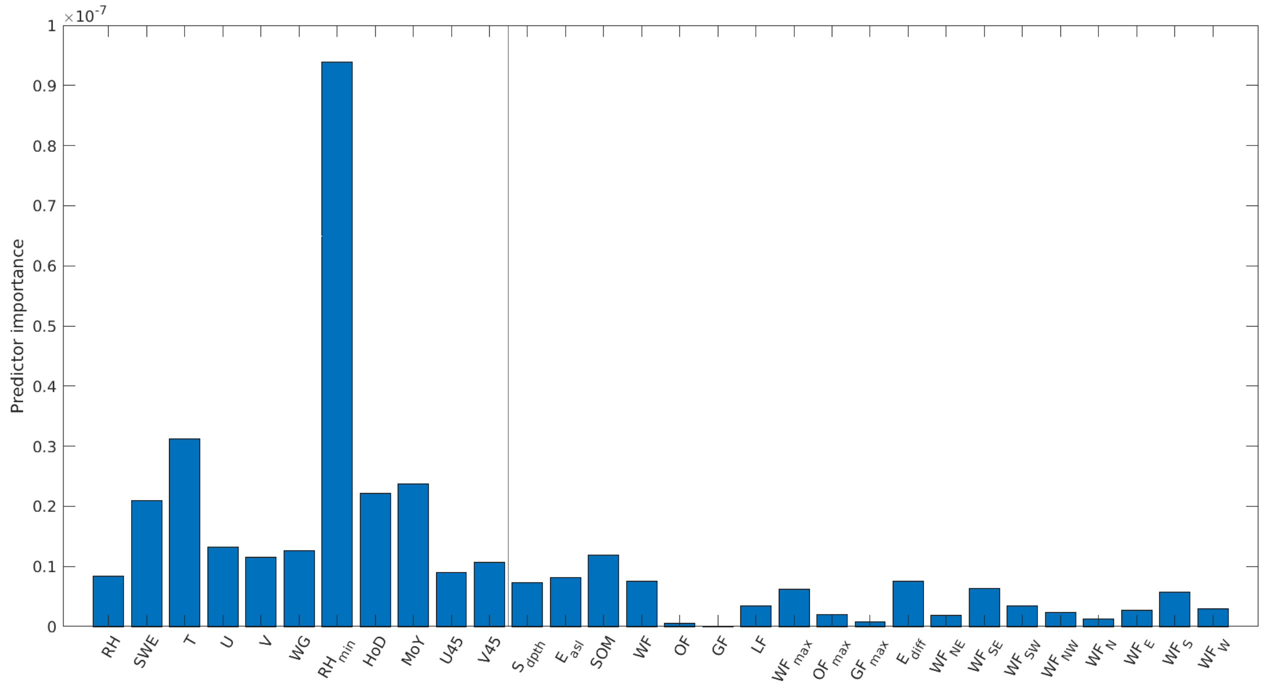

Figure B3. Relative importance of each fog predictor. The predictors to the left of the vertical line vary in time and space: 2-m relative humidity (RH), snowpack mass (SWE), 2-m temperature (T), 10-m wind components (U, V), 10-m wind gust speed (WG), minimum 2-m relative humidity on a 3x3 grid centered on the location of interest (RH_{min}), local solar time (HoD), month of the year (MoY) and 10-m wind components rotated by 45 degrees (U45, V45). The predictors to the right of the vertical line only vary in space: soil depth (S_{dpth}), elevation above sea level (E_{asl}), soil organic matter (SOM), water fraction (WF), ocean fraction (OF), glacier fraction (GF), lake fraction (LF), maximum water, ocean and glacier fraction on the surrounding 3x3 grid (WF_{max}, OF_{max}, GF_{max}), elevation with respect to the surrounding 3x3 grid (E_{diff}) and water fraction of each neighbouring grid cell (WF_{NE}, WF_{SE}, WF_{SW}, WF_{NW}, WF_{N}, WF_{E}, WF_{S}, WF_{W}).